공학박사 학위논문

Highly efficient deep-blue organic light emitting diodes utilizing triplet exciton harvesting strategies

삼중항 여기자 수확 전략을 활용한
고효율 진청색 유기발광소자

2020년 8월

서울대학교 대학원
재료공학 전공
임 형 철

Abstract

Highly efficient deep-blue organic light emitting diodes utilizing triplet exciton harvesting strategies

Hyoungcheol Lim
Department of Materials Science and Engineering
The Graduate School
Seoul National University

OLEDs have been commercialized in mobile display as well as flexible or large-area displays because they have various advantages such as high color gamut and light weight. In addition, OLEDs have been applied to lighting products because they can be fabricated as a surface or flexible light source, and have high color temperature and color rendering index. For several decades, the development of various emitters such as phosphorescence and TADF materials has enabled the production of highly efficient OLEDs and contributed to the commercialization of OLEDs. However, in order for OLED to become

more widely available in the future, more development and research must be conducted to increase the efficiency and color purity of blue OLED. In this research, triplet harvesting methods were explored and the efficient deep-blue OLEDs were developed.

In chapter 2, the high T_1 exciplex host suitable for deep-blue phosphorescent OLEDs (phOLEDs) is introduced. The exciplex hosts for deep-blue OLEDs had not been reported at that time because of the difficulties in identifying suitable molecules. A deep-blue-emitting exciplex system with an exciplex energy of 3.0 eV is developed based on the molecular property analysis. And the exciplex system is applied to the deep-blue phosphorescent OLEDs. The blue PhOLEDs exhibited maximum external quantum efficiency of 24% with CIE color coordinates of (0.15, 0.21) and longer lifetime than the single host devices.

In chapter3, thermally activated delayed fluorescent (TADF) emitters with narrow blue emission spectrum are introduced. Both emitters exhibit narrow emission spectra with the full width half maximum (FWHM) less than 65 nm due to the rigid donor and acceptor unit. Furthermore, long molecular structure along the transition dipole moment direction results in a high horizontal emitting dipole orientation ratio over 80%. By combining the effects, the OLED utilizing DBA-SAB as the emitter exhibits maximum EQE of 25.7% and CIE coordinates of (0.144, 0.212). Moreover, even a higher efficiency deep blue TADF OLED with a maximum EQE of 28.2% and 1931 Commission

Internationale de l'éclairage (CIE) coordinates of (0.142, 0.090) is realized.

In chapter 4, triplet-triplet annihilation process is studied and blue OLEDs with thin efficiency-enhancement layer (EEL) is developed. Insertion of a very thin EEL (3 nm) between the deep blue emitting layer (EML) and the electron transport layer enhanced the EQE of the blue device by 44% compared to the device without the EEL, resulting in an EQE of 7.9% and a current efficiency of 9.0 cd A−1 at 1000 cd m−2; the CIE coordinates of the emitting color were (0.13, 0.14). The transient electroluminescence showed that the efficiency enhancement originates from the triplet−triplet annihilation (TTA) process in the EEL, followed by energy transfer to the emitting dye in the EML.

.

Keywords: Deep-blue organic light-emitting diodes, phosphorescence, fluorescence, thermally activated delayed fluorescence, triplet-triplet annihilation, delayed fluorescence

Student Number: 2014-22529

Contents

List of Tables

List of Figures

Chapter 1. Introduction

1.1 Brief introduction to Organic Light-Emitting Diodes

In 1963, electroluminescence (EL) emission was observed from single crystal anthracene and tetracene doped anthracene by W. Helfrich and W. G. Schneider.[1] In 1987, C. W. Tang and S. A. Vanslyke reported the first bi-layered organic EL device and this device exhibited brightness of above 1,000 cd m^{-2}.[2] Since this discovery was reported, a lot of researches about organic light-emitting diodes (OLEDs) have been conducted intensively. More layers such as charge injection layer, charge transporting layer, exciton blocking layer and emitting layer (EML) have been added for improvements of efficiency and stability. Due to the different properties required for each layers, organic semiconductor materials have also been developed to meet the requirements.[3–6] Thanks to the much effort to improve the performance of OLEDs, OLED technologies are successfully commercialized in flat panel display and white lighting industry. (Figure 1.1)

Currently used OLEDs have multi-layered structure as explained above. The organic layers are usually thermally deposited between metal electrodes. Solution processes for OLED fabrication are also being studied because solution process is more efficient and cheap way for fabricating OLEDs. As an anode, transparent conducting film such as indium-tin oxide (ITO) is used that the light can come out of devices. The cathode electrode almost reflect the light

from EML. OLEDs can be fabricated on various substrates including flexible and transparent film, making rollable displays possible.

OLED market has been rapidly expanded in recent several years. OLED display have become dominant replace liquid crystal display (LCD) in small-sized displays and are beginning to be used in large area displays. Contrary to LCD, which were widely used as conventional displays, OLED panels do not require a light source due to their self-luminescent property. Therefore, OLED panels can be thinner and lighter compared with LCD. More importantly, OLED panels can control each pixel thus give high contrast ratio. Another advantages of OLED panels is low power consumption, high color purity, and fast repetition rate. Due to their advantages, OLEDs have been considered as a promising next-generation display, and are widely used as displays for various electronic devices. Also for a solid-state lighting, OLEDs have several advantages over conventional lightings. OLEDs are eco-friendly light source which have higher efficiency compared to light bulbs and incandescent lamp. In addition, OLEDs have high color temperature and color rendering index (CRI), and they can be manufactured as a large-area and flexible surface light source. Therefore, OLEDs are expanding their applications not only in displays but also in lighting.

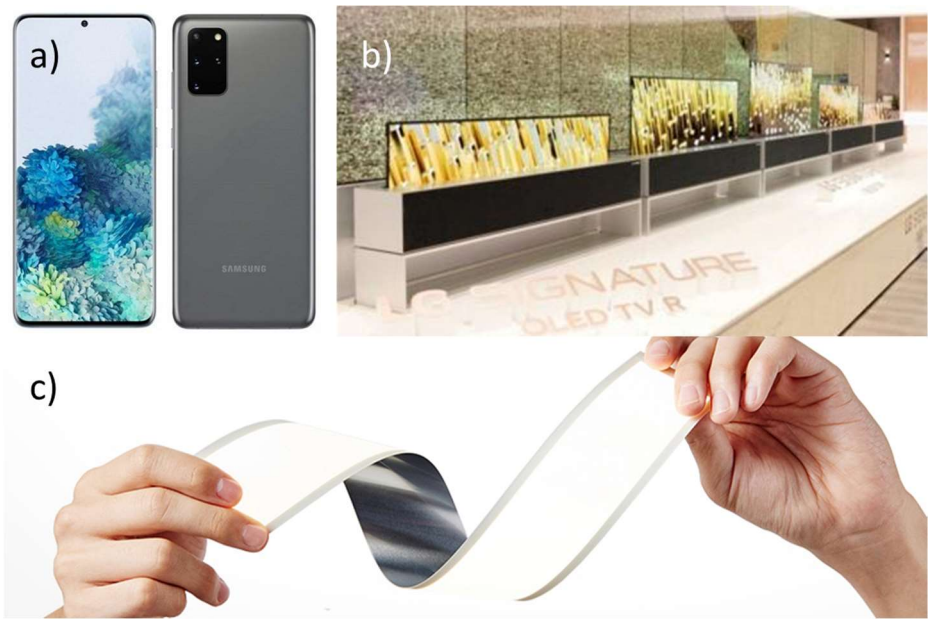

Figure 1.1 a) Samsung Galaxy S20 with OLED display (Samsung electronics 2020). b) LG rollable display (LG Electronics 2020). c) Flexible OLED lighting (LG display 2020)**.**

1.2 Parameters that governs the efficiency of OLEDs

The externa quantum efficiency (EQE) of OLEDs has been expressed as follows:[7–9]

$$EQE = \eta_{\text{int}} \times \eta_{out} = \eta_b \times \eta_{rad} \times q_{eff} \times \eta_{out} \quad (1.1)$$

where η_{int} is the internal quantum efficiency (IQE), and η_{out} is the out-coupling efficiency of OLEDs.

IQE can be expressed as the products of charge balance factor (η_b), radiative exciton ratio (η_{rad}) and effective photoluminescence (PL) quantum yield (q_{eff}). η_b expresses exciton formation efficiency, which means the ratio of generated excions to injected charge carrier. Thus η_b is unity when the same number of injected holes and electrons are recombined in OLEDs. q_{eff} expresses the radiative quantum yield of the emitter in a cavity structure. q_{eff} depends on PLQY (ϕ_{PL}) of emitter and can be reduced when the device is operating due to the exciton quenching by polarons.[10]

η_{rad} is the important factor influencing IQE of OLEDs. According to the spin-statistics, injected electrons and holes in OLEDs generate singlet and triplet excited states with a ratio of 1:3. The first-generation OLEDs were based on fluorescent emitters. Fluorescent emitters only utilize the singlet excited

states for the light-emission process and the triplet excited states decay as non-radiative process. Therefore, maximum IQE of conventional fluorescent OLEDs was limited to 25%. If the 75% of triplet excitons are harvested to the radiative process, the efficiency of OLEDs can be improves significantly, so many researchers have developed the methods to utilize 75% of triplet excited states in light-emitting process. Details about triplet harvesting methods will be covered in Chapter 1.3.

Because q_{eff} and η_b can be improved with optimized device structures, the structure of OLEDs have been changed to achieve the high efficiency. When the distance between emitters is close enough for energy transfer, q_{eff} is reduced because of the self-quenching. To reduce self-quenching of emitter, host-dopant system was introduced.[11] An EML structure in which a small amount of emitter was doped into the host material was devised, which reduced the self-quenching due to the sufficient distance between the emitters. For the high η_b values, charge imbalance have to be minimized. At low current density, low η_b value can be explained by the difference in energy barriers for holes and electrons to be injected into the device. Therefore the efficient charge injection from electrodes is required. Many materials and technics for efficient charge injection to the OLEDs have been developed.[12] One of the efficient methods to inject charge is electrical doping.[13,14] Some transition metal oxides and alkali metal carbonates have been

used as *p*-type and *n*-type dopants for hole injection and electron injection, respectively.[15–18] Injected charges have to recombine in EML for high efficiency because emitter is located in EML. To confine injected charges in EML, charge blocking layer have been adopted and the efficiency of OLEDs was enhanced.[19] Also, mixed-host and bipolar host materials have been developed for balanced charge transport in EML.[20,21]

η_{out} depends on the emitting dipole orientation(Θ) of emitters in EML and this value can be enhanced when the emitters have horizontal dipole orientation.[22–24] There was a report that maximum EQE of green OLEDs can increase around 26% to 46% without any light extraction structure when the Θ value of emitter, which has photoluminescence (PL) quantum yield (PLQY) of 1, changes from 0.67 (random orientation) to 1 (fully horizontal oriented).[9] In addition, OLEDs with maximum EQE over 40% can be realized in red and blue region when using the emitter has ϕ_{PL} =1 and Θ =1.[25,26] Many researches to achieve high Θ have been conducted and some of them successfully increased the η_{out} of OLEDs by developing efficient and horizontally oriented emitters.[27–29] Meanwhile, when the organic materials, which have low refractive indices, are used as transporting or host layer the η_{out} can be further increased due to the reduced substrate and wave-guided modes of OLEDs.[30,31] If the organic materials constituting OLEDs have a low refractive index of 1.5, theoretically achievable maximum EQE is over 60%.[32] Several efforts have been performed to increase the η_{out} through the development of organic

materials with low refractive indices or design of device structure considering the refractive indices of materials.[32,33]

1.3 Strategies for harvesting triplet excitons

The η_{rad} is one of the factors that can affect the efficiency of OLEDs, as described above. When only singlet excitons participate in radiative emission, η_{rad} is 25% due to the spin statics. For higher efficiency of the OLEDs, non-radiative triplet exciton should be harvested to emissive radiation. A lot of efforts have been made to enhance η_{rad}.

Triplet-tripelt annihilation (TTA) by fluorescent molecules such as rubrene or anthracene and their derivatives is used to harvest the electrically generated triplet excitons, thereby the IQE of such OLEDs may exceed the spin statistical limit of 25%.[34] The anthracene derivatives are usually used in blue emitting OLEDs and the TTA process can be expressed as in Figure 1.2. The annihilation of two triplet excitons leads to an intermediate state according to the spin statics (one singlet state, three triplet states and five quintet states). The lowest quintet state of anthracene monomer is not known but may be sufficiently high as to be inaccessible from the quintet intermediate state.[35] Then quintet state intermediate states are fully dissociated to two triplet excitons and quintet intermediate state do not affect to TTA process.

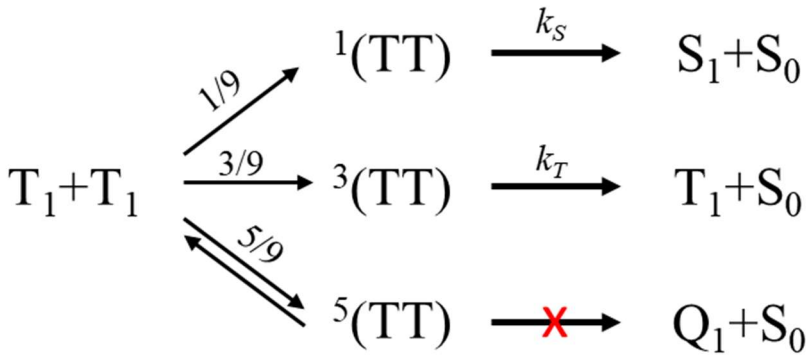

Figure 1.2 Triplet annihilation process (quintet state intermediate pair is fully dissociated to the two triplet excitons because of the higher quintet state energy than $2T_1$)

Now we can consider eight triplet excitons which generates one singlet state pair and three triplet state pair. Each pair will decay to the lowest singlet and triplet state. As a consequence, five triplet excitons give one singlet exciton and the triplet harvesting ratio through TTA process is 20%. However, when the energy state satisfies $T_2>2T_1$, triplet intermediate pair will dissociate to two triplet excitons.[36] In this case the maximum triplet harvesting efficiency from the TTA process is 50%, thus 37.5% of singlet excitons can be converted from the electrically generated triplet excitons. The theoretically achievable IQE of the OLEDs utilizing TTA process is considered to be 62.5%.[36,37]

In the late of 1990s, M. Baldo et al. reported novel emitters that contains heavy metal atom.[38] Because the heavy metal induced large spin-orbit coupling (SOC), fast intersystem crossing (ISC) from singlet state to triplet state as well as from triplet state to ground state is possible. Thus, the emissive transition from triplet state to ground state, which is called phosphorescent emission, enables η_{rad} of 100%. The OLEDs utilizing phosphorescent emtters, which are called phOLEDs, can achieve maximum IQE of 100% theoretically, significantly enhancing EQE of OLEDs.[39–41] A lot of efficient red, green and blue emitting phosphorescent emitters have been developed and most of them contains iridium (Ir) or platinum (Pt) atoms.[42–44]

Charge transfer (CT) type emitters can also give 100% of IQE by harvesting triplet excitons. CT type emitters have separated highet occupied molecular orbital (HOMO) and lowest occupied molecular orbital (LUMO).

The separated HOMO and LUMO minimizes electron exchange energy, resulting in small singlet-triplet energy level difference (ΔE_{ST}).[45] Because of the small ΔE_{ST}, reverse intersystem crossing (RISC) process from triplet state to singlet state can be increased. Non-radiative triplet excitons can be harvested to the radiative singlet state by efficient RISC process. The excited state CT between two different molecules can be occurred and this molecular pair is called excited state charge transfer complex (exciplex).[46,47] Intramolecular CT is also possible and the molecule exhibiting intramolecular CT is called thermally activated delayed fluorescent (TADF) material.[48–50] Despite the emission is released from the singlet excitons, both exciplex and TADF emitters can theoretically achieve the maximum IQE of 100% *via* RISC process. Because those CT type emitters do not contain heavy metal aoms, which are calssified as rare erth metal atoms, the cost for fabricating OLEDs can be saved as the CT type emitters are utilized.

The η_{rad} can be enhanced with conventional fluorescent emitters, which do not harvest triplet exciton. When the emitter is introduced to the triplet harvesting material, energy transfer from the triplet harvesting material to emitter, following triplet exciton harvesting process.[51–53] In this case, the light is released from the singlet exciton of conventionalf fluorescent, which have fast radiative decay lifetime (ns scale). Therefore, excitons can be cosumed very quickly and the exciton density in emitting layer (EL) can be lowered. As a results, the exciton-exciton quenching process, which brings about efficiency

roll-off and degradation of OLEDs, can be reduced.

Schematic illustration of triplet harvesting OLEDs are presented in Figure 1.3

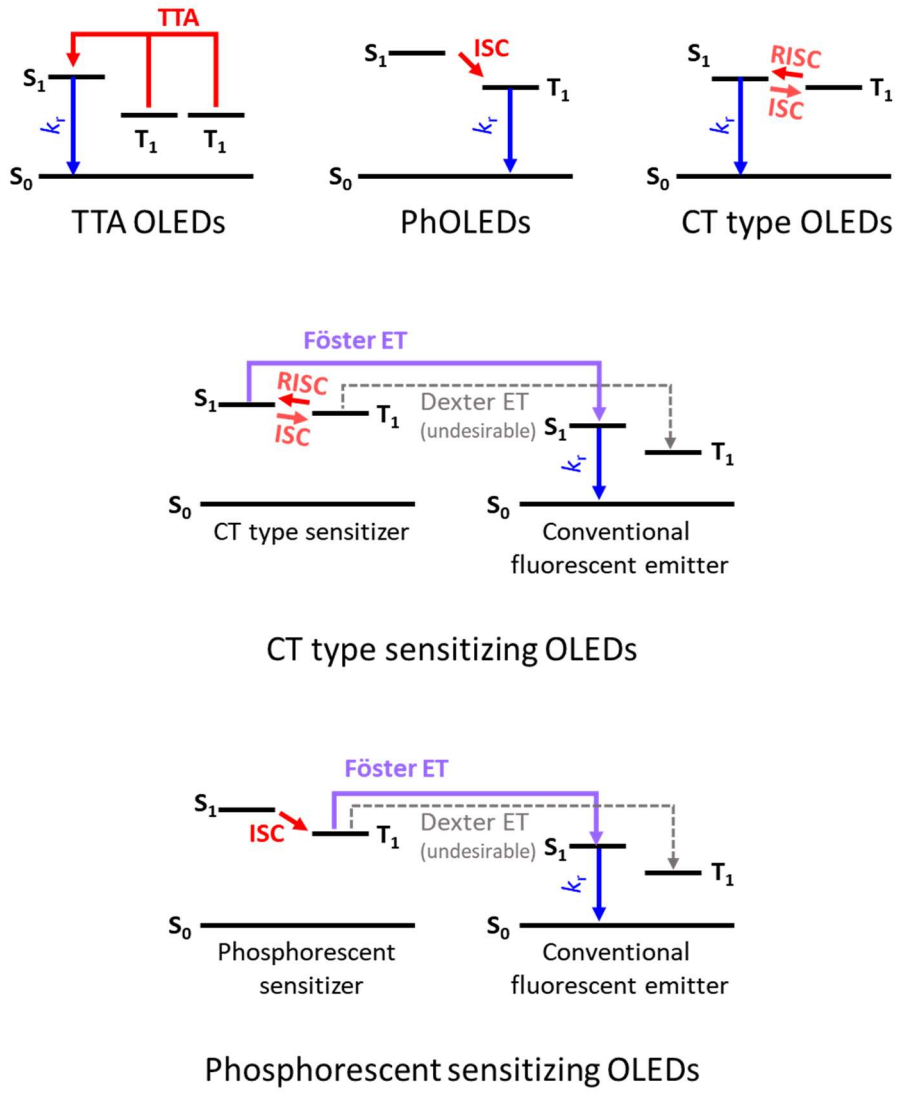

Figure 1.3 Schematic illustration for the methods to harvest triplet excitons in OLEDs.

1.4 Challenges for realizing high-efficiency deep blue OLEDs

The three principal color (red, green and blue) is required for the full-color OLED display. Among the three colors, blue-light-emitting materials and devices still need to be improved. The EQE of blue emitting devices is still inferior to that of the red and green devices and color purity also should be improved for large color gamut. Also it is well known that the power consumption of a full-color OLED is highly dependent upon the color purity of blue emission.[54] The color purity can be expressed with a Commission Internationale de l'Éclairage (CIE) coordinates and the smaller CIE *y*-value, the lower the power consumption (lm W^{-1}) of the device.

The main obstacle for the realization of high-efficiency deep-blue OLEDs is that only few materials can meet the requirements of deep blue emission, narrow FWHM, horizontally oriented and high PLQY properties. Therefore, more studies on the material properties should be conducted.

1.5 Outline of the thesis

In this thesis, deep-blue OLEDs utilizing various triplet harvesting methods will be presented. Color purity and efficiency of phOLEDs were improved using newly developed high T_1 exciplex system host. TADF OLEDs were developed that emits deep-blue using a TADF emitter with a narrow FWHM and a horizontally oriented emitting dipole moment. Also, highly bright and efficient blue fluorescent OLEDs were developed based on the understanding on the TTA process.

In chapter 2, it was verified the efficient blue phOLED can be fabricated using a deep-blue exciplex host. Using carbazole based donor and phosphine oxide based acceptor the deep-blue exciplex system was developed and used as a host system. The blue PhOLEDs doped with FCNIr achieved a turn-on voltage of 2.9 eV, a maximum EQE of 24% with CIE coordinates of (0.15, 0.21), and an EQE of 19% with CIE coordinates of (0.15, 0.19). Moreover, the exciplex host devices showed much better performances in EQE, power efficiency (PE), driving voltage, and operational lifetime than the single host devices.

In chapter 3, the analysis on the deep-blue TADF emitter was conducted. The emitters have long molecular structure along the direction of transition dipole moment and contain oxygen-bridged acceptor unit, which is highly rigid. A deep-blue OLED was fabricated using the TADF emitter, and it achieved EQE of 29.3% and CIE coordinate of (0.142, 0.090). The RISC mechanism was

analyzed using the electronic structures of emitter.

In chapter 4, TTA mechanism of anthracene based materials is analyzed. The three new anthracene based materials were presented, which were used as efficiency enhancement layer in blue fluorescent OLEDs. The charge mobility of anthracene based materials was a key factor affecting triplet harvesting efficiency by TTA process. Insertion of a very thin EEL (3 nm) between the blue EML and the electron transport layer enhanced the EQE of the blue device by 44% compared to the device without the EEL, resulting in an EQE of 7.9% and a current efficiency (CE) of 9.0 cd A^{-1} at 1000 cd m^{-2}; the CIE coordinates of the emitting color were (0.13, 0.14). Interestingly, one materials showed delayed emission ratio above 40%, which is higher value than spin statistical limit of TTA process. Electronic structure and transition orbital analysis of the material was conducted. As a consequence, deep-blue fluorescent OLEDs with better characteristics in terms of efficiency roll-off property and color purity were developed. Deep-blue fluorescent OLED exhibited a maximum EQE of 8.8% and a maximum CE of 6.3 cd A^{-1}, CIE coordinates of (0.136, 0.079). The maximum efficiencies were obtained at 5,000 cd m^{-2}.

Chapter 2. An Exciplex Host for Deep-Blue Phosphorescent Organic Light-Emitting Diodes

2.1 Introduction

The efficiency of OLEDs has improved significantly in recent years, largely because of improved device structures and new emitting materials with high PLQYs and horizontal emitting dipoles ratios (Θ).[25,48,55–62] Device structures utilizing a mixed host forming an excited state charge transfer complex (exciplex) are particularly interesting for their high efficiencies approaching the theoretical limit, as well as low driving voltage and low-efficiency roll-off.[32,63] A large number of high-efficiency OLEDs based on exciplex hosts have been reported using phosphorescent dyes, TADF dyes, and conventional fluorescent dyes for sky blue, green, yellow, and red colors.[51,64–70] However, there have been rare reports of efficient OLEDs based on exciplex hosts for deep blue, that is, a CIE *y*-coordinate approaching or less than 0.2. An efficient exciplex host for an OLED requires a hole-transporting material (HTM) and an electron-transporting material (ETM), where the triplet (T_1) energies of the constituent materials and the exciplex should be greater than the T_1 energy of the emitting dopants.[71] It is difficult to find host materials that satisfy these requirements for deep blue emission. Recently, exciplex system for deep blue phosphorescent OLEDs (phOLEDs) was reported.[72] However, the efficiency is still much lower than red, green and sky blue phOLEDs.

Here, we report an exciplex-forming mixed host composed of N,N′-dicarbazolyl-3,5-benzene (mCP) as the HTM and 2,4-bis(4-(diphenyl-phosphoryl)phenyl)pyridine (BM-A10) as the ETM. Both molecules have T_1 energies greater than 2.8 eV.[73,74] The mixed layer forms an exciplex with an emission energy of 3.0 eV. Because the exciplex system has a small singlet−triplet energy difference (ΔE_{ST}), it satisfies the requirements for efficient blue PhOLED for tris((3,5-difluoro-4-cyanophenyl)-pyridine) iridium (FCNIr), where the T_1 energy is 2.73 eV with the peak wavelength of 455 nm. The fabricated devices exhibited a maximum EQE of 24% with CIE coordinates of (0.15, 0.21), and a turn-on voltage of 2.9 V. The efficiency is much higher than the recently reported OLEDs based on the different exciplex host from ours.

2.2 Experimental

Fabrication and PL Measurement of Organic Thin Films. Organic thin films were fabricated by thermal evaporation onto clean quartz substrates in a vacuum chamber (base pressure < 5×10^{-7} Torr). PL spectra were measured using a continuous-wave Xe lamp (300 nm) at room temperature. Transient PL was measured using an N_2 laser (337 nm, Usho Optical Systems Co.) and a streak camera (Hamamatsu, C10627).

Fabrication of Hole-Only Devices (HOD), Electron-Only Devices (EOD), and Blue PhOLEDs. 150 nm-thick ITO substrates were used for the HOD and EOD devices, and 70 nm-thick ITO substrates were used for the PhOLEDs. These substrates were cleaned using acetone and boiling isopropyl alcohol. After they were dried in an oven at 80 °C, the ITO substrates were exposed to ultraviolet light and ozone. The organic layers and Al electrodes were then thermally evaporated in a vacuum chamber (base pressure <5×10^{-7} Torr). All devices were encapsulated in a glovebox following evaporation.

Measurement of Angle-Dependent PL and EL. Angle dependent *p*-polarized PL spectra were measured to determine the fraction of Θ, which was calculated using the classical dipole model. The emission patterns of the PhOLEDs were measured using an angle dependent EL setup. The experimental setup contained a motorized rotation stage, a programmable source meter (Keithley 2400), and a fiber optic spectrometer (Ocean Optics S2000).

Device Characterization. $J-V-L$ and $J-V$ characteristics were measured using a programmable source meter (Keithley 2400), and EL spectra were measured in the normal direction using spectrophotometer PR650 (Photo Research).

2.3 Result and discussion

Figure 2.1a and b show the chemical structures and the highest occupied molecular orbital (HOMO) levels and the lowest unoccupied molecular orbital (LUMO) levels of mCP, BMA10, and FCNIr, respectively.[57,66,73,74] Figure 2.1c shows the absorbance spectra of FCNIr and normalized photoluminescence (PL) spectra of mCP, BM-A10, an mCP:BM-A10 mixed layer (1:1 molar ratio), and mCP:BM-A10:FCNIr. Exciplex formation in the mCP:BM-A10 mixed layer is evidenced by the featureless broad emission spectrum, which is red-shifted from the constituent materials. The emission energy was 3.0 eV, which is close to the energy difference (2.9 eV) between the LUMO level of BM-A10 and the HOMO level of mCP. One must note that the T_1 energy of the exciplex estimated from the peak position of the exciplex emission is higher than those of the constituting molecules of mCP and BM-A10 (Figure 2.1b).[73,74] In other words, the T_1 energy of the exciplex is not confined in this exciplex forming mixed host system as displayed in the bottom of Figure 2.1b. The PLQY of the exciplex emission was 0.17 and that of FCNIr doped in the exciplex was 0.82 as measured using an integrating sphere. The fraction of Θ of FCNIr in the exciplex host was 0.77 (Figure 2.2).

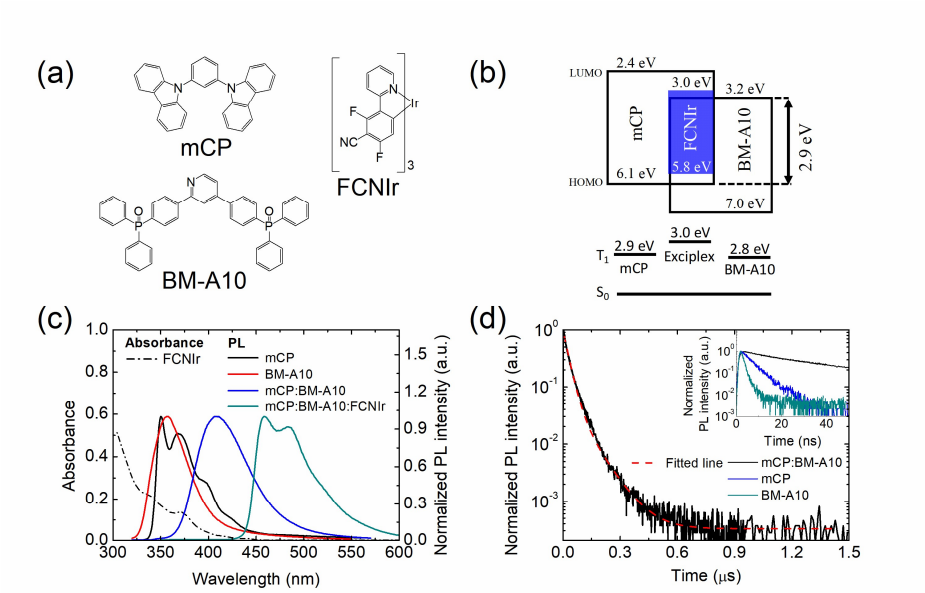

Figure 2.1 The (a) chemical structures and (b) HOMO and LUMO levels of mCP, BM-A10, and FCNIr. T1 energies of mCP, BM-A10, and exciplex are compared in the bottom of panel b. (c) The absorption spectrum of FCNIr (dichloromethane solvent, 5 mol %) and normalized PL spectra of mCP, BM-A10, mCP:BM-A10 (1:1 molar ratio), and mCP:BM-A10:FCNIr films. (d) Transient PL intensity of mCP:BM-A10 film at 300 K. The red dashed lines are the fitting curve using a double exponential function. The inset shows transient PL intensities of mCP, BM-A10, and mCP:BMA10 films up to 50 ns.

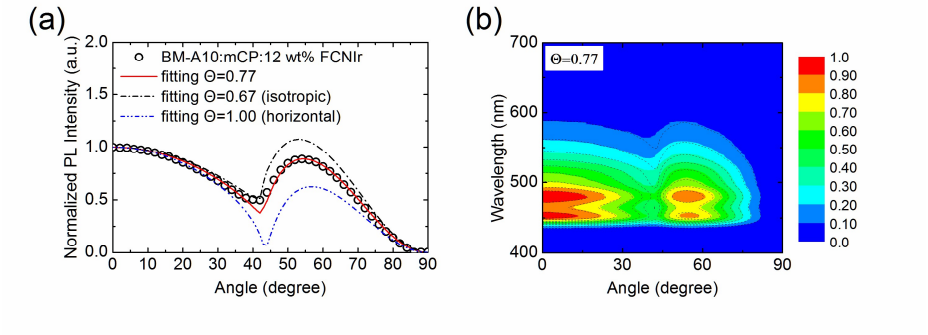

Figure 2.2 (a) Experimentally obtained angle-dependent PL (open circles) and simulated PL (solid line) of a 30-nm-thick BM-A10:mCP:FCNIr (12wt%) film at 455 nm. (b) Simulated (dashed line) and experimentally obtained (contour plot) angle-dependent PL spectra of an mCP:BM-A10:FCNIr (12 wt%) film.

The transient PL of the mCP:BM-A10 film is presented in Figure 2.1d and compared with those of the mCP and BM-A10 films (inset). It was well fitted with a double exponential curve with the excited state lifetimes of 26 and 86 ns, which are much longer than those of mCP or BM-A10. However, the lifetimes are much shorter than those of the delayed components of the normal transient PL of T_1 confined exciplex systems where T_1 of exciplex is lower than host T_1's.[46,64] This relatively short decay time of the mCP:BM-A10 exciplex system is attributed to the weakened T_1 harvesting of the exciplex with reverse intersystem crossing because the T_1 energy of the exciplex is not confined. Also, T_1 fusion can also contribute to the delayed emission as reported by Monkman et al.[75]

Blue PhOLEDs were fabricated via vacuum deposition. The structure of the devices is as follows: indium tin oxide (ITO) (70 nm)/6 wt % ReO_3-doped mCP (30 nm)/mCP (20 nm)/emitting layer (EML, 30 nm)/BM-A10 (20 nm)/12 wt % Rb_2CO_3 doped BM-A10 (20 nm)/Al (100 nm). The EML was formed of an mCP:BM-A10 mixed film (1:1 molar ratio) doped with 12 wt % FCNIr. The thicknesses of the ETL (*n*-BM-A10 layer) were optimized in terms of efficiency and emission color. The devices based on the mCP and the BM-A10 single host were also fabricated with the same structure and the same doping concentration for comparison.

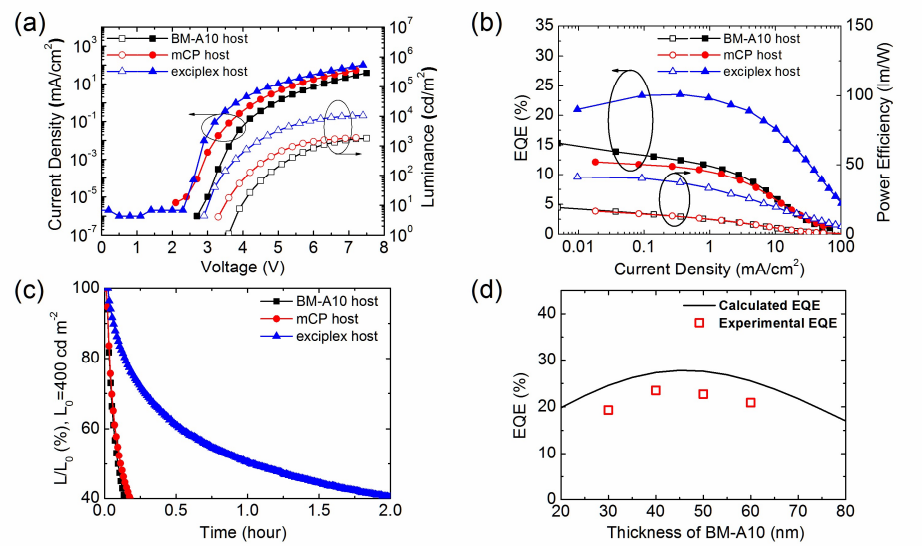

Figure 2.3 (a) Current density−voltage−luminance characteristics of the single host and exciplex host-based devices. (b) The EQEs and PEs of the devices as a function of current density. The devices have the same structure except for the host materials, and the thickness of n-BM-A10 was 20 nm. (c) Relative luminance decay curves of devices at the initial luminance of 400 cd m^{-2}. (d) Calculated and experimentally measured EQEs of the blue PhOLEDs.

The device characteristics are compared in Figure 2.3. The exciplex host devices showed higher EQE, higher PE, lower driving voltage, and lower efficiency roll-off than the single host devices. The device with the exciplex host exhibited a maximum EQE of 24% and maximum power efficiency (PE) of 41 lm W^{-1} with a CIE *y*-coordinate of 0.21. The efficiencies are the highest among the devices reported up to now based on the FCNIr as the dopant to our best knowledge (Table 2.1).[55,56,59,60,72,76–79] The turn-on voltage of the device using the exciplex host was the lowest with 2.9 V among the devices, probably due to the no injection barrier from the hole and electron transporting layers to the EML in the device. The device with a 10 nm-thick *n*-BM-A10 layer exhibited a little deeper blue color with a CIE *y*-coordinate of 0.19 at the expense of efficiencies with a maximum EQE of 19%, a maximum power efficiency (PE) of 33 lm W^{-1} (Figure 2.4). Table 2 lists a summary of the device characteristics. The CIE coordinates of the devices at the current density of 50 mA cm^{-2} are compared with those at the current density of 10 mA cm^{-2} in Table 2. The CIE *y*-coordinates of the OLEDs based on the BM-A10 single host changes by 0.02 (red shift) as the current density increases from 10 to 50 mA cm^{-2}. In contrast, the CIE coordinates of the OLED based on the exciplex host at 50 mA cm^{-2} are similar to those at a current density of 10 mA cm^{-2}, indicating that the recombination zone of the exciplex system does not shift much at high current densities even at 50 mA cm^{-2}. This fact may be related to the lower efficiency roll-off and higher stability.

Table 2.1 Summarized performances of PhOLEDs with CIE *y*–coordinate close to 0.2.

Host	Dopant	V_{on} [V]	EQE [%][a)]	PE [lm W^{-1}][a)]	CIE (*x*, *y*)	Ref.
mCP:BM-A10 (exciplex)	FCNIr	2.9	24 / 23 / 21	41 / 34 / 23	(0.15, 0.21)	This work
t-DCDPA:DBFTrz (exciplex)	FCNIr	4.0	16.4 / – / 14.7	– / – / –	(0.14, 0.20)	72
pBCb2Cz:TSPO1 (mixed)	tBUCN-FIrmMes	3.0	22.4 / – / 22.4	31.9 / – / 24.9	(0.14, 0.21)	56
TSPO1	*fac*-Ir(pmp)$_3$	4.0	10.1 / – / 9.0	– / – / –	(0.16, 0.09)	55
TSPO1	*mer*-Ir(pmp)$_3$	3.0	14.4 / – / 13.3	– / – / –	(0.16, 0.15)	
BCPO	(fpmi)$_2$Ir(dmpypz)	3.2	17.1 / 16.5 / 15.1	19.8 / 15.0 / 11.2	(0.13, 0.16)	76
PPO2	FCNIr	–	18.4 / 13.5 / –	16.6 /9.1 / –	(0.14, 0.15)	59
PPO21	FCNIr	3.5	20.4 / – / 11.9	26.1 / – / 6.6	(0.14, 0.19)	60
PO9	Ir(dbfmi)	2.6	18.6 / 13.6 / 6.2	35.9 / 19.6 / 6.3	(0.15, 0.19)	77
mCP	(dfpypy)$_2$Ir(dpm)	3.5	20.4 / 20.4 / 18.5	24.7 / – / –	(0.14, 0.18)	78
mCPPO1	FCNIrpic	3.5	25.1 / 24.8 / 23.1	21.5 / 21.5 / 15.1	(0.14, 0.18)	79

[a)] Data were measured at the maximum value/100 cd m^{-2}/1000 cd m^{-2}

Table 2.2 Turn-on voltage, EQE, PE, and CIE coordinates of the PhOLEDs.

Host	THK. of *n*–ETL (nm)	V_{on} (V)	EQE (%)[a)]	PE (lm W^{-1})[a)]	CIE (*x*, *y*)[b)]	CIE (*x*, *y*)[c)]
mCP: BM-A10 exciplex	10	2.9	19 / 19 / 17	33 / 30 / 21	(0.15, 0.19)	(0.15, 0.20)
	20	2.9	24 / 23 / 21	41 / 37 / 26	(0.15, 0.21)	(0.15, 0.21)
	30	2.9	23 / 23 / 21	40 / 35 / 24	(0.15, 0.24)	(0.16, 0.24)
	40	2.9	21 / 21 / 19	37 / 33 / 23	(0.15, 0.27)	(0.16, 0.28)
mCP	20	3.3	12 / 11 / 6	17 / 12 / 5	(0.15, 0.19)	(0.15, 0.19)
BM-A10	20	3.6	15 / 12 / 6	19 / 11 / 4	(0.15, 0.19)	(0.16, 0.21)

[a)] Data were measured at maximum value/100 cd m^{-2}/1000 cd m^{-2}

[b)] Data were measured at a current density of 10 mA cm^{-2} and [c)] at 50 mA cm^{-2}

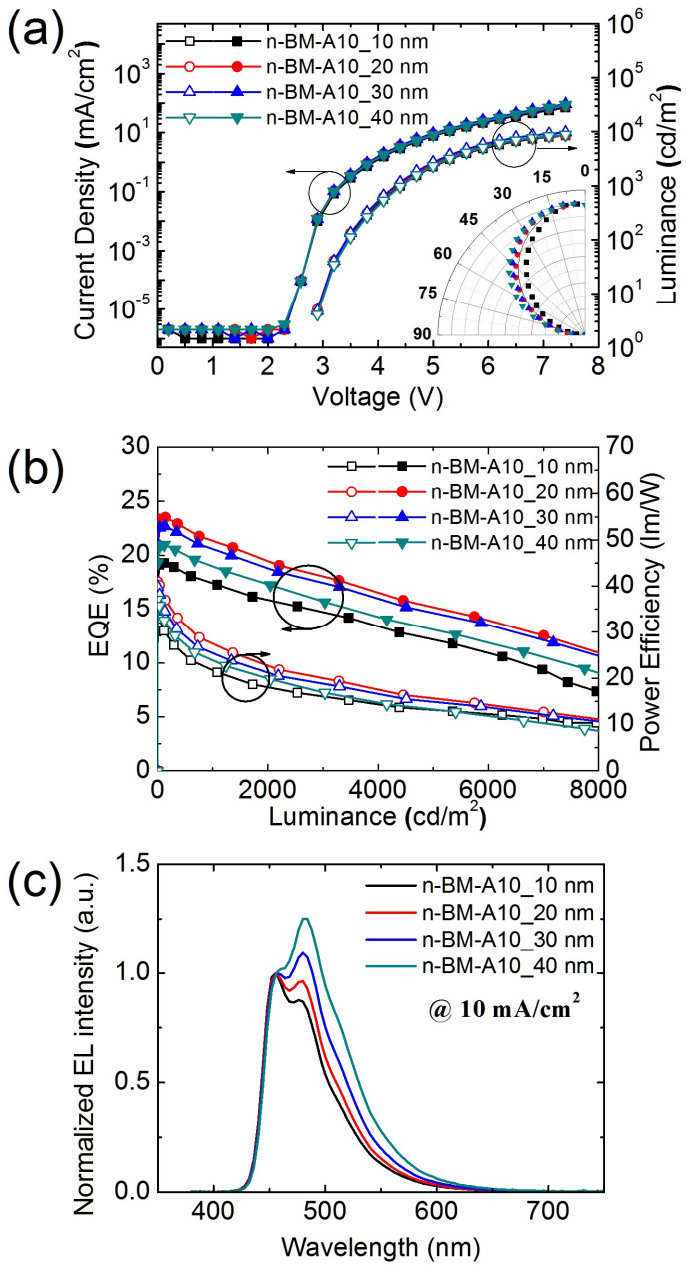

Figure 2.4 (a) *J–V–L* characteristics of the devices. (b) The EQEs and PEs of the devices. (c) Normalized EL spectra of devices with various thicknesses of the BM-A10 layer.

Figure 2.4a shows the *J*–*V*–*L* characteristics of the devices with the different thicknesses of the electron injection layer. The device structure was indium tin oxide (ITO) (70 nm)/6 wt% ReO_3 doped mCP (30 nm)/mCP (20 nm)/emitting layer (EML, 30 nm)/BM-A10 (20 nm)/12 wt% Rb_2CO_3 doped BM-A10 (10, 20, 30, 40 nm)/Al (100 nm). The turn-on voltage was 2.9 V. Efficient hole and electron injection was achieved from the electrodes by *p*– and *n*–doping, respectively, and the simple device structure with few interfaces resulted in the low turn-on voltage. Figure 2.4b shows the Lambertian corrected EQEs and power efficiencies. The emission patterns of the devices were measured via angle-dependent EL, where the Lambertian correction factors were 0.86, 1.04, 1.06, and 1.14 for *n*–doped BM-A10 layers that were 10-, 20-, 30-, and 40-nm-thick, respectively. Lambertian correction was implemented according to the method reported elsewhere.[32] Figure 2.4c shows normalized EL spectra of the devices at a current density of 10 mA cm^{-2}. As the thickness of the *n*–BM-A10 layer increased, the intensity of the vibronic peak of FCNIr increased, which is attributed to the microcavity effect.[80] The CIE *y*–coordinate varied from 0.19 to 0.27 as the thickness of the *n*–BM-10 layer increased from 10 to 40 nm. The device with a 10-nm-thick *n*–BM-A10 layer exhibited a maximum EQE of 19% with a power efficiency (PE) of 33 lm W^{-1}. The device with a 20-nm-thick *n*–BM-A10 layer exhibited a maximum EQE of 24% and maximum PE of 41 lm W^{-1} with a CIE *y*–coordinate of 0.21.

The exciplex host used device showed ten times extended operational lifetime (operational half lifetime LT50 of about 1 hr at 400 cd m^{-2}) compared to other single host devices (a few minutes at the same condition) as shown in Figure 2.3c. The materials are not thermally stable very much with the glass transition temperatures (T_g) of 55.4 and 102 °C for mCP and BM-A10, respectively.[74,81] Therefore, the T_g of the mixed film is expected to be lower than 100 °C. Even with the low thermal stability, the device lifetime extended more than ten times, demonstrating the potential of exciplex system for high efficiency and long lifetime OLEDs. Even though the lifetime is too short to be practical in this system, it can be much longer if more stable donor and acceptor materials for blue exciplex are developed.

The experimentally obtained efficiencies are compared with the theoretically calculated maximum achievable efficiencies under the assumption of no electrical losses in Figure 2.3d. The experimentally measured EQEs are approximately 4% smaller than the simulated data. The reason why this device shows lower efficiency than the theoretically achievable maximum efficiencies in contrast to our previous devices based on exciplex hosts is not clear yet and is under investigation. We speculate that the lower efficiencies may originate from the non-confined exciplex T_1 or charge imbalance. Even though the energy of the host T_1 exciplex can be transferred to the host T_1 and finally to dopant molecules, the energy transfer processes are in competition with the non-radiative decay of the host T_1 excitons, which can reduce the efficiency

from the theoretically achievable ones.[66] Carrier mobility should be investigated for the charge balance factor. The hole-only and electron-only devices were fabricated and the structure of hole-only device was indium tin oxide (ITO) (150 nm)/ReO_3 (1 nm)/mCP or mCP:BM-A10 (100 nm)/ReO_3 (1 nm)/Al (100 nm) and that of electron-only device was ITO (150 nm)/BM-A10 or mCP:BM-A10 (100 nm)/Rb_2CO_3 (1 nm)/Al (100 nm). To provide Ohmic contact, rhenium oxide (ReO_3) and rubidium carbonate (Rb_2CO_3) were used as a hole and electron injection layer, respectively.[12] The $J-V$ characteristics were presented in Figure 2.5a and the space charge limited current (SCLC) regime was analyzed according to the Mott−Gurney theory which is expressed as:

$$J_{\mathrm{SCLC}} = \frac{9}{8}\varepsilon_0\varepsilon_r\mu\frac{V^2}{L^3} \tag{2.1}$$

where J is the current density, ε_0 is the vacuum permittivity, ε_r is the dielectric constant, μ is the carrier mobility, V is the applied voltage, and L is the film thickness.[82] At the low electric field region, $J-V$ characteristics show Ohmic current. As the electric field increases, $J-V$ characteristics show SCLC in the region of 150−700 kV cm^{-1}. The extracted mobilities from equation 2.1 are presented in Figure 2.5b. The mobility values are fitted by the Poole−Frenkel model, which is expressed by

$$\mu = \mu_0 \exp(0.89\beta\sqrt{F}) \tag{2.2}$$

where μ_0 is the zero field carrier mobility, β is the Poole−Frenkel coefficient, and F is the electric field.[83] Almost 2 orders of magnitude difference between electron and hole mobilities in the EML can lead to the charge imbalance or at least shifted exciton profile toward the ETL inducing exciton loss.[84]

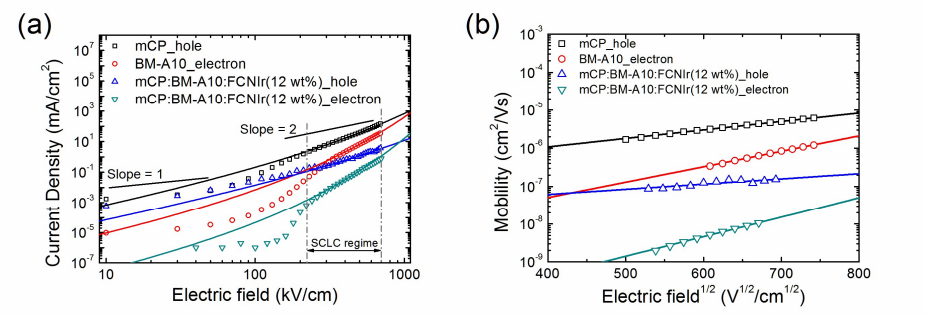

Figure 2.5 (a) Current density−voltage (J−V) characteristics of the hole and the electron only devices. (Open symbols: measured data, solid lines: fitted by space charge limited current (SCLC) model) (b) The hole mobilities of mCP and mCP:BM-A10:FCNIr mixed films, as well as the electron mobilities of BM-A10 and mCP:BM-A10:FCNIr mixed films. (Open symbols: Extracted from the J−V characteristics. Solid lines: Fitted by Poole-Frenkel model.)

2.4 Conclusion

In summary, we have developed an exciplex-forming mixed host for deep-blue PhOLEDs. The exciplex host was composed of mCP as the donor and BM-A10 as the acceptor. The emission energy of the exciplex was 3.0 eV, which is sufficiently large for the use of deep-blue dopants. The blue PhOLEDs doped with FCNIr achieved a turn-on voltage of 2.9 eV, a maximum EQE of 24% with CIE coordinates of (0.15, 0.21), and an EQE of 19% with CIE coordinates of (0.15, 0.19). This represents superior color purity compared to blue FIrpic-based devices, which have CIE coordinates of (0.16, 0.33). The exciplex host devices showed much better performances in EQE, PE, driving voltage, and operational lifetime than the single host devices.

Chapter 3. Highly efficient deep blue OLEDs using TADF emitter with narrow emission spectrum and high horizontal emitting dipole orientation

3.1 Introduction

The development of thermally activated delayed fluorescent (TADF) emitters has greatly improved the efficiency of the fluorescent organic-light emitting diodes (OLEDs).[48–50,85] In contrast to the conventional fluorescent emitters, which can only utilize singlet excitons for radiation, TADF emitters can harvest triplet excitons *via* reverse intersystem crossing (RISC) process and thus enable 100% internal quantum efficiency (IQE). TADF emitters have separated the highest occupied molecular orbital (HOMO) and lowest unoccupied molecular orbital (LUMO) on donor and acceptor units, respectively. The separated HOMO and LUMO minimizes electron exchange energy, resulting in small singlet (S_1)-triplet (T_1) energy level difference (ΔE_{ST}).[45] Because of the separated HOMO and LUMO orbitals, TADF emitters show charge transfer (CT) characteristics in radiative emissions. Therefore, the emission energy of TADF emitters can be adjusted by selecting appropriate donors and acceptors. Various donor and acceptor moieties have been utilized to develop blue TADF emitters. Examples include carbazole[48,86–88], acridine[89–

[91], phenoxazine[49,92], azasiline[93–95], and spiro-flourene[96] moieties for donor units and cyano[97–101], nitrogen heterocycles[50,96,102,103], oxygen heterocycles[104,105], sulfone[49,88,106], methanone[28,107], and boron[108–111] moieties for acceptor units. Even after the large development and despite the importance of deep blue emitters with CIE y<0.1 for full-color display and lighting, there have been few reports on highly efficient deep blue emitting TADF emitters due to broad emission spectra of TADF emitters with the full width at half maximum (FWHM) of 70~80 nm. Lee et al. developed a deep blue emitting TADF emitter with large steric hindrance, which exhibited a narrow emission spectrum with the FWHM of 48nm.[112] However, the EQE was relatively low (14.0%) compared to blue TADF OLEDs.[94–96,108]

Recently, novel TADF emitters with narrow FWHM have been reported. Hatakeyama et al. reported deep blue emitting TADF emitters with narrow FWHM using a nitrogen-bridged boron structure inducing multiple resonance effects.[113,114] Kwon et al. and Adachi et al. reported D-A type deep blue emitting TADF emitters adopting an oxygen-bridged boron acceptor unit, which is rigid and has symmetric structure.[115,116] The FWHM of the emitters was effectively reduced compared to the emitters using a non-rigid and symmetric acceptor unit, indicating that the nitrogen-bridged or oxygen-bridged boron structures are promising acceptor units for deep blue TADF emitters. Nevertheless, the efficient deep blue TADF OLEDs with EQEs near 30% and the CIE *y* coordinate under 0.1 have not been reported yet to our best knowledge. The

selection of a proper donor unit must be important to realize efficient deep blue TADF emitters because the ^{1}CT and ^{3}CT energy levels are influenced by the donor unit as well as the acceptor unit in the emitters.

In this paper, we report two new TADF emitters for efficient deep blue OLEDs by adopting rigid spiro-type donors and oxygen bridged boron acceptors to demonstrate an unprecedented highly efficient deep blue TADF OLED exhibiting EQE of 28.2% with CIE coordinates of (0.142, 0.090). The high color purity with narrow emission and high efficiency is discussed based on the energies level of the donor units, rigidity, and orientation of emitters. The high RISC rate of emitters was discussed based on TD-DFT calculation and experimentally measured energy levels.

3.2 Experimental

Materials preparation. The highly efficient TADF emitters (TDBA-SAF and DBA-SAB) were designed and synthesized in the Department of Chemistry and Research Institute of Natural Science of Gyeongsang National University supervised by professor Yun-Hi Kim.

Fabrication and PL measurement of organic thin film. Organic thin film was deposited by thermal evaporation on cleaned fused silica substrate in vacuum chamber of which the base pressure was under 5×10^{-7} Torr. PL spectra measured using continuous He-Cd laser (325 nm, Kimmon Koha Laser Systems) and Maya200 Pro (Ocean Optics Inc.) detector at room temperature.

Measurement of transient PL. Transient PL was measured using an N_2 laser (337 nm, Usho Optical Systems Co.) as an excitation source and a streak camera (Hamamatsu, C10627) as a detector.

Fabrication of OLEDs. ITO substrates were cleaned by acetone and boiling isopropyl alcohol. After drying in 80℃ oven, organic layers were thermally evaporated in vacuum chamber of which the base pressure was under 5×10^{-7} Torr. After the end of evaporation, all devices were encapsulated in globe box.

Measurement of OLEDs. *J–V* character was measured using Keithley 2400 source meter and EL spectra and intensities were measured using PR650 (Photo Research) in normal direction.

3.3 Result and discussion

The spiroacridine fluorene –based donor was designed to lower the HOMO energy level due to sp^2-hybridized spirofluorene. The spiro-type spiro-biacridine (SAB) and spiro-acridine fluorine (SAF) are expected to have deeper HOMO levels than dimethyl acridine (DMAC) structure with sp^3 hybridized CH_3 groups due to higher electron-withdrawing property originating from the stronger s character. Kwon et al. reported deep blue emitting TADF emitter consisting of *tert*-butyl dioxa boranaphtho anthracene (TDBA) and DMAC TDBA-Ac which exhibits blue emission of 458 nm in toluene.[115] Therefore, the combination of TDBA and SAB or SAF will give deeper blue emission than TDBA-Ac. In addition, the high rigid structure of spiroacridine fluorene can reduce the vibronic transitions to increase the quantum efficiency and to narrow down the emission spectrum. Moreover, the spiro-type donors construct a longer molecular structure, which is advantageous for increasing the horizontal emitting dipole moment ratio (Θ). Based on the consideration, we designed 10-(2,12-di-tert-butyl-5,9-dioxa-13b-boranaphtho[3,2,1-de]anthracen-7-yl)-10H-spiro[acridine-9,9'-fluorene] (TDBA-SAF), a donor (D)-acceptor (A) type emitter, and 10,10'-di(5,9-dioxa-13b-boranaphtho[3,2,1-de]anthracen-7-yl)-10H,10'H-9,9'-spirobi[acridine] (DBA-SAB), an A-D-A type emitter, respectively (Figure 3.1b).

The design concept is supported by the density functional theory (DFT) and time-dependent DFT (TD-DFT) calculations. Optimization of excited state

geometry was performed with Gaussian 09 employing the functional of CAM-B3LYP and M06-2X for ^{1,3}CT and ^{3}LE state, respectively. Natural transition orbitals (NTOs) were performed using optimized excited geometry with Schrodinger's Materials Suite Jaguar, employing ωB97X-D (ω=0.1) for ^{1,3}CT transition and M06-2X for ^{3}LE transition. For performing all geometry optimization and single-point energy calculations, the 6-31G (d,p) basis set was employed. Calculated NTOs corresponding to transition from excited state to ground state are depicted in Figure 3.1. The highest occupied natural transition orbital (HONTO) is mainly located at the spiro-acridine fluorene or spiro-biacridine donor unit and the lowest unoccupied natural transition orbital (LUNTO) is mainly located at the boron acceptor unit as expected. The orbital overlap between HONTO and LUNTO is very small and thus emitters would have CT-type transition with small ΔE_{ST}. In addition, the calculated NTOs corresponding to ^{3}LE transition turn to be located at the boron acceptor unit. The calculated energy levels of the ^{1}CT, ^{3}CT and ^{3}LE states are shown in Figure 3.1. The simulations forecast small ΔE_{ST} of 0.012 eV, as expected. Furthermore, the energy differences between ^{3}LE and ^{1}CT, and ^{3}LE and ^{3}CT are small with 0.093 eV and 0.105 eV for TDBA-SAF and 0.257 eV and 0.269 eV for DBA-SAB, respectively, anticipating fast RISC process in the emitters.

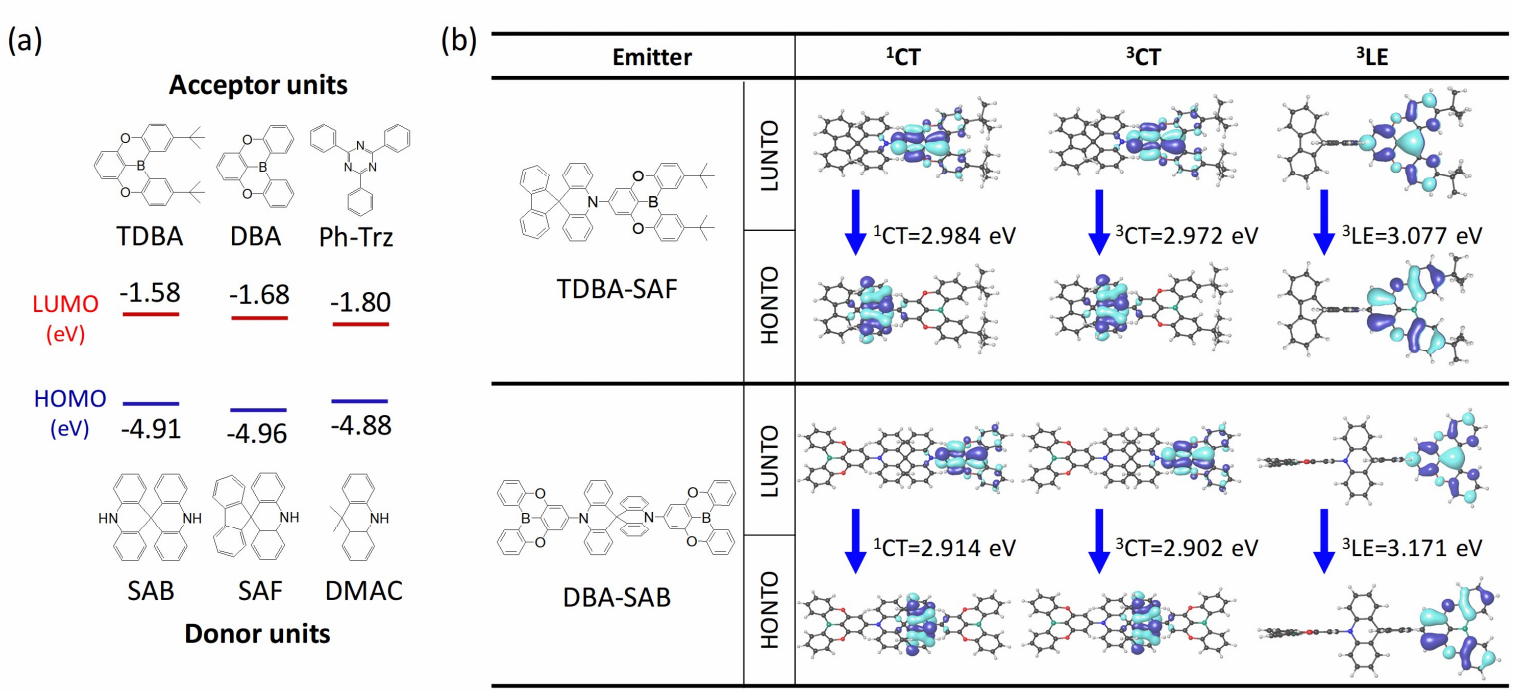

Figure 3.1 (a) Calculated LUMO level of acceptor units and HOMO levels of donor units. (Gaussian 09, B3LYP/6-31G(d)) (b) Calculated natural transition orbitals (NTOs) of TDBA-SAF and DBA-SAB for ^{1,3}CT and ^{3}LE states. NTO calculations were performed using optimized geometry of each excited states. (^{1,3}CT optimization: Gaussian 09, 6-31G (d,p)/CAM-B3LYP, ^{3}LE optimization: Gaussian 09, 6-31G (d,p)/M06-2X, ^{1,3}CT single point energy: Jaguar, 6-31G(d,p)/ωB97X-D (ω=0.1), ^{3}LE single point energy: Jaguar, 6-31G (d,p)/M06-2X)

The photophysical properties measured in solution state are shown in Figure 3.2a. The absorption peaks are located at the wavelengths of 381 nm and 375nm and the emission peaks at 450 nm and 460 nm for TDBA-SAF and for DBA-SAB in toluene, respectively. The Stokes shift is larger in DBA-SAB, which is attributed. TDBA-SAF exhibits smaller Stokes' shift than DBA-SAB because of the restriction of the Frank-Condon factor of the D-A structure than A-D-A structure.[108] The small Stokes' shift is beneficial for the realization of deep blue emission. One can note that the TDBA-SAF emits deeper blue spectrum than the previously reported TDBA-Ac because of the weaker electron donating property of spiro-fluorene substituted acridine than that of dimethyl substituted acridine, as discussed above (Figure 3.3).[95,96,115] The bathochromic shift of the PL spectrum with increasing solvent polarity in Figure 3.2 indicates the CT character of the emission of the molecules. The HOMO level was determined by cyclic voltammetry measurements **(**Figure 3.4**)** and the LUMO level was determined by adding the optical bandgap of materials to the HOMO level. The HOMO/LUMO level of TDBA-SAF and DBA-SAB was -5.5/-2.4 and -5.6/-2.5 eV, respectively.

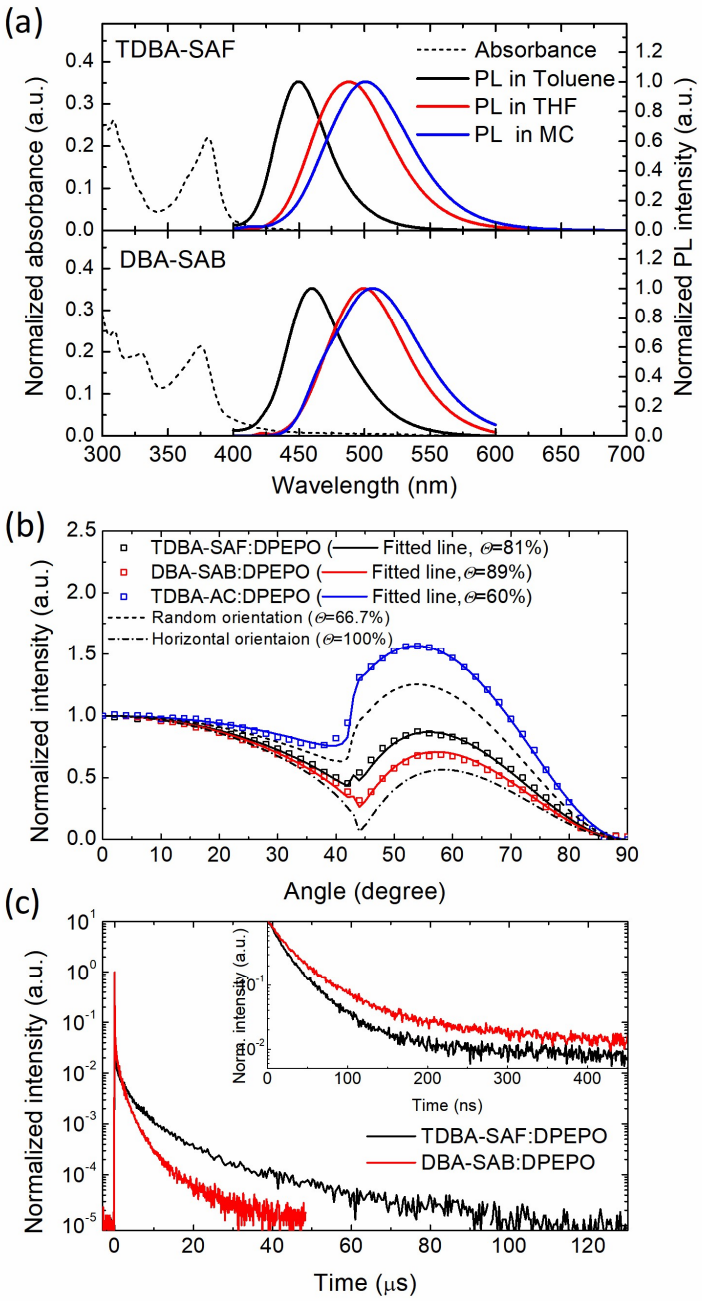

Figure 3.2 (a) The absorbance and photoluminescence (PL) spectra of TDBA-SAF and DBA-SAB in solution state. (b) Angle dependent PL (ADPL) intensity of p-polarized light from emitter doped DPEPO films. (c) Transient PL decay curves of emitter doped DPEPO films (inset: enlarged prompt decay curves).

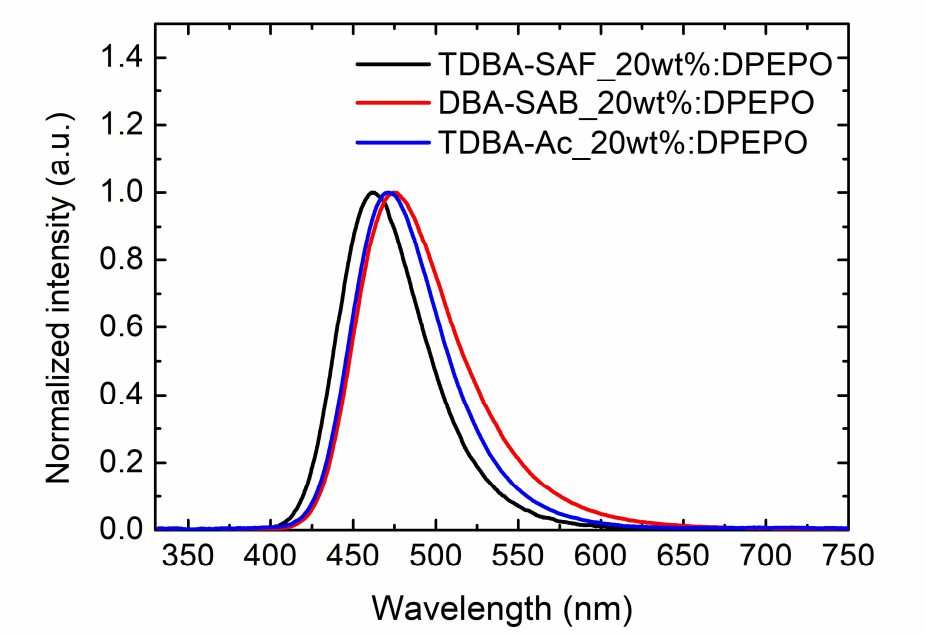

Figure 3.3 The photoluminescence (PL) spectra of TDBA-SAF, DBA-SAB and TDBA-Ac in DPEPO host.

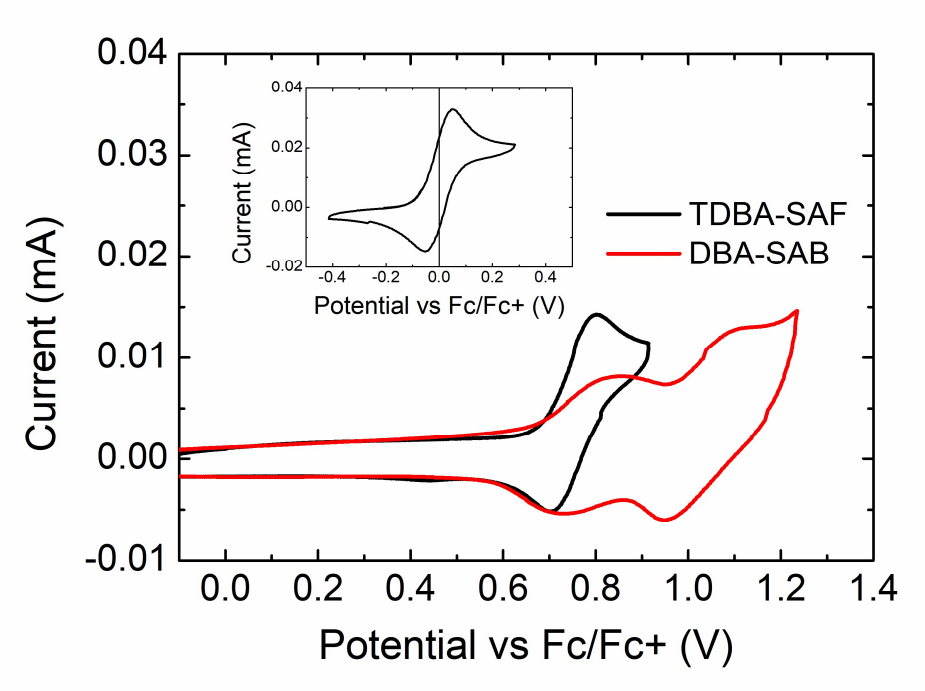

Figure 3.4 Cyclic voltammogram scans of solution, with methylene chloride, 0.1 M tetrabutylammonium hexafluorophosphate ($TBAPF_6$) and 1mM TADF emitter. $TBAPF_6$ was used as the supporting electrolyte.

The photoluminescence quantum yield (PLQY), EDO and transient decay curve measurements were conducted using the doped films in high T_1 host material, diphenyl-4-triphenylsilylphenyl-phosphine oxide (DPEPO). Both emitters have high PLQYs and horizontal EDO ratios (Θs, defined as the average ratio of the horizontal component of emitting dipole moment to the total emitting dipole moment) of 90 and 81% for TDBA-SAF and 87% and 89% for DBA-SAB, respectively, measured from the 20wt% doped films, respectively (Θ: Figure 3.2b). In addition, both emitters have high Θ values above 80%, which are the dramatically enhanced values compared to that of TDBA-Ac. Especially, DBA-SAB showed much higher Θ than TDBA-SAF due to the longer molecular structure with the direction of CT transition, as discussed before. The transient PL decay curves of emitters (Figure 3.2c), the rate constants of the both emitters were analyzed according to the methods described in reference.[49] The calculated rate constants are summarized in Table 3.1. Both TDBA-SAF and DBA-SAB exhibited efficient RISC process with the RISC rates of 2.1×10^6 s^{-1} and 1.9×10^6 s^{-1}, respectively. These RISC rates are similar to that of recently reported TADF emitters using oxygen-bridged boron acceptor, but larger than previously reported blue TADF emitters.[92,100,115,116]

Table 3.1 Photophysical properties and rate constants of TDBA-SAF and DBA-SAB.

	PLQY (%)	$\boldsymbol{\Theta}$ **(%)**	$\boldsymbol{\Phi_{PF}}$ **(%)**	$\boldsymbol{\Phi_{TADF}}$ **(%)**	$\boldsymbol{\tau_p}$ **(ns)**	$\boldsymbol{\tau_d}$ **(µs)**	$\boldsymbol{k_r}$ **(x10^7)**	$\boldsymbol{k_{nr}}$ **(x10^6)**	$\boldsymbol{k_{ISC}}$ **(x10^7)**	$\boldsymbol{k_{RISC}}$ **(x10^6)**	$\boldsymbol{k_{nr}^T}$ **(x10^5)**	$\boldsymbol{\Phi_{RISC}}$ **(%)**	$\boldsymbol{\Delta E_{ST}}$ **(eV)**
TDBA-SAF	90	81	32	58	30.6	1.34	1.0	1.2	2.1	2.1	0.7	96.6	0.11
DBA-SAB	87	89	47	40	45.1	0.96	1.0	1.6	1.0	1.9	1.4	93.4	0.07

In order to further understand the high RISC rates of the emitters, time-resolved PL spectra was taken and the energy level of ^{1,3}CT state was obtained from the onset of the emission spectra (Figure 3.5). At room temperature, the spectral shifts from prompt (~5ns) to delayed emissions (0.5~1.5μs) was 12 nm, which attributed to the narrow conformational distribution or suppressed structural relaxation of TADF emitters.[94] The singlet-triplet level energy difference (ΔE_{ST}) of the emitters was acquired from the onset of fluorescence and phosphorescence spectra measure at 100K. Both emitters exhibited featureless phosphorescence emission spectra along with the fluorescence emission, ensuring that triplet emission has also the CT character. The measured energies of the ^{1}CT state, ^{3}CT state and the resulting ΔE_{ST} are 2.99 eV, 2.88 eV, and 0.11 eV for TDBA-SAF and 2.94 eV, 2.85eV, and 0.09 eV for DBA-SAB, respectively. The experimental values matched well with the calculated values, suggesting that the TD-DFT was conducted with appropriate basis sets and functionals. Despite the larger $\Delta E_{ST,}$ TDBA-SAF exhibited larger RISC rate constant than DBA-SAB. As Monkman et al. have analyzed, ^{3}LE state can participate in RISC process between ^{1}CT and ^{3}CT states and effectively enhances the RISC rate because larger spin-orbit coupling matrix elements between ^{1}CT and ^{3}LE states than ^{1}CT and ^{3}CT states.[117] Because the TD-DFT calculation results indicated that the ^{3}LE state of the emitters is located at boron acceptor unit, the T_1 level of the boron acceptors was measured. The measured T_1 level was 3.01 eV for TDBA and 3.03 eV for DBA. The *tert*-butyl substituted TDBA exhibited slightly lower T_1 level than DBA. The energy

levels of ^{1,3}CT and ^{3}LE states of each emitters are presented in Figure 3.5c. As shown in Figure 3.5c, TDBA-SAF have smaller energy level difference between ^{3}CT and ^{3}LE states, which enables more effective vibronic coupling between the states. As a result, TDBA-SAF shows larger RISC rate than DBA-SAB despite the larger $\Delta E_{ST.}$

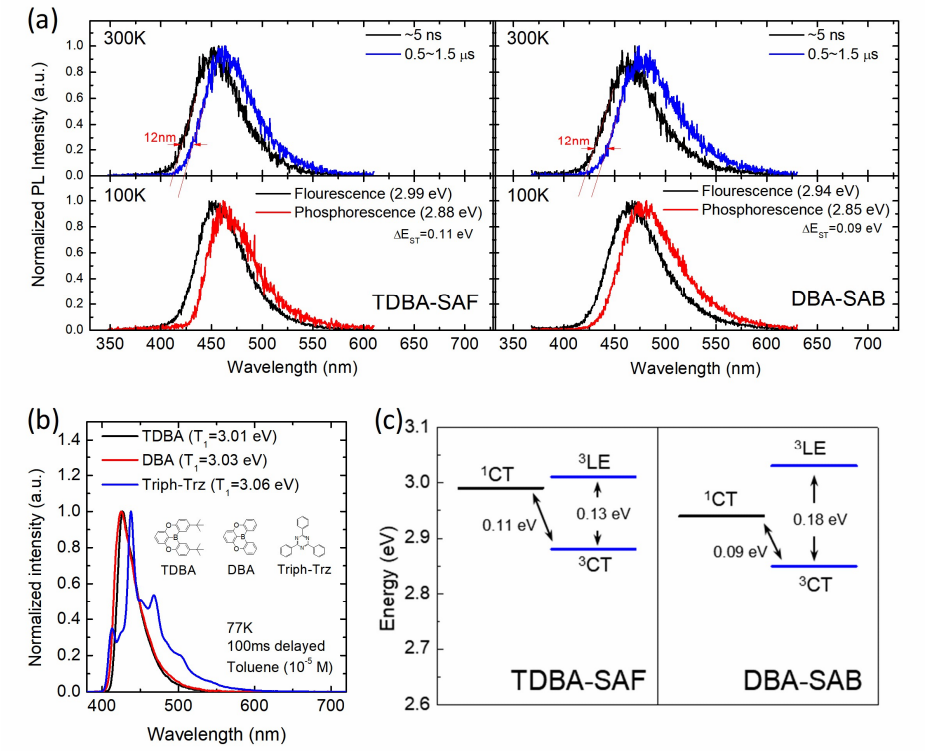

Figure 3.5 (a) Prompt and delayed emission spectra at 300K (upper) and 100K (lower) of TDBA-SAF and DBA-SAB. (b) Phosphorescent emission spectra of TDBA, DBA, Triph-Trz. (c) ^{1}CT, ^{3}CT and ^{3}LE state energy levels of TDBA-SAF and DBA-SAB.

To evaluate the TADF emitters in EL devices, we fabricated the devices which structure was as follows: ITO (70nm) / MoO_3 (1nm) / 1,1-bis((di-4-tolylamino)phenyl)cyclohexane (TAPC) (40nm) / tris(4-carbazoyl-9-ylphenyl)amine (TCTA) (10nm) / N,N′-dicarbazolyl-3,5-benzene (mCP) (10nm) / DPEPO:20wt% TADF emitter (25nm) / DPEPO (5nm) / Bathophenanthroline (Bphen) (30nm) / LiF (0.7nm) / Al (100nm). DPEPO was used as host and exciton blocking material (in ET side) to prevent exciton quenching because of their high T_1 (3.0 eV) level. Likewise mCP was used as exciton blocking layer in HT side because of their moderate hole transporting property and high T_1 (2.9 eV) level. Chemical structures and HOMO, LUMO energy levels of molecules used in device fabrication are presented in Figure 4a.

The current density–voltage–luminance (*J–V–L*) characteristics, EQE plots and EL emission spectra of devices are presented in Figure 3.6. The devices showed turn-on voltage of 3.6 V, which is lower than bandgap of DPEPO and similar to HOMO LUMO energy level difference between mCP and DPEPO. Therefore, it can be inferred that hole is injected into the EML through the HOMO level of emitter. The maximum EQEs of the devices with TDBA-SAF and DBA-SAB were 29.3% and 25.7%, respectively. The measured EQE values agreed well with the calculated EQE values (Figure 3.7). DBA-SAB used device showed better roll-off property in high current density which is attributed to shorter exciton decay lifetime than TDBA-SAF. The peak

position of EL emission spectra were 456nm for TDBA-SAF used device and 472nm for DBA-SAB used device. Both devices exhibited narrow emission spectrum with FWHM of 55 nm and 62 nm. This narrow emission spectrum is due to the rigidity of boron acceptor unit. This rigid acceptor unit have less vibronic transition compared to the phenyl-triazine unit (Figure 3.5b). Due to the narrow full-width at half-maximum (FWHM) of emission spectrum, CIE 1931 color coordination of (0.142, 0.090) and (0.144, 0.212) were achieved with TDBA-SAF and DBA-SAB. The inserted photos in Figure 3.6d show EL emission of each device at 300 cd m^{-2}. The characteristics of the devices are summarized in Table 3.2 and compared with previously reported blue TADF devices (CIE $y \leq 0.1$ and $EQE_{max} > 5\%$). The device fabricated with TDBA-SAF performed better than previously reported deep-blue TADF devices.

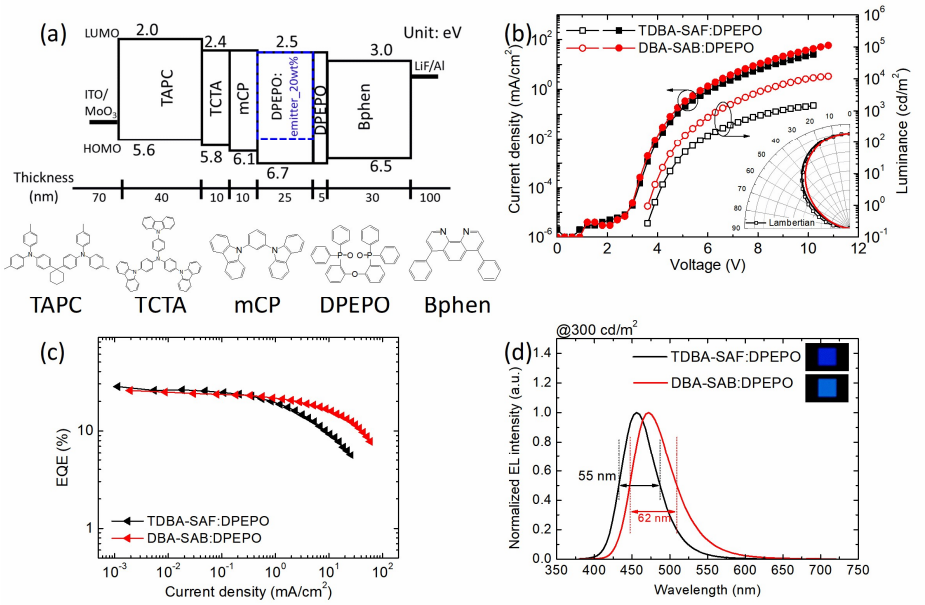

Figure 3.6 (a) Devices structure of OLEDs and molecular structures used in the device. (b) *J–V–L* characteristics (c) EQE plots and (d) EL emission spectra of devices. (inset in (b): simulated Lambertian emission patterns.)

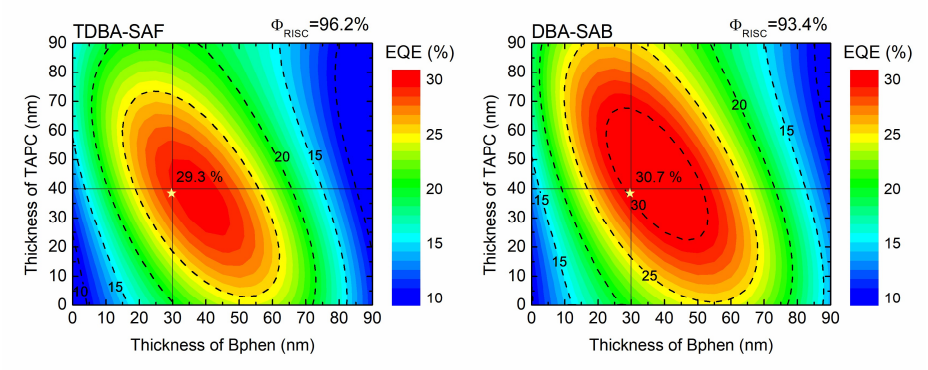

Figure 3.7 Theoretically achievable EQE of devices as the thickness of TAPC and Bphen changes.

Table 3.2 Summarized performances of OLEDs using TDBA-SAF and DBA-SAB and summary of reported deep-blue TADF OLED devices with CIE y ≤ 0.1 and EQE_{max} > 5%.

Emitter	PLQY [%]	λ_{max} [nm]	EQE_{max} [%]			CE_{max} [cd/A]			PE_{max} [lm/W]			CIE (x, y)	Ref.
			Max	100 cd m^{-2}	1000 cd m^{-2}	Max	100 cd m^{-2}	1000 cd m^{-2}	Max	100 cd m^{-2}	1000 cd m^{-2}		
TDBA-SAF	90	456	28.2	21.3	8.6	23.7	16.8	7.1	19.9	9.5	2.4	(0.142, 0.090)	This work
DBA-SAB	87	472	25.7	23.2	20.2	43.8	39.1	33.1	35.1	24.6	15.1	(0.144, 0.212)	This work
4	83	455	16.1	12.3	-	16.0	12.3	-	-	-	-	(0.141, 0.099)	[111]
Cz-TRZ3	92	450	19.2	-	-	-	-	-	-	-	-	(0.148, 0.098)	[103]
Cz-TRZ4	85	450	18.3	-	-	-	-	-	-	-	-	(0.150, 0.097)	[103]
ICzAc	95	454	13.7	-	-	11.8	-	-	10.6	-	-	(0.15, 0.09)	[91]
DABNA-1	88	464	13.5	-	-	10.6	-	-	8.3	-	-	(0.13, 0.09)	[113]
PXB-mIC	63	450	12.5	-	5.2	8.6	-	3.6	-	-	-	(0.15, 0.08)	[110]
CNICCz	46	449	12.4	6.4	-	9.9	4.6	-	8.8	2.6	-	(0.15, 0.08)	[87]
tDCz-DPS	80	423	9.9	-	-	-	-	-	-	-	-	(0.15, 0.07)	[88]
DCzBN2	66	417	7.7	-	-	3.9	-	-	2.7	-	-	(0.15, 0.07)	[100]
DCzBN3	76	414	10.3	5.4	-	5.1	-	-	3.5	-	-	(0.16, 0.06)	[100]
TDBA-AC	93	458	21.5	-	9.69	8.51	-	3.8	7.64	-	1.6	(0.15, 0.06)	[115]

3.4 Conclusion

In conclusion, deep blue and blue emitting TADF emitters, TDBA-SAF and DBA-SAB, were newly developed by incorporating spiro-biacridine or spiro-acridine fluorene donor units and oxygen-bridged borane acceptor unit by prof. Yun-Hi Kim. The deeper HOMO levels of the acceptor unit resulted in (deep) blue emissions. The donor and acceptor units are rigid so that the emission spectra are narrow with the FWHM less than 62 nm. It turns out that ΔE_{ST}'s of the molecules are smaller than 0.11 eV, and the triplet LE state of the molecules are located in the borane unit with a little higher energy than ^{1}CT and ^{3}CT whose energy difference is smaller than 0.18 eV, resulting in high RISC rate and high PLQYs approaching 90%. In addition, the large aspect ratio of the molecules gives rise to high Θ above 80% (81% for TDBA-SAF and 89% for DBA-SAB). All the combined effects bring out a deep blue OLED using TDBA-SAF as an emitter with the EQE of 28.2%, CIE coordinate of (0.142, 0.090) and low efficiency roll-off.

Chapter 4. Enhanced Triplet−Triplet annihilation of Blue Fluorescent Organic Light-Emitting diodes by Generating Excitons in Trapped Charge-Free Regions

4.1 Introduction

Conventional fluorescent organic light-emitting diodes (FOLEDs) have several advantages over phosphorescent OLEDs and thermally activated delayed fluorescent (TADF) OLEDs in terms of longevity, especially in the blue region. The narrower emission spectra of conventional fluorescent emitters than TADF and phosphorescent emitters are advantageous for achieving better color purity. The short exciton lifetime of emitters is also an important advantage in terms of increasing the operational lifetime and efficiency roll-off of OLEDs. The key limitation of conventional FOLEDs is the low efficiency, because conventionally fluorescent molecules only use singlet excitons as the radiative source. Thus, improving the efficiency of blue FOLEDs is one of the critical issues for OLEDs.

Triplet−triplet annihilation (TTA), which can convert two triplet excitons into a radiative singlet exciton, is a practical method for enhancing the efficiency of conventional FOLEDs.[36,37,118–120] Anthracene-cored molecules have been widely used as blue emitters in nondoped emitting layers (EMLs)

because of the presence of the TTA process.[121–125] Wang et al. reported anthracene-cored blue emitters with carbazole and benzonitrile side groups.[126] The nondoped devices using this donor−acceptor emitter exhibited external quantum efficiencies (EQEs) of 10.06% and CIE coordinates of (0.14, 0.14). Kim et al. developed anthracene-cored blue emitters with high horizontal emitting dipole ratios (Θ) of 90% in neat film. The enhanced horizontal dipole ratio enabled the fabrication of highly efficient deep blue FOLEDs with an EQE of 6.6% and CIE coordinates of (0.145, 0.068).[127] In the doped EML system, anthracene derivatives have also been used as host molecules or emitters, and devices exceeding theoretical EQEs have been reported.[128–131] Fukagawa et al. developed anthracene derivatives with spirobifluorene, and Zhu et al. developed anthracene derivatives with triphenylimidazole.[132,133] Cheng et al. used a dipyrenylbenzene derivative as a host and achieved an EQE greater than 10%.[134,135] Suh et al. developed a benzoanthracene-cored emitter and reported a very high EQE of 14.8% with CIE coordinates of (0.14, 0.11).[136] Kido et al. developed a bisanthracene-based donor−acceptor type deep blue emitter and also reported a high EQE of 12% and CIE coordinates of (0.15, 0.06).[137] Although many anthracene derivatives used in blue FOLEDs with high EQE have been reported, there has been much interest on the EML, such as the host or emitters. There have been few reports on how the layers adjacent to the EML affect the TTA process. Kido et al. enhanced the EQE of blue FOLEDs by optimizing the charge balance.[138] Efficiency-enhancement layers (EELs) were first reported in 2010.[139] Hosokawa et al. reported that inserting a layer called

an EEL between the EML and electron transport layer (ETL) can boost TTA processes. Unfortunately, because of the lack of sufficient information about the molecules used in EELs, such as the molecular structure and photophysical properties, the mechanisms governing the efficiency enhancement are not yet clearly understood. For better understanding, the EEL should be analyzed systematically.

In this study, we analyzed EEL materials, which were newly developed by Y. H. Kim group, for efficient blue FOLEDs and systematically investigated the mechanism that enhances the efficiency. The device with a 3 nm-thick ADP3Py EEL inserted between the EML and the ETL exhibited a 44% higher maximum EQE than the reference device without the EEL but with the same EML, resulting in an EQE of 7.9% and a current efficiency of 9.0 cd A^{-1} at 1000 cd m^{-2} with CIE coordinates of the emitting color of (0.13, 0.14). The mechanism for improving the efficiencies of the devices appears to be TTA in the EEL followed by energy transfer to the emitting dye in the EML.

4.2 Experimental

Materials preparation: Three anthracene-based materials, 3,3'-(5-(10-(naphthalen-1-yl)anthracen-9-yl)-1,3-phenylene)dipyridine (AP3Py-Na), 3,3'-(5-(10-(naphthalen-2-yl)anthracen-9-yl)-1,3-phenylene)dipyridine (AP3Py-2Na), and 9,10-bis(3,5-di(pyridin-3-yl)phenyl)anthracene (ADP3Py), were designed and synthesized in the Department of Chemistry and Research Institute of Natural Science of Gyeongsang National University supervised by professor Yun-Hi Kim.

Fabrication and PL Measurement of Organic Thin Film: Organic thin film was deposited by thermal evaporation on a cleaned fused silica substrate in a vacuum chamber with a base pressure of under 5×10^{-7} torr. The PL spectra were measured using a continuous He−Cd laser (325 nm) at room temperature.

Fabrication of HODs, EODs, and OLEDs: ITO substrates were cleaned by using acetone and boiling isopropyl alcohol. After drying in an 80 °C oven, organic layers were thermally evaporated in a vacuum chamber with a base pressure of less than 5×10^{-7} torr. Following the evaporation, all devices were encapsulated in a glovebox. The structure of HODs was ITO/MoO3 (1 nm)/test material (50 nm)/MoO3 (1 nm)/Al (100 nm), and the structure of EODs was ITO/LiF (1 nm)/test material (50 nm)/LiF (1 nm)/Al (100 nm).

Measurement of Devices: The J−V characteristics were measured using a Keithley 2400 source meter, and the EL spectra and intensities were measured using a PR650 spectrometer (Photo Research) in the normal direction.

Measurement of Transient EL: Transient EL data were obtained using a pulse generator (8114A, Agilent) and a spectrometer (SpectraPro-300i, Princeton Instruments) which were connected to a photomultiplier tube (PD-438, Acton Research). A pulsed voltage with a pulse width of 500 μs and a frequency of 100 Hz was applied to the device. The detection wavelength was 465 nm.

4.3 Result and discussion

The photoluminescence (PL) spectra of the deposited films are presented in Figure 4.1a. The highest occupied molecular orbital (HOMO) levels of the materials were determined by the cyclic voltammetry (CV) measurements shown in the Supporting Information (Figure 4.2), and the lowest unoccupied molecular orbital (LUMO) levels were calculated by adding the optical band gap to the HOMO level. The HOMO/LUMO levels of AP3Py-Na, AP3Py-2Na, and ADP3Py are −5.88/−2.98, −5.84/−2.92, and −5.76/−2.84 eV, respectively.

The device structure and energy levels of the materials used in OLED fabrication are shown in Figure 1b, and the chemical structures of the molecules are shown in Figure 4.1c. A 1 nm molybdenum oxide (MoO_3) layer was used as a hole-injecting layer. N,N′-di(1-naphthyl)-N,N′-diphenyl-(1,1′-biphenyl)-4,4′-diamine and tris(4-carbazoyl-9-ylphenyl)amine were used as a hole-transporting layer and electron-blocking layer, respectively. Bathophenanthroline (BPhen) served as an ETL, and 1 nm of lithium fluoride (LiF) was used as an electroninjecting layer. To investigate the effect of the EEL, 3 nm-thick EELs were inserted between the EML and ETL. A device without an EEL (non-EEL device) was also fabricated as a reference. 2-Methyl-9,10-bis(naphthalen-2-yl)anthracene (MADN) doped with 5 wt % N,N′-bis(3-methylphenyl)-N,N′-bis[3-(9-phenyl-9H-fluoren-9-yl)phenyl]-pyrene-1,6-diamine (BD) was used as the EML. Because blue emitters with a pyrene core and amine side groups exhibit high PL quantum yields (PLQYs) and high

stability, BD was selected as an emitter in this work.[129,140,141] The absorption spectrum of the BD and the emission spectra of the MADN and materials used as the EEL are presented in Figure 4.1a. Because of the sufficient spectral overlap between the MADN and BD, energy transfer from the MADN to the BD can be efficient. The horizontal emitting dipole ratios and PLQY of 5 wt % BD-doped MADN film were 0.80 and 0.82, respectively. The results of the horizontal emitting dipole measurements are shown in Figure 4.3. The maximum EQE of the device structure was calculated to be 5.8%, assuming the ideal charge balance and ratio of radiative excitons to be 25%.

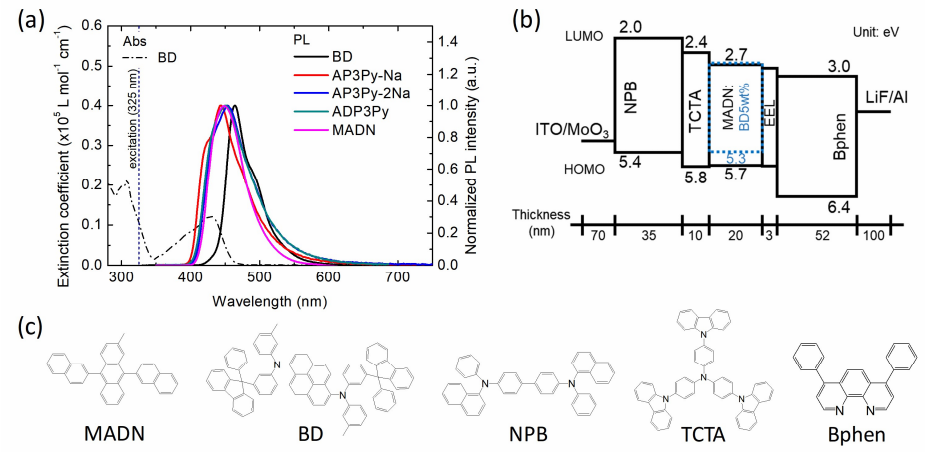

Figure 4.1 (a) Extinction coefficient of BD and PL emission spectra of BD, AP3Py-Na, AP3Py-2Na, ADP3Py and MADN films deposited on fused silica substrate. (b) Devices structure of OLEDs and (c) molecular structures used in the device.

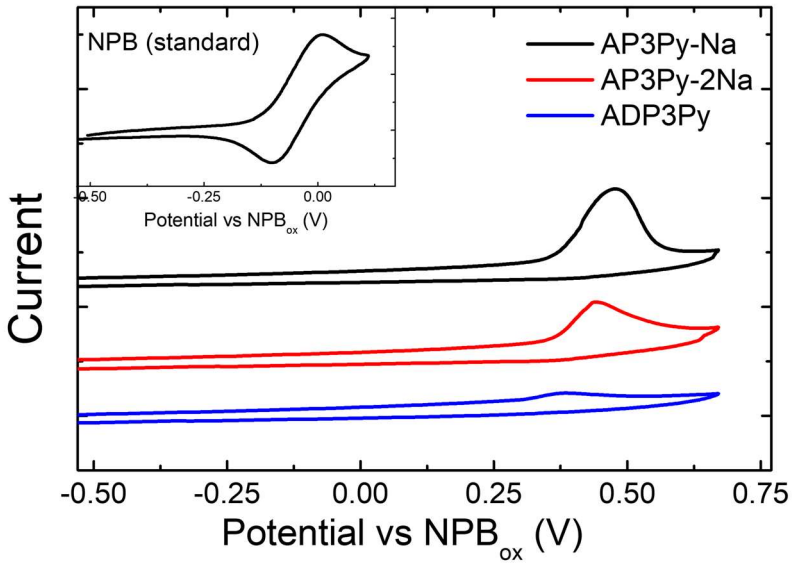

Figure 4.2 Cyclic voltammetry scans of AP3Py-Na, AP3Py-2Na and ADP3Py (1 mM in dichloromethane with 0.1 M $TBAHF_6$, scan rate of 100 mV s^{-1}).

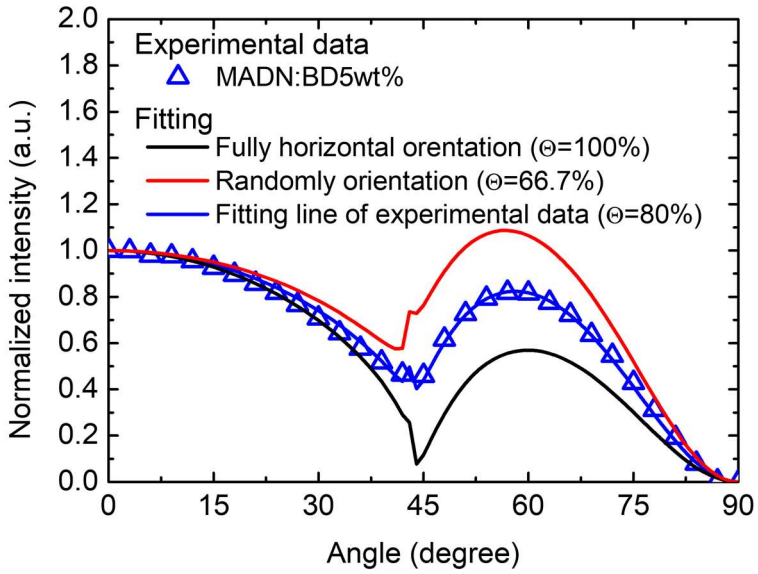

Figure 4.3 Experimentally obtained angle-dependent PL (open symbol) and simulated values (solid line) of a 30-nm-thick MADN:BD(5wt%) film.

Figure 4.4 shows the current density−voltage−luminance ($J-V-L$) characteristics, the EQE, and the electroluminescence (EL) spectra of the OLEDs. Insertion of the EEL reduced the current density compared to the reference device (without the EEL), as expected. However, the emission spectra are exactly the same for all of the devices, indicating that the emission is wholly from the emitter (BD) in the EML, whether or not the device has an EEL. Interestingly, however, the EQE of the devices with the EEL (EEL devices) was enhanced significantly compared to that of the non-EEL device, as shown in Figure 4.4b. The device with no EEL (non-EEL device) exhibited a maximum EQE of 5.5%, whereas the device with the ADP3Py EEL had a maximum EQE of 7.9%, which is 44% higher than that of the non-EEL device. The high EQE of the device approached 8%, which exceeds the theoretical maximum EQE (5.8%). This indicates that a large portion of the triplet excitons are harvested for emission following the insertion of the EEL. Details of the device characteristics are summarized in Table 4.1.

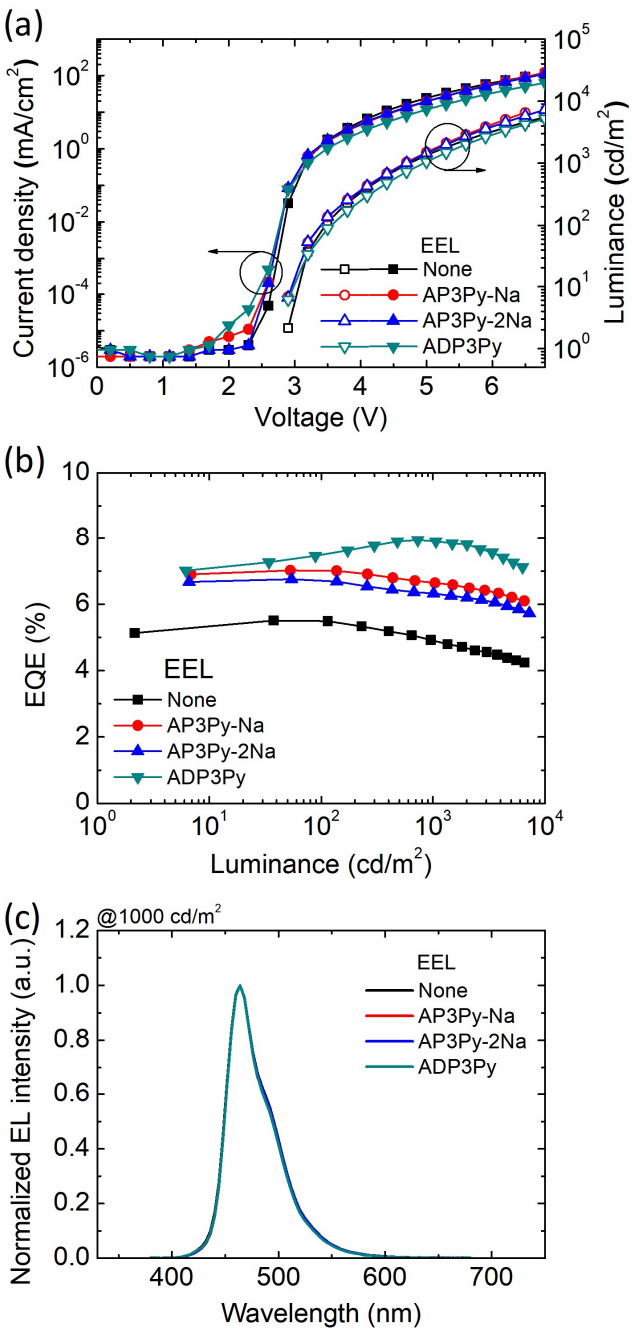

Figure 4.4 (a) *J-V-L* characteristics, (b) EQE plots and (c) EL emission spectra of the devices.

Table 4.1 Turn-on Voltage, EQE, CE, PE, and CIE Coordinates of the devices.

[a]Data were measured at maximum value/100 cd m^{-2}/1000 cd m^{-2}.

EEL	V_{on} (V)	EQE (%)[a]	CE (cd A^{-1})[a]	PE (lm W^{-1})[a]	CIE (*x*, *y*)[b]
None	2.9	5.5/5.5/4.9	6.8/6.5/5.6	7.3/5.9/3.7	(0.13, 0.14)
AP3Py-Na 3 nm	2.9	7.0/7.0/6.7	8.5/8.4/7.8	8.9/7.8/5.3	(0.13, 0.14)
AP3Py-2Na 3 nm	2.9	6.8/6.7/6.3	8.1/8.1/7.4	8.6/7.5/5.0	(0.13, 0.14)
ADP3Py 3 nm	2.9	7.9/7.5/7.9	9.0/8.5/9.0	8.6/7.5/5.7	(0.13, 0.14)
ADP3Py 10 nm	3.0	7.1/6.9/7.0	8.4/8.2/8.4	7.7/6.5/4.8	(0.13, 0.15)

[b]Data were measured at a luminance of 1000 cd m^{-2}.

The origin of the enhancement of the EQEs by the EELs was investigated using the transient EL, as shown in Figure 4.5. Rectangular voltage pulses (500 μs) were applied to the devices at a repetition rate of 100 Hz. The pulse height was adjusted to obtain a current density of 10 mA cm^{-2}. All of the devices exhibited delayed fluorescence, indicating that the TTA contributes to the emission. However, the contribution of the delayed fluorescence to the total emission varied with the device, increasing from 0.05 for the non-EEL device to 0.20, 0.16, and 0.41 for the devices with AP3Py-Na, AP3Py-2Na, and ADP3Py as the EEL, increasing the EQEs from 5.5 to 6.7, 6.4, and 7.9%, respectively. The enhancement of the EQE or delayed fluorescence by TTA was further confirmed by analyzing the time dependence of the triplet exciton density, as follows

$$\frac{\partial[\mathrm{T}(t)]}{\partial t} = -\beta[T(t)] - \gamma_{total}[\mathrm{T}(t)]^2 \tag{4.1}$$

where *T(t)* is the triplet exciton density, β is the monomolecular decay rate constant, and γ_{total} is the overall bimolecular annihilation rate constant. Under high exciton density conditions ($\gamma_{total}[T(t)]^2 \gg [T(t)]$), the solution of eq 4.1 becomes[119,142]

$$[\mathrm{T}(t)]^{-1} = \gamma_{totla} \cdot t + \frac{1}{[\mathrm{T}(0)]} \tag{4.2}$$

The intensity of the delayed fluorescence (I_{df}) induced by the TTA process can be expressed as:

$$I_{df} = \frac{1}{2} f \gamma_{total} [T(t)]^2 \tag{4.3}$$

or

$$I_{df}{}^{-1/2} \propto [T(t)]^{-1} = \gamma_{total} \cdot t + \frac{1}{[T(0)]} \tag{4.4}$$

where f is the fraction of TTA that leads to the delayed fluorescence. We predicted a linear relationship between the inverse of the square root of I_{df} and time using eq 4.4, and the experimental data are plotted in the inset of Figure 4.5. The transient behaviors of all of the devices exhibited a linear relationship between $I_{df}{}^{-1/2}$ versus time, demonstrating that the delayed fluorescence originated from the TTA process. One should note that the linear relationship expressed by eq 4.4 holds only for a short time after the pulse-off in the transient data because the assumption $\gamma_{total}[T(t)]^2 \gg \beta[T(t)]$ in eq 4.1 is valid only when the triplet exciton density is high.

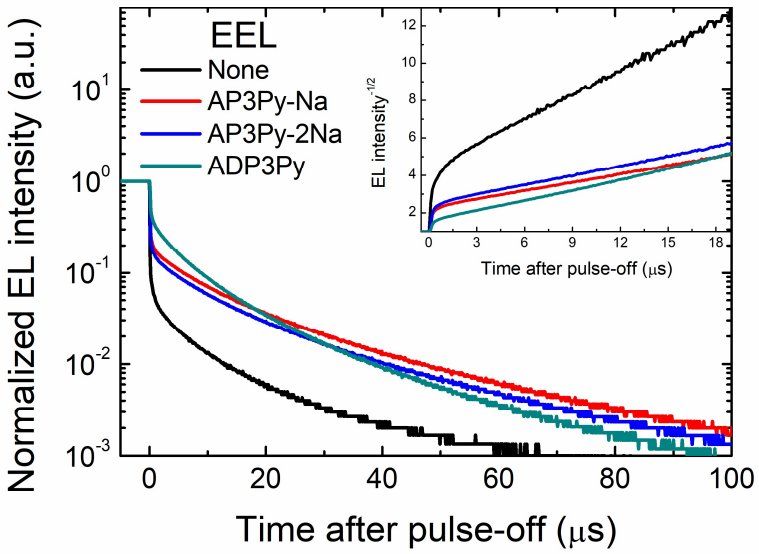

Figure 4.5 Transient EL decay curves of device. Inset shows (EL intensity)$^{-1/2}$ vs time.

The non-EEL device exhibited a very small delayed fluorescence, of 5% of the total emission, even though the host material, MADN, is an anthracene derivative. This weak TTA process in the non-EEL device, therefore, seems to be abnormal because anthracene derivatives are known to exhibit efficient TTA.[37,143] This weak TTA in the non-EEL device can be understood by considering the recombination mechanism. The BD in the EML can behave as a hole trap with a trap depth of 0.4 eV, as shown in Figure 4.1b, in which the energy levels are determined using the CV measurements shown in Figure4.6. In contrast, the LUMO levels of MADN and BD are almost the same. Therefore, the emitter sites act as hole traps because the immobility of the trapped holes on the emitter molecules increases their capture cross sections to electrons, making emitters act as electron−hole recombination centers. The triplet excitons are generated directly on the emitters, which are spatially confined to each other, which causes inefficient TTA, as previously discussed by Luo and Aziz.[144]

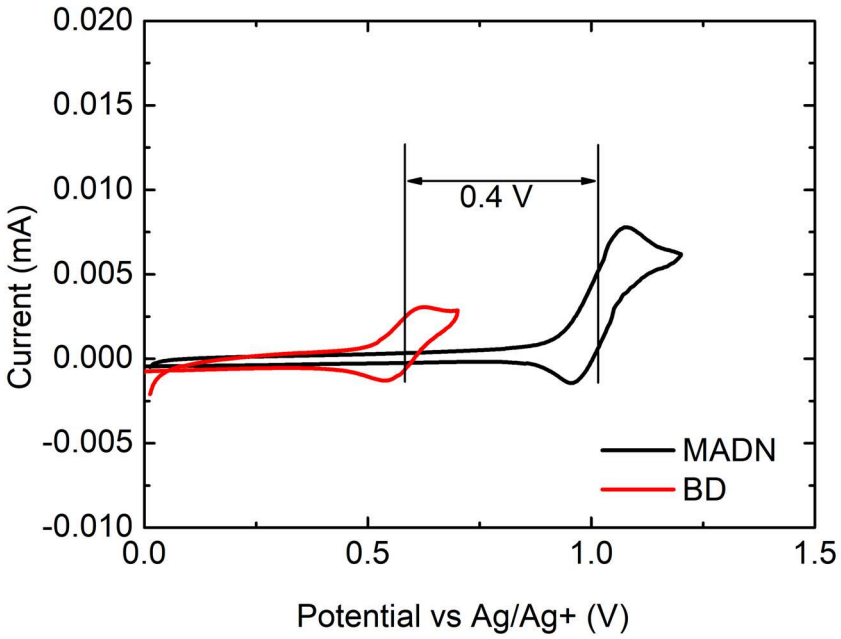

Figure 4.6 Cyclic voltammetry results of MADN and BD (1 mM in dichloromethane with 0.1 M $TBAHF_6$, scan rate of 100 mV s^{-1}).

The fact that the devices with the EEL, despite having the same EML structure, exhibited much higher delayed fluorescence indicates that the TTA process takes place efficiently in the EEL. In other words, the excitons are mainly formed in the EEL. The exciton generation region in the devices with and without the EEL can be inferred from the carrier mobility of the EML and EELs. The hole and electron mobilities of the 5 wt % BD-doped MADN, BPhen, AP3Py-Na, AP3Py-2Na, and ADP3Py layers were measured using the hole-only devices (HODs) and electron-only devices (EODs) whose structures are described in the Chapter 4.2. The current density−electric field ($J-F$) curves are shown in Figure 4.7a,b, and the space charge limited current (SCLC) regime was analyzed by Mott-Gurney theory.[82] The extracted mobility values are presented in Figure 4.7c,d as fitted to the Poole−Frenkel model.[83] In the EML, hole mobility is three times higher than electron mobility, indicating that the exciton generation region is located near the EML/BPhen interface in the non-EEL device. The EEL layers also exhibited higher hole mobility than electron mobility. Because the MADN and EEL molecules have similar HOMO levels, holes can be injected from the EML to the EEL without any energy barrier. Therefore, excitons are expected to be generated mainly at the MADN/BPhen (non-EEL device) or EEL/BPhen (the device with the EEL) interface.

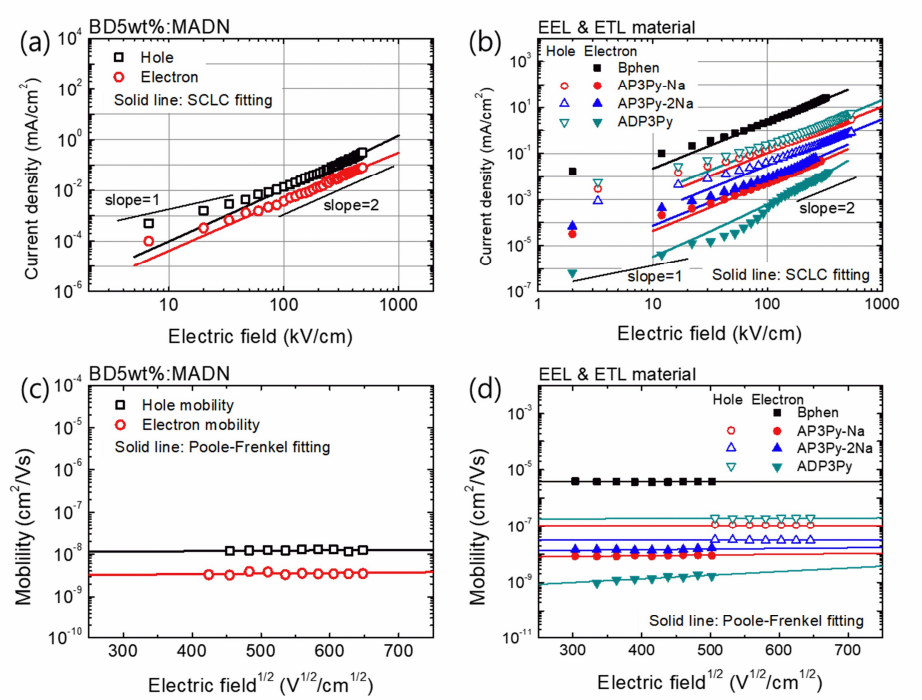

Figure 4.7 J-F curves of hole-only and electron-only devices of (a) 5wt% BD doped MADN and (c) EEL & ETL materials. (Solid lines: fitting lines in SCLC region using child's law) Hole and electron mobility of (c) 5wt% BD doped MADN and (d) EEL & ETL materials. (Solid lines: fitting lines using Poole-Frenkel equation.)

In order to validate that the delayed emission of the transient EL is due to the TTA of the EEL, it is necessary to confirm the TTA characteristics of the EEL. Kondakov et al. and So et al. have shown that the emission intensity−current density (*L*−*J*) plot of OLEDs exhibiting TTA characteristics has quadratic relationship in the weak-annihilation regime because of low triplet exciton density.[36,118,145] As the triplet exciton density increases, the linear relationship is observed because the TTA process becomes dominant. In this work, the single-layer electroluminescent devices of indium tin oxide (ITO)/MoO_3 (1 nm)/EEL (50 nm)/LiF (1 nm)/Al (100 nm) were fabricated to confirm the TTA characteristics of the EEL and the results are presented in Figure 4.8. The results clearly show two distinct regimes, weak-annihilation regime (at low current density) and strong-annihilation regime (at high current density). At low current density, the slopes were almost quadratic, 1.6 and 1.7, and at high current density, the slopes were 1.2 which are almost linearly dependent, confirming that EELs exhibit TTA characteristics. As the molecules used in EELs show TTA characteristics and there are no emitters which act as hole trap sites in the EEL, the TTA process can proceed efficiently in the EEL device. Because of the sufficient spectral overlap between the absorption of the emitter and the emission of AP3Py-Na, AP3Py-2Na, and ADP3Py, efficient Förster resonance energy transfer (FRET) is possible from the EEL to the emitters (Figure 4.1a). As a result, we observed the same EL spectra despite the differences between their exciton generation regions.

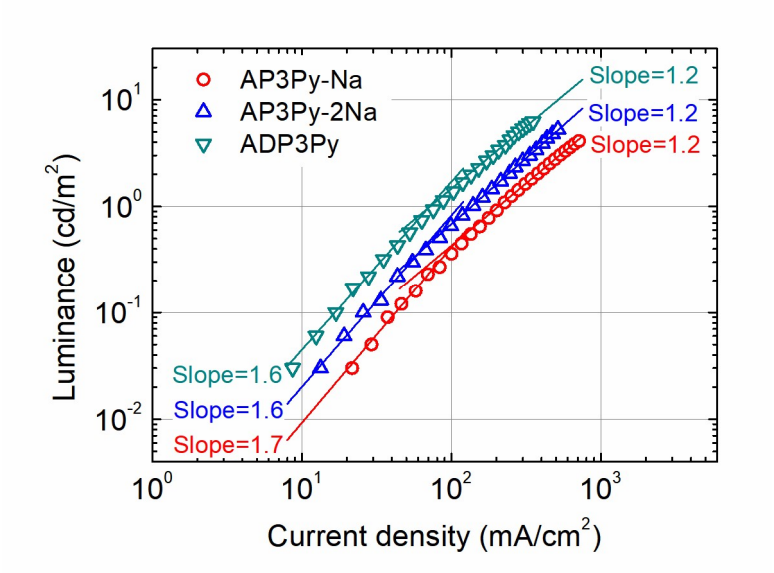

Figure 4.8 Luminance vs current density characteristics of single layer electroluminescent devices.

To verify the above speculation, that is, TTA in the EEL followed by FRET to BD in the EML, the emission characteristics of a device with a thicker (10 nm) ADP3Py layer were analyzed (Figure 4.9a). The device has a 45 nm-thick BPhen layer, whereas the other layers were the same as in Figure 4.1b. We anticipate that ADP3Py emission is observed if the energy transfer from the ADP3Py excitons to BDs is not complete. The EL emission spectrum of the device with the 3 nm-thick ADP3Py layer is exactly the same as that of the non-EEL device, implying that the energy transfer is complete. In contrast, the device with the 10 nm-thick ADP3Py layer exhibited higher intensities in short wavelength regions than the devices with no EEL and a 3 nm ADP3Py layer. The increased EL emission exactly matches the ADP3Py emission, demonstrating that the difference originates from the incomplete energy transfer from the ADP3Py exciton to BD. The ADP3Py emission intensity increases as the driving voltage increases as shown in Figure 4.10. The maximum EQE of the device with a 10 nm-thick ADP3Py layer is lower than that of the device with the 3 nm-thick ADP3Py layer, but higher than the non-EEL device (Figure 4.9b), supporting the fact that the energy transfer is incomplete, but these results support the hypothesis that the excitons generated in the EEL can enhance the device efficiency by FRET to the emitters in the EML.

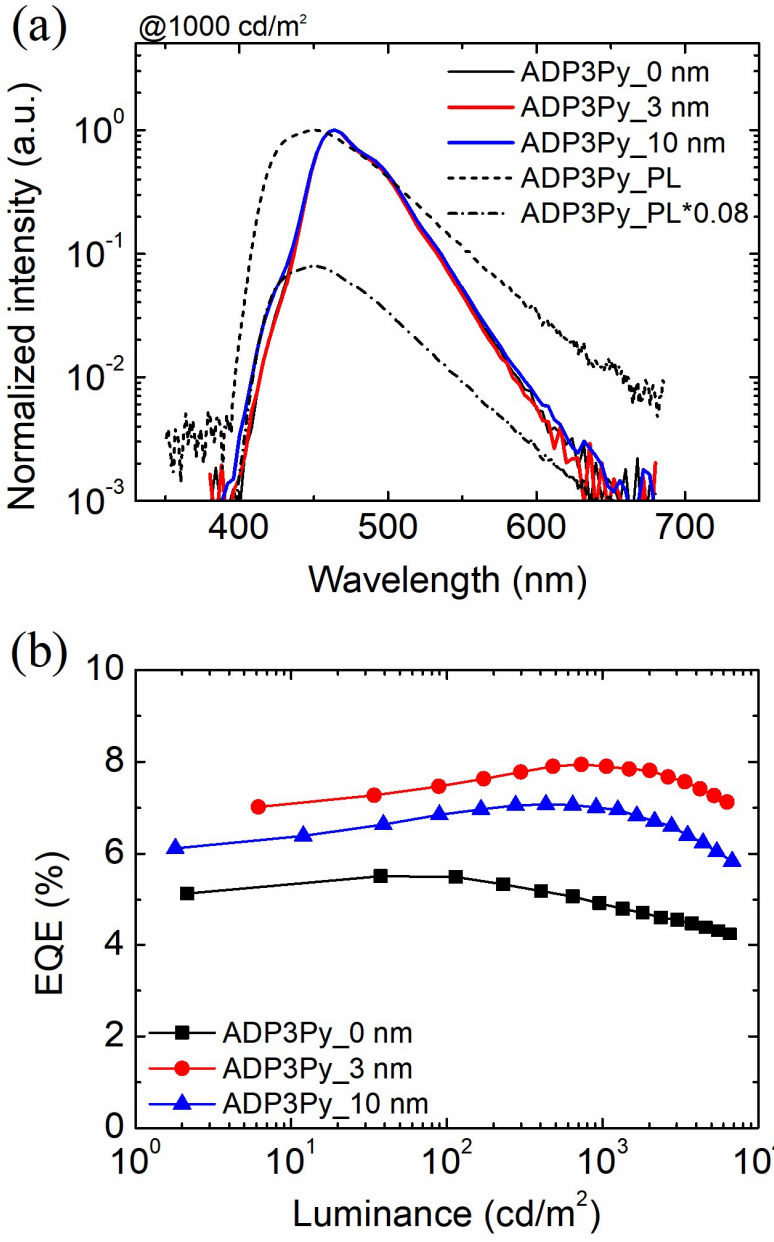

Figure 4.9 Device properties as the thickness of ADP3Py layer changes. (a) EL emission spectra and (b) EQE plots.

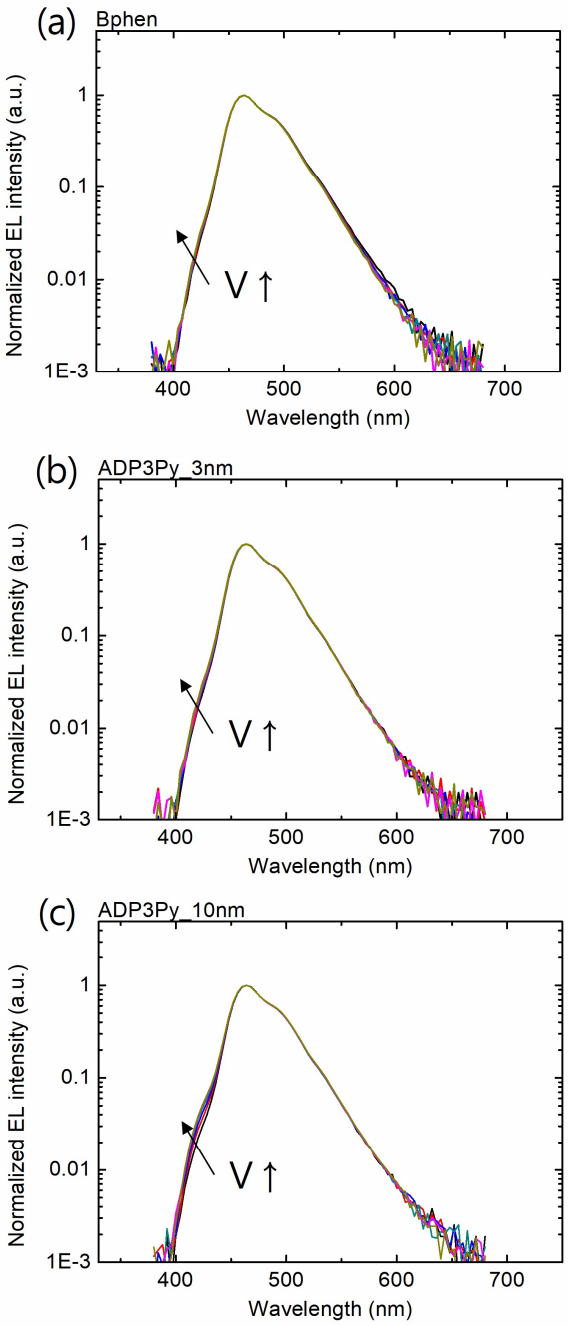

Figure 4.10 EL emission spectra change of (a) non EEL device, (b) 3-nm-thcin ADP3Py used device, (c) 10-nm-thick ADP3Py used device as driving voltage increase.

The reason why ADP3Py exhibits the highest EQE among the three EELs can be understood based on the exciton density profiles in the EELs, conceived from the electron and hole mobilities (Figure 4.7d). The materials used in the EEL exhibited lower electron mobilities than BPhen, and ADP3Py had the lowest mobility. Because of the large electron mobility difference between the BPhen and EEL, electrons will accumulate at the EEL/BPhen interface. On the other hand, the hole mobilities are higher than the electron mobilities in the EELs, and the mobility difference between the hole and electron in the EELs is ADP3Py > AP3Py-Na > AP3Py-2Na, so that holes will be more filed up at the EEL/BPhen interface and the width of the recombination zone becomes narrower in the same sequence. Therefore, we can expect that the exciton density at the interface, TTA process (proportional to the square of triplet exciton density), and resultantly device efficiency are ADP3Py > AP3Py-Na > AP3Py-2Na, which is consistent with the experimental EQEs in Figure 4.4b. It can be said, therefore, that the low electron mobility combined with the large difference between hole and electron mobilities of the materials used in EELs results in narrow exciton distribution in the EEL, leading to efficient TTA processes.

The ADP3Py used device exhibited 41% of the delayed emission ratio (Figure 4.5). This is little higher than the theoretically limited value of 37.5%. Thus we consider other triplet harvesting channel. The triplet exciton harvesting via intersystem crossing (ISC) can be considered. In Figure 4.11 I described the TTA process in EEL. In this diagram, ISC process from $[TT]^3$ state to S_1+S_0 state *via* T_n+S_0 state can be considered and expressed with second-order perturbation theory. With second-order perturbation theory, ISC rate can be expressed as below[146]

$$k_{ISC} = \frac{2\pi}{\hbar}\sum_{f}\left|\langle\Psi_f|\hat{H}_{int}|\Psi_i\rangle + \sum_{n}\frac{\langle\Psi_f|\hat{H}_{int}|\Psi_n\rangle\langle\Psi_n|\hat{H}_{int}|\Psi_i\rangle}{E_i - E_n}\right|^2 \delta(E_f - E_i) \tag{4.5}$$

Where Ψ_i, Ψ_n and Ψ_f are the wave function of initial, intermediate and final state. Similarly, E_i, E_n and E_f express energy level of initial, intermediate and final state. Considering the calculated S_n and T_n levels, ISC transition to S_1 would be energetically possible due to the lower energy level of S_1 than $2T_1$ (Figure 4.12). Thus the initial state is $[TT]^3$, the intermediate state is T_n+S_0 and the final state is S_1+S_0. For electron spin conversion process, the spin-orbit coupling (SOC) should be considered and for internal decay electron-electron interaction should be considered. As a results, equation 4.5 can be expressed as below[147]

$$k_{\mathrm{ISC}} = \frac{2\pi}{\hbar}\left|\left\langle \Psi_{S_1+S_0}\left|\hat{H}_{SOC}\right|\Psi_{[\mathrm{TT}]^3}\right\rangle + \sum_{\mathrm{n}} \frac{\left\langle \Psi_{S_1+S_0}\left|\hat{H}_{SOC}\right|\Psi_{\mathrm{T_n+S_0}}\right\rangle\left\langle \Psi_{\mathrm{T_n+S_0}}\left|\hat{H}_{\mathrm{el}}\right|\Psi_{[TT]^3}\right\rangle}{E_{[TT]^3} - E_{\mathrm{T_n+S_0}}}\right|^2 \delta(E_{S_1+S_0} - E_{[TT]^3}) \quad (4.6)$$

The first term can be ignored because of the small spin-orbit coupling matrix element (SOCME) between $[TT]^3$ state and S_1+S_0 state and the second term couples the $[TT]^3$ state and the S_1+S_0 state using the T_n+S_0 state as an intermediate state.

The natural transition orbitals (NTOs) of ADP3Py corresponding to the S_1 and T_n (n = 1~5) transition were calculated by Gaussian 09 (B3LYP/6-31G(d)) and the results are presented in Figure 4.13. Spin-orbit coupling (SOC) is allowed between the states of different orbital symmetry and spin multiplicity (El-sayed rule) then ISC rate from T_5 and S_1 would be unneglectable. Furthermore, T_5 is the energetically closest state to $[TT]^3$, which can minimize $E_{[TT]^3} - E_{\mathrm{T_n+S_0}}$. Thus, delayed emission ratio above 40% would be possible for non-doped ADP3Py layer, due to the triplet harvesting channel via ISC.

The optimized device was fabricated with more efficient (MBD 106) and narrow spectrum (M-tDABNA) emitters. The device structure and the absorption and emission spectra of emitters are depicted in Figure 4.14. The HOMO level of B3PYMPM is deeper than that of Bphen, allowing the efficient hole blocking. The $J-V-L$ characteristics, the EQE, and the EL spectra of the OLEDs are presented in Figure 4.15. The devices showed efficiency roll-on

characteristics (efficiency increases in higher current density region). The EQE_{max} was obtained near the luminance of 5000 cd m^{-2}.

The origin of the roll-on characteristics of the devices was investigated using the transient EL, as shown in Figure 4.16. Rectangular voltage pulses (5 ms) were applied to the devices at a repetition rate of 20 Hz. The pulse height was changed from the low current density (1 mA cm^{-2}) to the high current density (80 mA cm^{-2}). The delayed emission was well fitted by TTA model (equation 4.4). Both devices exhibited similar delayed emission ratio and the largest value was obtained when the 80 mA cm^{-2} pulse was applied. On the basis of the delayed emission ratio, EQE by the TTA process can be extracted. As can be seen in figure 4.17, the EQE by the prompt emission exhibits efficiency roll-off property. The EQE roll-on is attributed to the efficient TTA process in EEL.

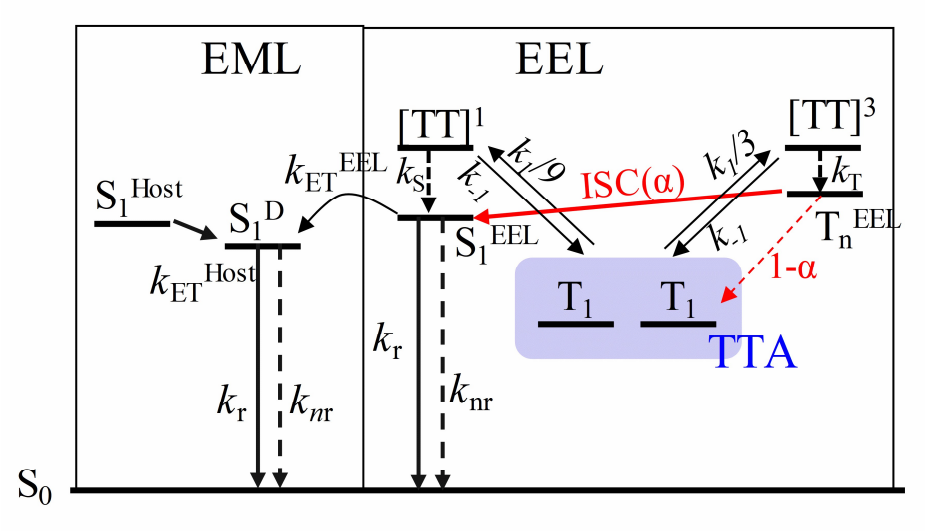

Figure 4.11. Schematic illustration of TTA process in EEL considering ISC process from $[TT]^3$ to S_1.

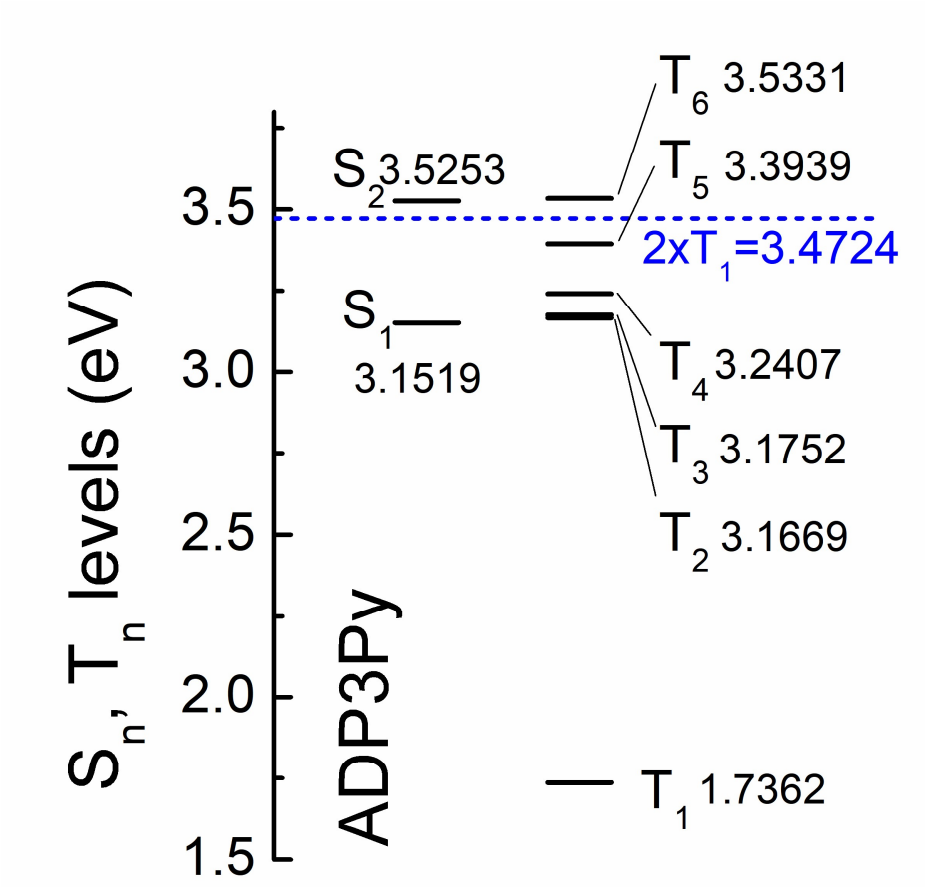

Figure 4.12 Calculated S_n and T_n levels of ADP3Py (Gaussian 09, B3LYP/6-31G(d))

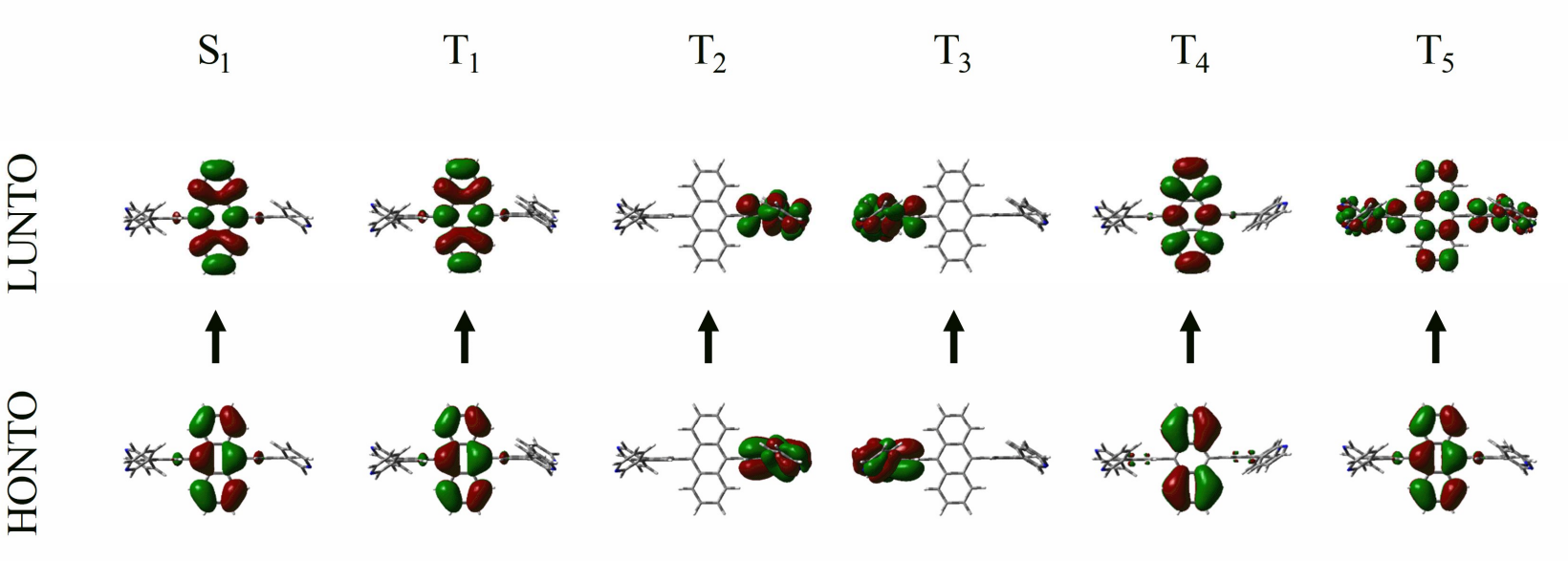

Figure 4.13 Calculated natural transition orbital (NTO) of ADP3Py

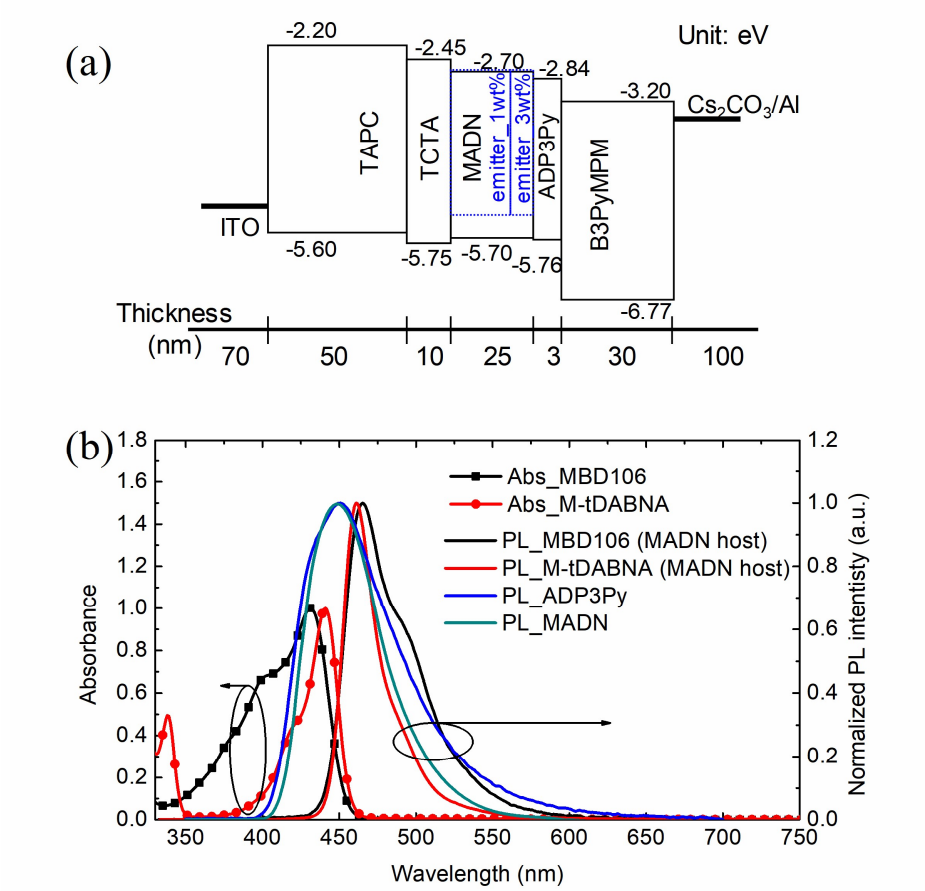

Figure 4.14 (a) Device structure using MBD 106 and M-tDABNA as emitter. (b) Absorption and emission spectra of molecules used in the device.

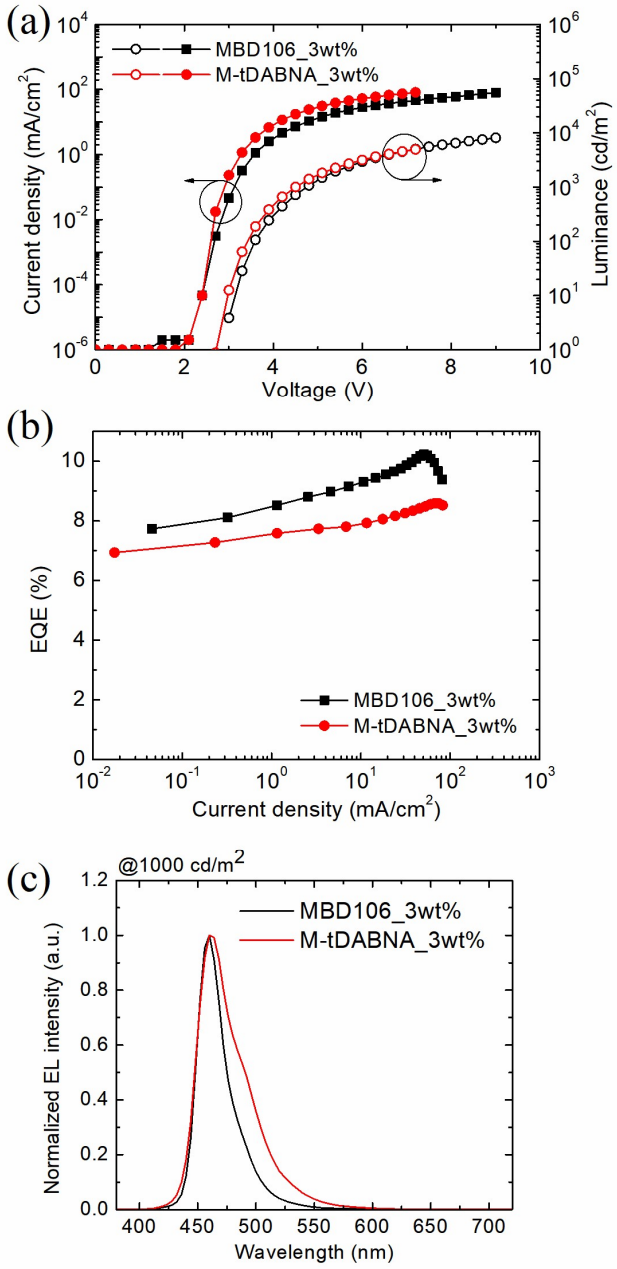

Figure 4.15 (a) *J-V-L* characteristics, (b) EQE plots and (c) EL emission spectra of the devices.

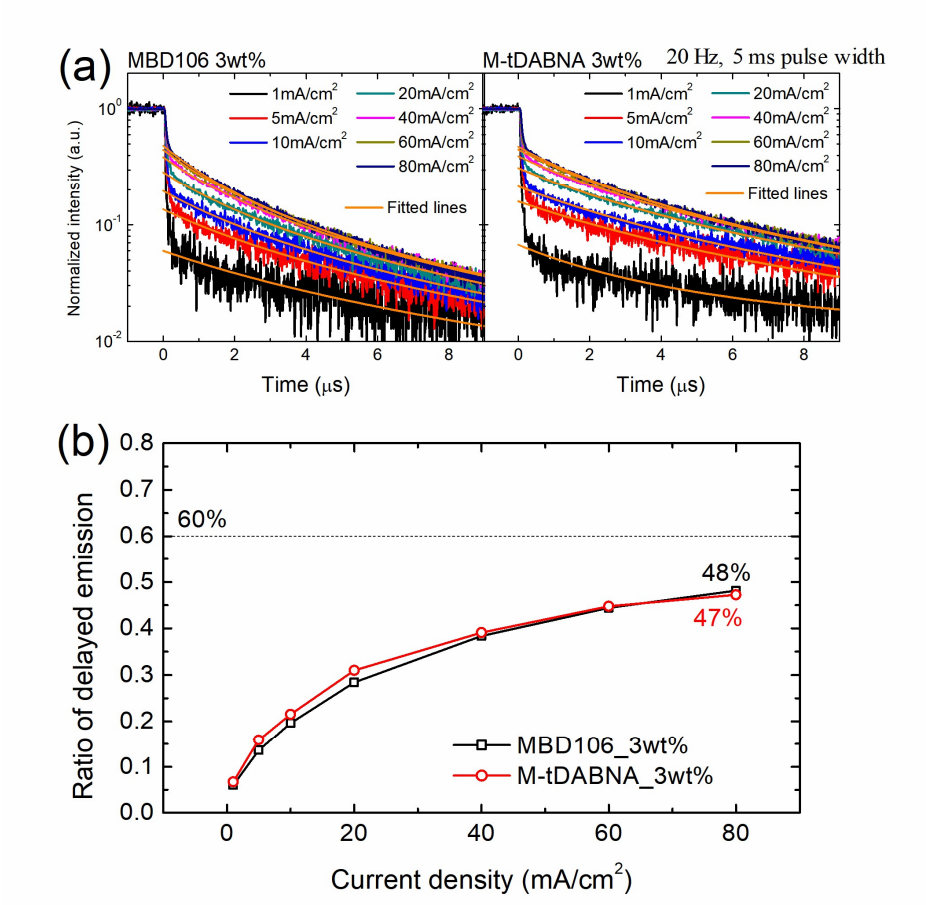

Figure 4.16 (a) Transient EL results and (b) delayed emission ratio as the current density changes. (Orange lines in (a): fitted line by TTA model)

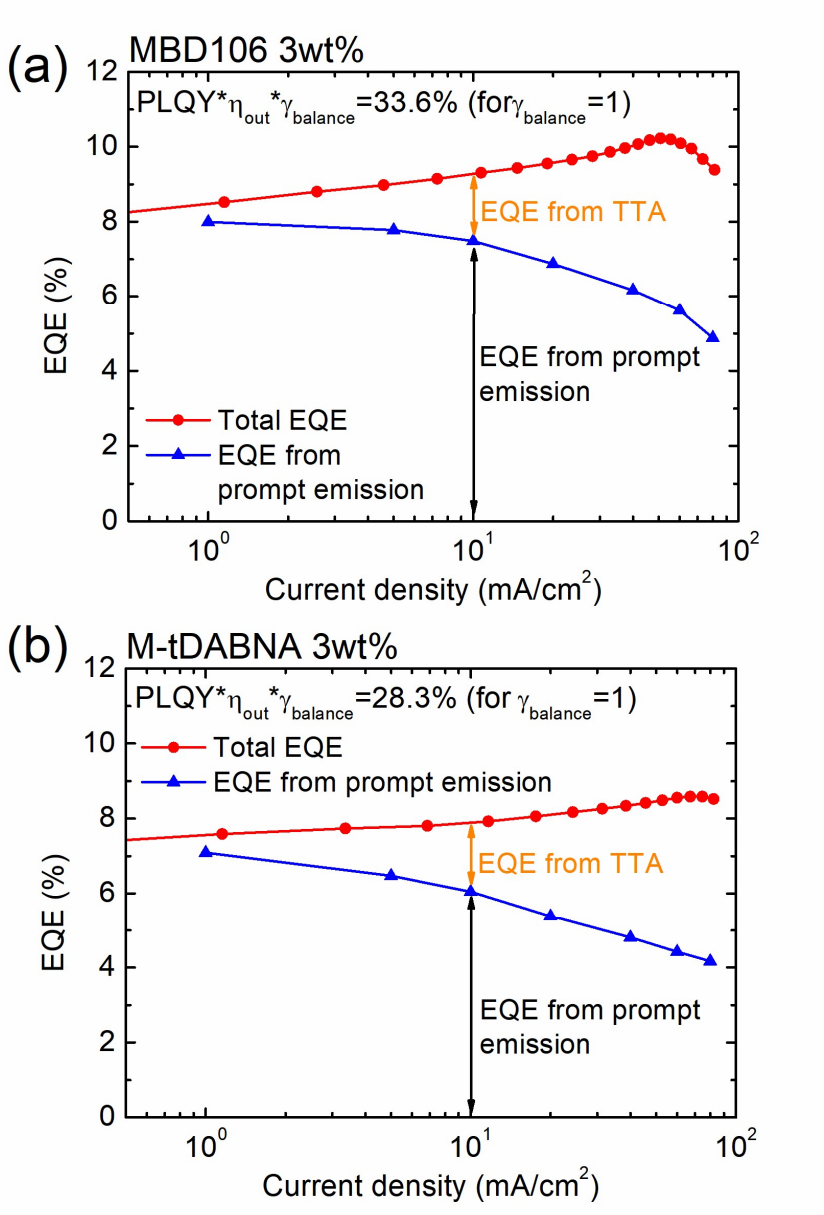

Figure 4.17 Analysis of efficiency composed of the EQE from prompt emission and TTA process of (a) MBD106 doped and (b) M-tDABNA doped device.

4.4 Conclusion

In summary, we analyzed three anthracene-cored molecules, AP3Py-Na, AP3Py-2Na, and ADP3Py, which can be used as EELs in blue fluorescent OLEDs. A very thin EEL inserted between the EML and ETL increased the EQE of the device by 44% compared to the non-EEL device. Transient EL measurements clearly show that the enhanced emission comes from the increased delayed emission that originates from the TTA in the EEL, followed by energy transfer to the BD in the EML. Interestingly, the contribution of the delayed fluorescence to the total emission of the optimized device with the EEL was 0.41, which exceeds the theoretical maximum TTA contribution (37.5%) calculated based on spin statistics.[148] The TTA process in the EELs is more efficient than that in the EML because there are no trap sites in the EEL. In contrast, the BD in the EML behaves as a hole trap to induce the direct generation of the triplet excitons on the emitters, which are spatially confined, leading to inefficient TTA. These findings also reveal that the relative energy level differences between the TTA-inducing host (e.g., anthracene moieties) and BD play a role of paramount importance in terms of avoiding direct trap-induced triplet generation on dopants and thus leading to efficient TTA. The difference in electron and hole mobilities affect the exciton distribution in EELs to influence TTA. Large difference results in the narrow recombination zone to facilitate efficient TTA.

Chapter 5. Summary and Conclusion

Even with the importance of deep-blue OLEDs, there has been few reports about efficient deep-blue OLEDs because of the difficulty in satisfying narrow spectrum and high efficiency for blue host-emitter systems. In order to realize highly efficient deep-blue OLEDs we explored various triplet harvesting methods and tried to solve their limitation. Based on these researches, efficient deep-blue OLEDs have been developed.

In Chapter 2, an exciplex-forming mixed host for deep-blue PhOLEDs was developed and applied to the OLED. The emission energy of the exciplex was 3.0 eV, which is sufficiently large for the use of deep-blue dopants. The blue PhOLEDs doped with FCNIr achieved a turn-on voltage of 2.9 eV, a maximum EQE of 24% with CIE coordinates of (0.15, 0.21), and an EQE of 19% with CIE coordinates of (0.15, 0.19). This represents superior color purity compared to blue FIrpic-based devices, which have CIE coordinates of (0.16, 0.33). The exciplex host devices showed much better performances in EQE, PE, driving voltage, and operational lifetime than the single host devices.

In chapter 3, deep blue and blue emitting TADF emitters developed and synthesized by prof. Yun-Hi Kim was introduced. We investigated the origin of narrow spectrum, efficient RISC process and high Θ values. The deeper HOMO levels of the acceptor unit resulted in (deep) blue emissions. The donor and acceptor units are rigid so that the emission spectra are narrow with the

FWHM less than 62 nm. It turns out that ΔE_{ST}'s of the molecules are smaller than 0.11 eV, and the triplet LE state of the molecules are located in the boron unit with a little higher energy than ^{1}CT and ^{3}CT whose energy difference is smaller than 0.18 eV, resulting in high RISC rate and high PLQYs approaching 90%. In addition, the large aspect ratio of the molecules gives rise to high Θ above 80% (81% for TDBA-SAF and 89% for DBA-SAB). All the combined effects bring out a deep blue OLED using TDBA-SAF as an emitter with the EQE of 28.2%, CIE coordinate of (0.142, 0.090) and low efficiency roll-off.

In Chapter 4, we analyzed three anthracene-cored molecules, AP3Py-Na, AP3Py-2Na, and ADP3Py, which can be used as EELs in blue fluorescent OLEDs. A very thin EEL inserted between the EML and ETL increased the EQE of the device by 44% compared to the non-EEL device. Transient EL measurements clearly show that the enhanced emission comes from the increased delayed emission that originates from the TTA in the EEL, followed by energy transfer to the BD in the EML. The TTA process in the EELs is more efficient than that in the EML because there are no trap sites in the EEL. The difference in electron and hole mobilities affect the exciton distribution in EELs to influence TTA. Large difference results in the narrow recombination zone to facilitate efficient TTA

We believe that the development of fluorescent OLEDs using exciplex cohost and phosphorescent sensitizer has provided a direction for achieving OLEDs with high efficiency and long operational lifetime. Since we demonstrate that the phosphorescent sensitization can be applied even in blue fluorescent OLEDs, the development of stable host, deep-blue phosphorescent

materials, and a deep-blue exciplex with high triplet energy and efficient RISC will lead to the development of highly efficient blue OLEDs with long operational lifetime, which has been the goal of many researchers working on OLEDs.

Bibliography

[1] Helfrich, W.; Schneider, W. G. Recombination Radiation in Anthracene Crystals. *Phys. Rev. Lett.* **1965**, *14* (7), 229–231.

[2] Tang, C. W.; Vanslyke, S. A. Organic Electroluminescent Diodes. *Appl. Phys. Lett.* **1987**, *51* (12), 913–915.

[3] Yuan, X.-D.; Liang, J.; He, Y.-C.; Li, Q.; Zhong, C.; Jiang, Z.-Q.; Liao, L.-S. A Rational Design of Carbazole-Based Host Materials with Suitable Spacer Group towards Highly-Efficient Blue Phosphorescence. *J. Mater. Chem. C* **2014**, *2* (31), 6387–6394.

[4] Kim, S. J.; Kim, Y. J.; Son, Y. H.; Hur, J. A.; Um, H. A.; Shin, J.; Lee, T. W.; Cho, M. J.; Kim, J. K.; Joo, S.; Yang, J. H.; Chae, G. S.; Choi, K.; Hyuk Kwon, J.; Hoon Choi, D. High-Efficiency Blue Phosphorescent Organic Light-Emitting Diodes Using a Carbazole and Carboline-Based Host Material. *Chem. Commun.* **2013**, *49* (60), 6788.

[5] Song, W.; Lee, I.; Lee, J. Y. Host Engineering for High Quantum Efficiency Blue and White Fluorescent Organic Light-Emitting Diodes. *Adv. Mater.* **2015**, *27* (29), 4358–4363.

[6] Chang, C.-H.; Kuo, M.-C.; Lin, W.-C.; Chen, Y.-T.; Wong, K.-T.; Chou, S.-H.; Mondal, E.; Kwong, R. C.; Xia, S.; Nakagawa, T.; Adachi, C. A Dicarbazole–Triazine Hybrid Bipolar Host Material for Highly Efficient Green Phosphorescent OLEDs. *J. Mater. Chem.* **2012**, *22* (9), 3832.

[7] Tsutsui, T.; Aminaka, E.; Lin, C. P.; Kim, D. U. Extended Molecular Design Concept of Molecular Materials for Electroluminescence: Sublimed–Dye Films, Molecularly Doped Polymers and Polymers with Chromophores. *Philos. Trans. R. Soc. London. Ser. A Math. Phys. Eng. Sci.* **1997**, *355* (1725), 801–814.

[8] Nowy, S.; Krummacher, B. C.; Frischeisen, J.; Reinke, N. A.; Brütting, W. Light Extraction and Optical Loss Mechanisms in Organic Light-Emitting Diodes: Influence of the Emitter Quantum Efficiency. *J. Appl. Phys.* **2008**, *104* (12), 123109.

[9] Kim, S.-Y.; Jeong, W.-I.; Mayr, C.; Park, Y.-S.; Kim, K.-H.; Lee, J.-H.; Moon, C.-K.; Brütting, W.; Kim, J.-J. Organic Light-Emitting Diodes with 30% External Quantum Efficiency Based on a Horizontally Oriented Emitter. *Adv. Funct. Mater.* **2013**, *23* (31), 3896–3900.

[10] Sim, B.; Moon, C.; Kim, K.-H.; Kim, J. Quantitative Analysis of the Efficiency of OLEDs. *ACS Appl. Mater. Interfaces* **2016**, *8* (48), 33010–33018.

[11] Powell, R. C.; Kepler, R. G. Evidence for Long-Range Exciton-Impurity Interaction in Tetracene-Doped Anthracene Crystals. *Phys. Rev. Lett.* **1969**, *22* (13), 636–639.

[12] Tokito, S.; Noda, K.; Taga, Y. Metal Oxides as a Hole-Injecting Layer for an Organic Electroluminescent Device. *J. Phys. D. Appl. Phys.* **1996**, *29* (11), 2750–2753.

[13] Plans, J.; Baltá Calleja, F. J. Electrical Conductivity in Doped Polyethylene. *Polym. Bull.* **1981**, *5* (6), 311–316.

[14] Lee, J. H.; Kim, J. J. Interfacial Doping for Efficient Charge Injection in Organic Semiconductors. *Phys. Status Solidi Appl. Mater. Sci.* **2012**, *209* (8), 1399–1413.

[15] Greiner, M. T.; Chai, L.; Helander, M. G.; Tang, W.-M.; Lu, Z.-H. Transition Metal Oxide Work Functions: The Influence of Cation Oxidation State and Oxygen Vacancies. *Adv. Funct. Mater.* **2012**, *22* (21), 4557–4568.

[16] Yoo, S.-J.; Lee, J.-H.; Lee, J.-H.; Kim, J.-J. Doping-Concentration-Dependent Hole Mobility in a ReO 3 Doped Organic Semiconductor of 4,4′,4″-Tris(N -(2-Naphthyl)- N -Phenyl-Amino)-Triphenylamine. *Appl. Phys. Lett.* **2013**, *102* (18), 183301.

[17] Yoo, S. J.; Chang, J. H.; Lee, J. H.; Moon, C. K.; Wu, C. I.; Kim, J. J. Formation of Perfect Ohmic Contact at Indium Tin Oxide/N,N′-Di(Naphthalene-1-Yl)-N,N′-Diphenyl-Benzidine Interface Using ReO 3. *Sci. Rep.* **2014**, *4*, 1–6.

[18] Kim, J.-M.; Yoo, S.-J.; Moon, C.-K.; Sim, B.; Lee, J.-H.; Lim, H.; Kim, J. W.; Kim, J.-J. N-Type Molecular Doping in Organic Semiconductors: Formation and Dissociation Efficiencies of a Charge Transfer Complex. *J. Phys. Chem. C* **2016**, *120* (17), 9475–9481.

[19] O'Brien, D. F.; Baldo, M. A.; Thompson, M. E.; Forrest, S. R. Improved Energy Transfer in Electrophosphorescent Devices. *Appl. Phys. Lett.* **1999**, *74* (3), 442–444.

[20] Naka, S.; Shinno, K.; Okada, H.; Onnagawa, H.; Miyashita, K. Organic Electroluminescent Devices Using a Mixed Single Layer. *Jpn. J. Appl. Phys.* **1994**, *33* (12B), L1772–L1774.

[21] Chaskar, A.; Chen, H. F.; Wong, K. T. Bipolar Host Materials: A Chemical Approach for Highly Efficient Electrophosphorescent Devices. *Adv. Mater.* **2011**, *23* (34), 3876–3895.

[22] Wasey, J. A. E.; Barnes, W. L. Efficiency of Spontaneous Emission from Planar Microcavities. *J. Mod. Opt.* **2000**, *47* (4), 725–741.

[23] Kim, J. S.; Ho, P. K. H.; Greenham, N. C.; Friend, R. H. Electroluminescence Emission Pattern of Organic Light-Emitting Diodes: Implications for Device Efficiency Calculations. *J. Appl. Phys.* **2000**, *88* (2), 1073–1081.

[24] Frischeisen, J.; Yokoyama, D.; Endo, A.; Adachi, C.; Brütting, W. Increased Light Outcoupling Efficiency in Dye-Doped Small Molecule Organic Light-Emitting Diodes with Horizontally Oriented Emitters. *Org. Electron.* **2011**, *12* (5), 809–817.

[25] Kim, K.-H.; Lee, S.; Moon, C.; Kim, S.-Y.; Park, Y.; Lee, J.-H.; Woo Lee, J.; Huh, J.; You, Y.; Kim, J. Phosphorescent Dye-Based Supramolecules for High-Efficiency Organic Light-Emitting Diodes. *Nat. Commun.* **2014**, *5* (1), 4769.

[26] Shin, H.; Lee, S.; Kim, K.; Moon, C.; Yoo, S.; Lee, J.; Kim, J. Blue Phosphorescent Organic Light-Emitting Diodes Using an Exciplex Forming Co-Host with the External Quantum Effi Ciency of Theoretical Limit. **2014**, 4730–4734.

[27] Lee, J. H.; Sarada, G.; Moon, C. K.; Cho, W.; Kim, K. H.; Park, Y. G.; Lee, J. Y.; Jin, S. H.; Kim, J. J. Finely Tuned Blue Iridium Complexes with Varying Horizontal Emission Dipole Ratios and Quantum Yields for Phosphorescent Organic Light-Emitting Diodes. *Adv. Opt. Mater.* **2015**, *3* (2), 211–220.

[28] Rajamalli, P.; Senthilkumar, N.; Huang, P. Y.; Ren-Wu, C. C.; Lin, H. W.; Cheng, C. H. New Molecular Design Concurrently Providing Superior Pure Blue, Thermally Activated Delayed Fluorescence and Optical Out-Coupling Efficiencies. *J. Am. Chem. Soc.* **2017**, *139* (32), 10948–10951.

[29] Kim, K. H.; Ahn, E. S.; Huh, J. S.; Kim, Y. H.; Kim, J. J. Design of Heteroleptic Ir Complexes with Horizontal Emitting Dipoles for Highly Efficient Organic Light-Emitting Diodes with an External Quantum Efficiency of 38%. *Chem. Mater.* **2016**, *28* (20), 7505–7510.

[30] Smith, L. H.; Barnes, W. L. Using a Low-Index Host Layer to Increase Emission from Organic Light-Emitting Diode Structures. *Org. Electron.* **2006**, *7* (6), 490–494.

[31] Callens, M. K.; Yokoyama, D.; Neyts, K. Anisotropic Materials in OLEDs for High Outcoupling Efficiency. *Opt. Express* **2015**, *23* (16), 21128.

[32] Shin, H.; Lee, J.; Moon, C.; Huh, J.; Sim, B.; Kim, J. Sky-Blue Phosphorescent OLEDs with 34.1% External Quantum Efficiency Using a Low Refractive Index Electron Transporting Layer. *Adv. Mater.* **2016**, *28* (24), 4920–4925.

[33] Yokoyama, D.; Nakayama, K. I.; Otani, T.; Kido, J. Wide-Range Refractive Index Control of Organic Semiconductor Films toward Advanced Optical Design of Organic Optoelectronic Devices. *Adv. Mater.* **2012**, *24* (47), 6368–6373.

[34] Kondakov, D. Y. Role of Triplet-Triplet Annihilation in Highly Efficient Fluorescent Devices. *J. Soc. Inf. Disp.* **2009**, *17* (2), 137.

[35] Saltiel, J.; March, G. R.; Smothers, W. K.; Stout, S. A.; Charlton, J. L. Spin-Statistical Factor in the Triplet-Triplet Annihilation of Anthracene Triplets. *J. Am. Chem. Soc.* **1981**, *103* (24), 7159–7164.

[36] Kondakov, D. Y.; Pawlik, T. D.; Hatwar, T. K.; Spindler, J. P. Triplet Annihilation Exceeding Spin Statistical Limit in Highly Efficient Fluorescent Organic Light-Emitting Diodes. *J. Appl. Phys.* **2009**, *106* (12), 124510.

[37] Chiang, C. J.; Kimyonok, A.; Etherington, M. K.; Griffiths, G. C.; Jankus, V.; Turksoy, F.; Monkman, A. P. Ultrahigh Efficiency Fluorescent Single and Bi-Layer Organic Light Emitting Diodes: The Key Role of Triplet Fusion. *Adv. Funct. Mater.* **2013**, *23* (6), 739–746.

[38] Baldo, M. A.; O'Brien, D. F.; You, Y.; Shoustikov, A.; Sibley, S.; Thompson, M. E.; Forrest, S. R. Highly Efficient Phosphorescent Emission from Organic Electroluminescent Devices. *Nature* **1998**, *395* (6698), 151–154.

[39] Adachi, C.; Baldo, M. A.; Thompson, M. E.; Forrest, S. R. Nearly 100% Internal Phosphorescence Efficiency in an Organic Light Emitting Device. *J. Appl. Phys.* **2001**, *90* (10), 5048–5051.

[40] Adachi, C.; Baldo, M. A.; Forrest, S. R.; Lamansky, S.; Thompson, M. E.; Kwong, R. C. High-Efficiency Red Electrophosphorescence Devices. *Appl. Phys. Lett.* **2001**, *78* (11), 1622–1624.

[41] Baldo, M. A.; Lamansky, S.; Burrows, P. E.; Thompson, M. E.; Forrest, S. R. Very High-Efficiency Green Organic Light-Emitting Devices Based on Electrophosphorescence. *Appl. Phys. Lett.* **1999**, *75* (1), 4–6.

[42] Xiao, L.; Chen, Z.; Qu, B.; Luo, J.; Kong, S.; Gong, Q.; Kido, J. Recent Progresses on Materials for Electrophosphorescent Organic Light-Emitting Devices. *Adv. Mater.* **2011**, *23* (8), 926–952.

[43] Jeong, H.; Shin, H.; Lee, J.; Kim, B.; Park, Y.-I.; Yook, K. S.; An, B.-K.; Park, J. Recent Progress in the Use of Fluorescent and Phosphorescent Organic Compounds for Organic Light-Emitting Diode Lighting. *J. Photonics Energy* **2015**, *5* (1), 057608.

[44] Im, Y.; Byun, S. Y.; Kim, J. H.; Lee, D. R.; Oh, C. S.; Yook, K. S.; Lee, J. Y. Recent Progress in High-Efficiency Blue-Light-Emitting Materials

for Organic Light-Emitting Diodes. *Adv. Funct. Mater.* **2017**, *27* (13), 1603007.

[45] Frederichs, B.; Staerk, H. Energy Splitting between Triplet and Singlet Exciplex States Determined with E-Type Delayed Fluorescence. *Chem. Phys. Lett.* **2008**, *460* (1–3), 116–118.

[46] Goushi, K.; Yoshida, K.; Sato, K.; Adachi, C. Organic Light-Emitting Diodes Employing Efficient Reverse Intersystem Crossing for Triplet-to-Singlet State Conversion. *Nat. Photonics* **2012**, *6* (4), 253–258.

[47] Park, Y.; Kim, K.; Kim, J.; Park, Y.; Kim, K.; Kim, J. Efficient Triplet Harvesting by Fluorescent Molecules through Exciplexes for High Efficiency Organic Light-Emitting Diodes Efficient Triplet Harvesting by Fluorescent Molecules through Exciplexes for High Efficiency Organic Light-Emitting Diodes. **2014**, *153306* (2013), 1–6.

[48] Uoyama, H.; Goushi, K.; Shizu, K.; Nomura, H.; Adachi, C. Highly Efficient Organic Light-Emitting Diodes from Delayed Fluorescence. *Nature* **2012**, *492* (7428), 234–238.

[49] Zhang, Q.; Li, B.; Huang, S.; Nomura, H.; Tanaka, H.; Adachi, C. Efficient Blue Organic Light-Emitting Diodes Employing Thermally Activated Delayed Fluorescence. *Nat. Photonics* **2014**, *8* (4), 326–332.

[50] Hirata, S.; Sakai, Y.; Masui, K.; Tanaka, H.; Lee, S. Y.; Nomura, H.; Nakamura, N.; Yasumatsu, M.; Nakanotani, H.; Zhang, Q.; Shizu, K.; Miyazaki, H.; Adachi, C. Highly Efficient Blue Electroluminescence Based on Thermally Activated Delayed Fluorescence. *Nat. Mater.* **2015**, *14* (3), 330–336.

[51] Kim, K.-H.; Moon, C.; Sun, J. W.; Sim, B.; Kim, J. Triplet Harvesting by a Conventional Fluorescent Emitter Using Reverse Intersystem Crossing of Host Triplet Exciplex. *Adv. Opt. Mater.* **2015**, *3* (7), 895–899.

[52] Zhang, D.; Song, X.; Cai, M.; Duan, L. Blocking Energy-Loss Pathways for Ideal Fluorescent Organic Light-Emitting Diodes with Thermally Activated Delayed Fluorescent Sensitizers. *Adv. Mater.* **2018**, *30* (6), 1705250.

[53] Kim, H.-G.; Kim, K.-H.; Moon, C.-K.; Kim, J.-J. Harnessing Triplet Excited States by Fluorescent Dopant Utilizing Codoped Phosphorescent Dopant in Exciplex Host for Efficient Fluorescent Organic Light Emitting Diodes. *Adv. Opt. Mater.* **2017**, *5* (3), 1600749.

[54] Tung, Y.-J.; Ngo, T.; Hack, M.; Brown, J.; Koide, N.; Nagara, Y.; Kato, Y.; Ito, H. 5.2: A High Efficiency Phosphorescent White OLED for LCD Backlight and Display Applications. *SID Symp. Dig. Tech. Pap.* **2004**,

35 (1), 48.

[55] Lee, J.; Chen, H.; Batagoda, T.; Coburn, C.; Djurovich, P. I.; Thompson, M. E.; Forrest, S. R. Deep Blue Phosphorescent Organic Light-Emitting Diodes with Very High Brightness and Efficiency. *Nat. Mater.* **2016**, *15* (1), 92–98.

[56] Sarada, G.; Sim, B.; Moon, C.-K.; Cho, W.; Kim, K.-H.; Sree, V. G.; Park, E.; Kim, J.-J.; Jin, S.-H. Synthesis and Characterization of Highly Efficient Blue Ir(III) Complexes by Tailoring β-Diketonate Ancillary Ligand for Highly Efficient PhOLED Applications. *Org. Electron.* **2016**, *39*, 91–99.

[57] Kim, S. H.; Jang, J.; Lee, S. J.; Lee, J. Y. Deep Blue Phosphorescent Organic Light-Emitting Diodes Using a Si Based Wide Bandgap Host and an Ir Dopant with Electron Withdrawing Substituents. *Thin Solid Films* **2008**, *517* (2), 722–726.

[58] Adachi, C.; Baldo, M. A.; Thompson, M. E.; Forrest, S. R. Nearly 100% Internal Phosphorescence Efficiency in an Organic Light Emitting Device. *J. Appl. Phys.* **2001**, *90* (10), 5048–5051.

[59] Jeon, S. O.; Yook, K. S.; Joo, C. W.; Lee, J. Y. Phenylcarbazole-Based Phosphine Oxide Host Materials For High Efficiency In Deep Blue Phosphorescent Organic Light-Emitting Diodes. *Adv. Funct. Mater.* **2009**, *19* (22), 3644–3649.

[60] Son, H. S.; Lee, J. Y. Structure–Property Relationship in High Triplet Energy Host Materials with a Phenylcarbazole Core and Diphenylphosphine Oxide Substituent. *Org. Electron.* **2011**, *12* (6), 1025–1032.

[61] Sasabe, H.; Pu, Y.; Nakayama, K.; Kido, J. M-Terphenyl-Modified Carbazole Host Material for Highly Efficient Blue and Green PHOLEDS. *Chem. Commun.* **2009**, No. 43, 6655.

[62] Lee, D. R.; Kim, B. S.; Lee, C. W.; Im, Y.; Yook, K. S.; Hwang, S.-H.; Lee, J. Y. Above 30% External Quantum Efficiency in Green Delayed Fluorescent Organic Light-Emitting Diodes. *ACS Appl. Mater. Interfaces* **2015**, *7* (18), 9625–9629.

[63] Lee, J. H.; Lee, S.; Yoo, S. J.; Kim, K. H.; Kim, J. J. Langevin and Trap-Assisted Recombination in Phosphorescent Organic Light Emitting Diodes. *Adv. Funct. Mater.* **2014**, *24* (29), 4681–4688.

[64] Park, Y.; Lee, S.; Kim, K.-H.; Kim, S.-Y.; Lee, J.; Kim, J. Exciplex-Forming Co-Host for Organic Light-Emitting Diodes with Ultimate Efficiency. *Adv. Funct. Mater.* **2013**, *23* (39), 4914–4920.

[65] Seino, Y.; Sasabe, H.; Kimura, M.; Inomata, S.; Nakao, K.; Kido, J.

Novel Blue Exciplex Comprising Acridine and Sulfone Derivatives as a Host Material for High-Efficiency Blue Phosphorescent OLEDs. *Chem. Lett.* **2016**, *45* (3), 283–285.

[66] Lee, J.; Cheng, S.; Yoo, S.; Shin, H.; Chang, J.; Wu, C.; Wong, K.; Kim, J. An Exciplex Forming Host for Highly Efficient Blue Organic Light Emitting Diodes with Low Driving Voltage. *Adv. Funct. Mater.* **2015**, *25* (3), 361–366.

[67] Goushi, K.; Adachi, C. Efficient Organic Light-Emitting Diodes through up-Conversion from Triplet to Singlet Excited States of Exciplexes. *Appl. Phys. Lett.* **2012**, *101* (2), 023306.

[68] Hung, W. Y.; Fang, G. C.; Chang, Y. C.; Kuo, T. Y.; Chou, P. T.; Lin, S. W.; Wong, K. T. Highly Efficient Bilayer Interface Exciplex for Yellow Organic Light-Emitting Diode. *ACS Appl. Mater. Interfaces* **2013**, *5* (15), 6826–6831.

[69] Seino, Y.; Sasabe, H.; Pu, Y. J.; Kido, J. High-Performance Blue Phosphorescent OLEDs Using Energy Transfer from Exciplex. *Adv. Mater.* **2014**, *26* (10), 1612–1616.

[70] Liu, X. K.; Chen, Z.; Zheng, C. J.; Chen, M.; Liu, W.; Zhang, X. H.; Lee, C. S. Nearly 100% Triplet Harvesting in Conventional Fluorescent Dopant-Based Organic Light-Emitting Devices through Energy Transfer from Exciplex. *Adv. Mater.* **2015**, *27* (12), 2025–2030.

[71] Adachi, C.; Kwong, R. C.; Djurovich, P.; Adamovich, V.; Baldo, M. A.; Thompson, M. E.; Forrest, S. R. Endothermic Energy Transfer: A Mechanism for Generating Very Efficient High-Energy Phosphorescent Emission in Organic Materials. *Appl. Phys. Lett.* **2001**, *79* (13), 2082–2084.

[72] Song, W.; Lee, H. L.; Lee, J. Y. High Triplet Energy Exciplex Hosts for Deep Blue Phosphorescent Organic Light-Emitting Diodes. *J. Mater. Chem. C* **2017**, *5* (24), 5923–5929.

[73] Holmes, R. J.; Forrest, S. R.; Tung, Y. J.; Kwong, R. C.; Brown, J. J.; Garon, S.; Thompson, M. E. Blue Organic Electrophosphorescence Using Exothermic Host-Guest Energy Transfer. *Appl. Phys. Lett.* **2003**, *82* (15), 2422–2424.

[74] Von Ruden, A. L.; Cosimbescu, L.; Polikarpov, E.; Koech, P. K.; Swensen, J. S.; Wang, L.; Darsell, J. T.; Padmaperuma, A. B. Phosphine Oxide Based Electron Transporting and Hole Blocking Materials for Blue Electrophosphorescent Organic Light Emitting Devices. *Chem. Mater.* **2010**, *22* (20), 5678–5686.

[75] Jankus, V.; Chiang, C. J.; Dias, F.; Monkman, A. P. Deep Blue Exciplex

Organic Light-Emitting Diodes with Enhanced Efficiency; P-Type or E-Type Triplet Conversion to Singlet Excitons? *Adv. Mater.* **2013**, *25* (10), 1455–1459.

[76] Lu, K.-Y.; Chou, H.-H.; Hsieh, C.-H.; Yang, Y.-H. O.; Tsai, H.-R.; Tsai, H.-Y.; Hsu, L.-C.; Chen, C.-Y.; Chen, I.-C.; Cheng, C.-H. Wide-Range Color Tuning of Iridium Biscarbene Complexes from Blue to Red by Different N ^ N Ligands: An Alternative Route for Adjusting the Emission Colors. *Adv. Mater.* **2011**, *23* (42), 4933–4937.

[77] Sasabe, H.; Takamatsu, J.; Motoyama, T.; Watanabe, S.; Wagenblast, G.; Langer, N.; Molt, O.; Fuchs, E.; Lennartz, C.; Kido, J. High-Efficiency Blue and White Organic Light-Emitting Devices Incorporating a Blue Iridium Carbene Complex. *Adv. Mater.* **2010**, *22* (44), 5003–5007.

[78] Park, J.; Oh, H.; Oh, S.; Kim, J.; Park, H. J.; Kim, O. Y.; Lee, J. Y.; Kang, Y. Deep Blue Phosphorescent Organic Light-Emitting Diodes with Excellent External Quantum Efficiency. *Org. Electron.* **2013**, *14* (12), 3228–3233.

[79] Jeon, S. O.; Jang, S. E.; Son, H. S.; Lee, J. Y. External Quantum Efficiency above 20% in Deep Blue Phosphorescent Organic Light-Emitting Diodes. *Adv. Mater.* **2011**, *23* (12), 1436–1441.

[80] Tokito, S.; Tsutsui, T.; Taga, Y. Microcavity Organic Light-Emitting Diodes for Strongly Directed Pure Red, Green, and Blue Emissions. *J. Appl. Phys.* **1999**, *86* (5), 2407–2411.

[81] Wu, M.-F.; Yeh, S.-J.; Chen, C.-T.; Murayama, H.; Tsuboi, T.; Li, W.-S.; Chao, I.; Liu, S.-W.; Wang, J.-K. The Quest for High-Performance Host Materials for Electrophosphorescent Blue Dopants. *Adv. Funct. Mater.* **2007**, *17* (12), 1887–1895.

[82] Mott, N. F.; Gurney, R. W. *Electronic Processes in Ionic Crystals*; Academic Press: New York, 1964.

[83] Murgatroyd, P. N. Theory of Space-Charge-Limited Current Enhanced by Frenkel Effect. *J. Phys. D. Appl. Phys.* **1970**, *3* (2), 151–156.

[84] Chopra, N.; Lee, J.; Zheng, Y.; Eom, S.; Xue, J.; So, F. Effect of the Charge Balance on High-Efficiency Blue-Phosphorescent Organic Light-Emitting Diodes. *ACS Appl. Mater. Interfaces* **2009**, *1* (6), 1169–1172.

[85] Endo, A.; Ogasawara, M.; Takahashi, A.; Yokoyama, D.; Kato, Y.; Adachi, C. Thermally Activated Delayed Fluorescence from Sn4+-Porphyrin Complexes and Their Application to Organic Light Emitting Diodes - A Novel Mechanism for Electroluminescence. *Adv. Mater.* **2009**, *21* (47), 4802–4806.

[86] Yokoyama, M.; Inada, K.; Tsuchiya, Y.; Nakanotani, H.; Adachi, C. Trifluoromethane Modification of Thermally Activated Delayed Fluorescence Molecules for High-Efficiency Blue Organic Light-Emitting Diodes. *Chem. Commun.* **2018**, *54* (59), 8261–8264.

[87] Im, Y.; Han, S. H.; Lee, J. Y. Deep Blue Thermally Activated Delayed Fluorescent Emitters Using CN-Modified Indolocarbazole as an Acceptor and Carbazole-Derived Donors. *J. Mater. Chem. C* **2018**, *6* (18), 5012–5017.

[88] Zhang, Q.; Li, J.; Shizu, K.; Huang, S.; Hirata, S.; Miyazaki, H.; Adachi, C. Design of Efficient Thermally Activated Delayed Fluorescence Materials for Pure Blue Organic Light Emitting Diodes. *J. Am. Chem. Soc.* **2012**, *134* (36), 14706–14709.

[89] Ganesan, P.; Chen, D. G.; Liao, J. L.; Li, W. C.; Lai, Y. N.; Luo, Di.; Chang, C. H.; Ko, C. L.; Hung, W. Y.; Liu, S. W.; Lee, G. H.; Chou, P. T.; Chi, Y. Isomeric Spiro-[Acridine-9,9′-Fluorene]-2,6-Dipyridylpyrimidine Based TADF Emitters: Insights into Photophysical Behaviors and OLED Performances. *J. Mater. Chem. C* **2018**, *6* (37), 10088–10100.

[90] Sun, J. W.; Baek, J. Y.; Kim, K.-H.; Moon, C.-K.; Lee, J.-H.; Kwon, S.; Kim, Y.-H.; Kim, J. Thermally Activated Delayed Fluorescence from Azasiline Based Intramolecular Charge-Transfer Emitter (DTPDDA) and a Highly Efficient Blue Light Emitting Diode. *Chem. Mater.* **2015**, *27* (19), 6675–6681.

[91] Seo, J.-A.; Im, Y.; Han, S. H.; Lee, C. W.; Lee, J. Y. Unconventional Molecular Design Approach of High-Efficiency Deep Blue Thermally Activated Delayed Fluorescent Emitters Using Indolocarbazole as an Acceptor. *ACS Appl. Mater. Interfaces* **2017**, *9* (43), 37864–37872.

[92] Ohsawa, T.; Sasabe, H.; Watanabe, T.; Nakao, K.; Komatsu, R.; Hayashi, Y.; Hayasaka, Y.; Kido, J. A Series of Imidazo[1,2-f]Phenanthridine-Based Sky-Blue TADF Emitters Realizing EQE of over 20%. *Adv. Opt. Mater.* **2019**, *7* (5), 1801282.

[93] Sun, J. W.; Baek, J. Y.; Kim, K. H.; Huh, J. S.; Kwon, S. K.; Kim, Y. H.; Kim, J. J. Azasiline-Based Thermally Activated Delayed Fluorescence Emitters for Blue Organic Light Emitting Diodes. *J. Mater. Chem. C* **2017**, *5* (5), 1027–1032.

[94] Woo, S.-J.; Kim, Y.; Kwon, S.-K.; Kim, Y.-H.; Kim, J.-J. Phenazasiline/Spiroacridine Donor Combined with Methyl-Substituted Linkers for Efficient Deep Blue Thermally Activated Delayed Fluorescence Emitters. *ACS Appl. Mater. Interfaces* **2019**, *11* (7), 7199–7207.

[95] Woo, S.-J.; Kim, Y.; Kim, Y.-H.; Kwon, S.-K.; Kim, J.-J. A Spiro-Silafluorene–Phenazasiline Donor-Based Efficient Blue Thermally Activated Delayed Fluorescence Emitter and Its Host-Dependent Device Characteristics. *J. Mater. Chem. C* **2019**, *7* (14), 4191–4198.

[96] Lin, T.-A.; Chatterjee, T.; Tsai, W.-L.; Lee, W.-K.; Wu, M.-J.; Jiao, M.; Pan, K.-C.; Yi, C.-L.; Chung, C.-L.; Wong, K.-T.; Wu, C.-C. Sky-Blue Organic Light Emitting Diode with 37% External Quantum Efficiency Using Thermally Activated Delayed Fluorescence from Spiroacridine-Triazine Hybrid. *Adv. Mater.* **2016**, *28* (32), 6976–6983.

[97] Sun, J. W.; Kim, K.-H.; Moon, C.-K.; Lee, J.-H.; Kim, J.-J. Highly Efficient Sky-Blue Fluorescent Organic Light Emitting Diode Based on Mixed Cohost System for Thermally Activated Delayed Fluorescence Emitter (2CzPN). *ACS Appl. Mater. Interfaces* **2016**, *8* (15), 9806–9810.

[98] Zou, S. J.; Xie, F. M.; Xie, M.; Li, Y. Q.; Cheng, T.; Zhang, X. H.; Lee, C. S.; Tang, J. X. High-Performance Nondoped Blue Delayed Fluorescence Organic Light-Emitting Diodes Featuring Low Driving Voltage and High Brightness. *Adv. Sci.* **2020**, *7* (3).

[99] Drigo, N. A.; Kudriashova, L. G.; Weissenseel, S.; Sperlich, A.; Huckaba, A. J.; Nazeeruddin, M. K.; Dyakonov, V. Photophysics of Deep Blue Acridane- and Benzonitrile-Based Emitter Employing Thermally Activated Delayed Fluorescence. *J. Phys. Chem. C* **2018**, *122* (39), 22796–22801.

[100] Chan, C.; Cui, L.; Kim, J. U.; Nakanotani, H.; Adachi, C. Rational Molecular Design for Deep-Blue Thermally Activated Delayed Fluorescence Emitters. *Adv. Funct. Mater.* **2018**, *28* (11), 1706023.

[101] Zhang, D.; Cai, M.; Bin, Z.; Zhang, Y.; Zhang, D.; Duan, L. Highly Efficient Blue Thermally Activated Delayed Fluorescent OLEDs with Record-Low Driving Voltages Utilizing High Triplet Energy Hosts with Small Singlet–Triplet Splittings. *Chem. Sci.* **2016**, *7* (5), 3355–3363.

[102] Liu, M.; Komatsu, R.; Cai, X.; Hotta, K.; Sato, S.; Liu, K.; Chen, D.; Kato, Y.; Sasabe, H.; Ohisa, S.; Suzuri, Y.; Yokoyama, D.; Su, S.-J.; Kido, J. Horizontally Orientated Sticklike Emitters: Enhancement of Intrinsic Out-Coupling Factor and Electroluminescence Performance. *Chem. Mater.* **2017**, *29* (20), 8630–8636.

[103] Cui, L.; Nomura, H.; Geng, Y.; Kim, J. U.; Nakanotani, H.; Adachi, C. Controlling Singlet–Triplet Energy Splitting for Deep-Blue Thermally Activated Delayed Fluorescence Emitters. *Angew. Chemie Int. Ed.* **2017**, *56* (6), 1571–1575.

[104] Wong, M. Y.; Krotkus, S.; Copley, G.; Li, W.; Murawski, C.; Hall, D.; Hedley, G. J.; Jaricot, M.; Cordes, D. B.; Slawin, A. M. Z.; Olivier, Y.;

Beljonne, D.; Muccioli, L.; Moral, M.; Sancho-Garcia, J.-C.; Gather, M. C.; Samuel, I. D. W.; Zysman-Colman, E. Deep-Blue Oxadiazole-Containing Thermally Activated Delayed Fluorescence Emitters for Organic Light-Emitting Diodes. *ACS Appl. Mater. Interfaces* **2018**, *10* (39), 33360–33372.

[105] Li, Z.; Li, W.; Keum, C.; Archer, E.; Zhao, B.; Slawin, A. M. Z.; Huang, W.; Gather, M. C.; Samuel, I. D. W.; Zysman-Colman, E. 1,3,4-Oxadiazole-Based Deep Blue Thermally Activated Delayed Fluorescence Emitters for Organic Light Emitting Diodes. *J. Phys. Chem. C* **2019**, *123* (40), 24772–24785.

[106] Rajamalli, P.; Chen, D.; Li, W.; Samuel, I. D. W.; Cordes, D. B.; Slawin, A. M. Z.; Zysman-Colman, E. Enhanced Thermally Activated Delayed Fluorescence through Bridge Modification in Sulfone-Based Emitters Employed in Deep Blue Organic Light-Emitting Diodes. *J. Mater. Chem. C* **2019**, *7* (22), 6664–6671.

[107] Lee, S. Y.; Yasuda, T.; Yang, Y. S.; Zhang, Q.; Adachi, C. Luminous Butterflies: Efficient Exciton Harvesting by Benzophenone Derivatives for Full-Color Delayed Fluorescence OLEDs. *Angew. Chemie Int. Ed.* **2014**, *53* (25), 6402–6406.

[108] Numata, M.; Yasuda, T.; Adachi, C. High Efficiency Pure Blue Thermally Activated Delayed Fluorescence Molecules Having 10H-Phenoxaborin and Acridan Units. *Chem. Commun.* **2015**, *51* (46), 9443–9446.

[109] Hirai, H.; Nakajima, K.; Nakatsuka, S.; Shiren, K.; Ni, J.; Nomura, S.; Ikuta, T.; Hatakeyama, T. One-Step Borylation of 1,3-Diaryloxybenzenes Towards Efficient Materials for Organic Light-Emitting Diodes. *Angew. Chemie - Int. Ed.* **2015**, *54* (46), 13581–13585.

[110] Ahn, D. H.; Lee, H.; Kim, S. W.; Karthik, D.; Lee, J.; Jeong, H.; Lee, J. Y.; Kwon, J. H. Highly Twisted Donor–Acceptor Boron Emitter and High Triplet Host Material for Highly Efficient Blue Thermally Activated Delayed Fluorescent Device. *ACS Appl. Mater. Interfaces* **2019**, *11* (16), 14909–14916.

[111] Lee, Y. H.; Park, S.; Oh, J.; Woo, S.-J.; Kumar, A.; Kim, J.-J.; Jung, J.; Yoo, S.; Lee, M. H. High-Efficiency Sky Blue to Ultradeep Blue Thermally Activated Delayed Fluorescent Diodes Based on Ortho - Carbazole-Appended Triarylboron Emitters: Above 32% External Quantum Efficiency in Blue Devices. *Adv. Opt. Mater.* **2018**, *6* (17), 1800385.

[112] Cho, Y. J.; Jeon, S. K.; Lee, S.-S.; Yu, E.; Lee, J. Y. Donor Interlocked Molecular Design for Fluorescence-like Narrow Emission in Deep Blue

Thermally Activated Delayed Fluorescent Emitters. *Chem. Mater.* **2016**, *28* (15), 5400–5405.

[113] Hatakeyama, T.; Shiren, K.; Nakajima, K.; Nomura, S.; Nakatsuka, S.; Kinoshita, K.; Ni, J.; Ono, Y.; Ikuta, T. Ultrapure Blue Thermally Activated Delayed Fluorescence Molecules: Efficient HOMO-LUMO Separation by the Multiple Resonance Effect. *Adv. Mater.* **2016**, *28* (14), 2777–2781.

[114] Kondo, Y.; Yoshiura, K.; Kitera, S.; Nishi, H.; Oda, S.; Gotoh, H.; Sasada, Y.; Yanai, M.; Hatakeyama, T. Narrowband Deep-Blue Organic Light-Emitting Diode Featuring an Organoboron-Based Emitter. *Nat. Photonics* **2019**, *13* (10), 678–682.

[115] Ahn, D. H.; Kim, S. W.; Lee, H.; Ko, I. J.; Karthik, D.; Lee, J. Y.; Kwon, J. H. Highly Efficient Blue Thermally Activated Delayed Fluorescence Emitters Based on Symmetrical and Rigid Oxygen-Bridged Boron Acceptors. *Nat. Photonics* **2019**, *13* (8), 540–546.

[116] Kim, J. U.; Park, I. S.; Chan, C.-Y.; Tanaka, M.; Tsuchiya, Y.; Nakanotani, H.; Adachi, C. Nanosecond-Time-Scale Delayed Fluorescence Molecule for Deep-Blue OLEDs with Small Efficiency Rolloff. *Nat. Commun.* **2020**, *11* (1), 1765.

[117] Gibson, J.; Monkman, A. P.; Penfold, T. J. The Importance of Vibronic Coupling for Efficient Reverse Intersystem Crossing in Thermally Activated Delayed Fluorescence Molecules. *ChemPhysChem* **2016**, *17* (19), 2956–2961.

[118] Kondakov, D. Y. Characterization of Triplet-Triplet Annihilation in Organic Light-Emitting Diodes Based on Anthracene Derivatives. *J. Appl. Phys.* **2007**, *102* (11), 114504.

[119] Wallikewitz, B. H.; Kabra, D.; Gélinas, S.; Friend, R. H. Triplet Dynamics in Fluorescent Polymer Light-Emitting Diodes. *Phys. Rev. B* **2012**, *85* (4), 045209.

[120] Lee, M.-T.; Chen, H.-H.; Liao, C.-H.; Tsai, C.-H.; Chen, C. H. Stable Styrylamine-Doped Blue Organic Electroluminescent Device Based on 2-Methyl-9,10- Di (2-Naphthyl)Anthracene. *Appl. Phys. Lett.* **2004**, *85* (15), 3301–3303.

[121] Kim, S. K.; Yang, B.; Ma, Y.; Lee, J. H.; Park, J. W. Exceedingly Efficient Deep-Blue Electroluminescence from New Anthracenes Obtained Using Rational Molecular Design. *J. Mater. Chem.* **2008**, *18* (28), 3376–3384.

[122] Huang, Y.; Du, X.; Tao, S.; Yang, X.; Zheng, C.-J.; Zhang, X.; Lee, C.-S. High Efficiency Non-Doped Deep-Blue and

Fluorescent/Phosphorescent White Organic Light-Emitting Diodes Based on an Anthracene Derivative. *Synth. Met.* **2015**, *203*, 49–53.

[123] Zheng, C.-J.; Zhao, W.-M.; Wang, Z.-Q.; Huang, D.; Ye, J.; Ou, X.-M.; Zhang, X.-H.; Lee, C.-S.; Lee, S.-T. Highly Efficient Non-Doped Deep-Blue Organic Light-Emitting Diodes Based on Anthracene Derivatives. *J. Mater. Chem.* **2010**, *20* (8), 1560.

[124] Cho, I.; Kim, S. H.; Kim, J. H.; Park, S.; Park, S. Y. Highly Efficient and Stable Deep-Blue Emitting Anthracene-Derived Molecular Glass for Versatile Types of Non-Doped OLED Applications. *J. Mater. Chem.* **2012**, *22* (1), 123–129.

[125] Kim, B.; Park, Y.; Lee, J.; Yokoyama, D.; Lee, J.-H.; Kido, J.; Park, J. Synthesis and Electroluminescence Properties of Highly Efficient Blue Fluorescence Emitters Using Dual Core Chromophores. *J. Mater. Chem. C* **2013**, *1* (3), 432–440.

[126] Liu, W.; Ying, S.; Guo, R.; Qiao, X.; Leng, P.; Zhang, Q.; Wang, Y.; Ma, D.; Wang, L. Nondoped Blue Fluorescent Organic Light-Emitting Diodes Based on Benzonitrile-Anthracene Derivative with 10.06% External Quantum Efficiency and Low Efficiency Roll-Off. *J. Mater. Chem. C* **2019**, *7* (4), 1014–1021.

[127] Kim, K. H.; Baek, J. Y.; Cheon, C. W.; Moon, C. K.; Sim, B.; Choi, M. Y.; Kim, J. J.; Kim, Y. H. Highly Efficient Non-Doped Deep Blue Fluorescent Emitters with Horizontal Emitting Dipoles Using Interconnecting Units between Chromophores. *Chem. Commun.* **2016**, *52* (73), 10956–10959.

[128] Liao, C.-H.; Lee, M.-T.; Tsai, C.-H.; Chen, C. H. Highly Efficient Blue Organic Light-Emitting Devices Incorporating a Composite Hole Transport Layer. *Appl. Phys. Lett.* **2005**, *86* (20), 203507.

[129] Jung, H.; Kang, S.; Lee, H.; Yu, Y.-J.; Jeong, J. H.; Song, J.; Jeon, Y.; Park, J. High Efficiency and Long Lifetime of a Fluorescent Blue-Light Emitter Made of a Pyrene Core and Optimized Side Groups. *ACS Appl. Mater. Interfaces* **2018**, *10* (36), 30022–30028.

[130] Park, J. K.; Lee, K. H.; Kang, S.; Lee, J. Y.; Park, J. S.; Seo, J. H.; Kim, Y. K.; Yoon, S. S. Highly Efficient Blue-Emitting Materials Based on 10-Naphthylanthracene Derivatives for OLEDs. *Org. Electron.* **2010**, *11* (5), 905–915.

[131] Kim, Y. H.; Shin, D. C.; Kim, S.-H.; Ko, C.-H.; Yu, H.-S.; Chae, Y.-S.; Kwon, S. K. Novel Blue Emitting Material with High Color Purity. *Adv. Mater.* **2001**, *13* (22), 1690–1693.

[132] Fukagawa, H.; Shimizu, T.; Ohbe, N.; Tokito, S.; Tokumaru, K.;

Fujikake, H. Anthracene Derivatives as Efficient Emitting Hosts for Blue Organic Light-Emitting Diodes Utilizing Triplet–Triplet Annihilation. *Org. Electron.* **2012**, *13* (7), 1197–1203.

[133] Mu, G.; Zhuang, S.; Zhang, W.; Wang, Y.; Wang, B.; Wang, L.; Zhu, X. Efficient Blue Organic Light-Emitting Diodes Based on Triphenylimidazole Substituted Anthracene Derivatives. *Org. Electron.* **2015**, *21*, 9–18.

[134] Chen, Y. H.; Lin, C. C.; Huang, M. J.; Hung, K.; Wu, Y. C.; Lin, W. C.; Chen-Cheng, R. W.; Lin, H. W.; Cheng, C. H. Superior Upconversion Fluorescence Dopants for Highly Efficient Deep-Blue Electroluminescent Devices. *Chem. Sci.* **2016**, *7* (7), 4044–4051.

[135] Chou, P.-Y.; Chou, H.-H.; Chen, Y.-H.; Su, T.-H.; Liao, C.-Y.; Lin, H.-W.; Lin, W.-C.; Yen, H.-Y.; Chen, I.-C.; Cheng, C.-H. Efficient Delayed Fluorescence via Triplet–Triplet Annihilation for Deep-Blue Electroluminescence. *Chem. Commun.* **2014**, *50* (52), 6869–6871.

[136] Cha, S. J.; Han, N. S.; Song, J. K.; Park, S. R.; Jeon, Y. M.; Suh, M. C. Efficient Deep Blue Fluorescent Emitter Showing High External Quantum Efficiency. *Dye. Pigment.* **2015**, *120*, 200–207.

[137] Hu, J.-Y.; Pu, Y.-J.; Satoh, F.; Kawata, S.; Katagiri, H.; Sasabe, H.; Kido, J. Bisanthracene-Based Donor-Acceptor-Type Light-Emitting Dopants: Highly Efficient Deep-Blue Emission in Organic Light-Emitting Devices. *Adv. Funct. Mater.* **2014**, *24* (14), 2064–2071.

[138] Pu, Y. J.; Nakata, G.; Satoh, F.; Sasabe, H.; Yokoyama, D.; Kido, J. Optimizing the Charge Balance of Fluorescent Organic Light-Emitting Devices to Achieve High External Quantum Efficiency beyond the Conventional Upper Limit. *Adv. Mater.* **2012**, *24* (13), 1765–1770.

[139] Kawamura, M.; Kawamura, Y.; Mizuki, Y.; Funahashi, M.; Kuma, H.; Hosokawa, C. 39.4: Highly Efficient Fluorescent Blue OLEDs with Efficiency-Enhancement Layer. *SID Symp. Dig. Tech. Pap.* **2010**, *41* (1), 560.

[140] Suzuki, T.; Nonaka, Y.; Watabe, T.; Nakashima, H. Highly Ef Fi Cient Long-Life Blue Fl Uorescent Organic Light-Emitting Diode Exhibiting Triplet – Triplet Annihilation Effects Enhanced by a Novel Hole-Transporting Material. *Jpn. J. Appl. Phys.* **2014**, *052102*, 1–6.

[141] Heimel, P.; Mondal, A.; May, F.; Kowalsky, W.; Lennartz, C.; Andrienko, D.; Lovrincic, R. Unicolored Phosphor-Sensitized Fluorescence for Efficient and Stable Blue OLEDs. *Nat. Commun.* **2018**, *9* (1), 4990.

[142] Avakian, P.; Merrifield, R. E. Triplet Excitons in Anthracene Crystals—A Review. *Mol. Cryst.* **1968**, *5* (1), 37–77.

[143] Aydemir, M.; Haykir, G.; Battal, A.; Jankus, V.; Sugunan, S. K.; Dias, F. B.; Al-Attar, H.; Türksoy, F.; Tavasli, M.; Monkman, A. P. High Efficiency OLEDs Based on Anthracene Derivatives: The Impact of Electron Donating and Withdrawing Group on the Performance of OLED. *Org. Electron.* **2016**, *30*, 149–157.

[144] Luo, Y.; Aziz, H. Correlation between Triplet-Triplet Annihilation and Electroluminescence Efficiency in Doped Fluorescent Organic Light-Emitting Devices. *Adv. Funct. Mater.* **2010**, *20* (8), 1285–1293.

[145] Salehi, A.; Dong, C.; Shin, D.-H.; Zhu, L.; Papa, C.; Thy Bui, A.; Castellano, F. N.; So, F. Realization of High-Efficiency Fluorescent Organic Light-Emitting Diodes with Low Driving Voltage. *Nat. Commun.* **2019**, *10* (1), 2305.

[146] Henry, B. R.; Siebrand, W. Spin–Orbit Coupling in Aromatic Hydrocarbons. Analysis of Nonradiative Transitions between Singlet and Triplet States in Benzene and Naphthalene. *J. Chem. Phys.* **1971**, *54* (3), 1072–1085.

[147] Smith, M. B.; Michl, J. Singlet Fission. *Chem. Rev.* **2010**, *110* (11), 6891–6936.

[148] Kondakov, D. Y. Triplet–Triplet Annihilation in Highly Efficient Fluorescent Organic Light-Emitting Diodes: Current State and Future Outlook. *Philos. Trans. R. Soc. A Math. Phys. Eng. Sci.* **2015**, *373* (2044), 20140321.

초 록

유기발광다이오드(이하 OLED)는 디스플레이에 사용되는 경우 자체 발광 특성으로 인해 빛을 밝혀주는 광원(백라이트)가 불필요하다. 따라서 기존 액정 디스플레이에 비해 얇고 가벼운 디스플레이 제작이 가능하며 명암비가 우수하다. 또한 기판 선택에 제한이 적어 유연, 투명 기판에 적용될 수 있다는 장점이 있다. 이러한 장점들을 가진 유기발광다이오드는 소형 모바일 기기의 디스플레이에 적용되기 시작한 이래 디스플레이 및 조명 분야에서 활용되며 적용 범위를 넓혀가고 있다. 고효율과 긴 수명을 보이는 적색, 녹색 OLED 가 개발되었으나 아직까지 청색 OLED 의 성능은 그에 미치지 못한다. 따라서 고품질 디스플레이를 위해서는 청색 소자의 개선이 필요하다고 할 수 있다.

일반 형광 발광체는 전기적으로 생성되는 여기자 중 25%에 불과한 일중한 만을 발광 여기자로 사용하기 때문에 낮은 효율을 보인다. 효율을 높이기 위해서는 75%를 차지하는 삼중항을 효율적으로 활용하는 것이 중요하다. 진청색 발광을 위해서는 좁은 발광 스펙트럼과 높은 발광 에너지를 갖는 발광체를 사용해야 한다.

본 논문에서는 효율적인 진청색 발광체와 삼중항 수확 전략을 활용한 진청색, 고효율 OLED 개발에 대한 주제를 다루고 있다.

제 2 장에서는 청색 발광에 적합한 엑시플렉스 (exciplex) 호스트 개발에 대한 내용을 다룬다. 새롭게 개발된 엑시플렉스 호스트를와 일중항과 삼중항 모두 발광에 참여 가능한 인광 발광체를 이용해 고효율 청색 인광 소자를 제작할 수 있었다. 엑시플렉스 호스트를 사용하는 OLED 는 발광층으로의 전하 주입이 용이하며, 발광층의 전하 밀도가 상대적으로 낮아 소자의 성능이 단일 호스트에 비해 우수하다. 그러나 청색 OLED 의 경우 청색 발광체의 넓은 밴드갭과 높은 삼중항 에너지 (T_1)로 인해 엑시플렉스 호스트를 청색 소자에 적용하기가 쉽지 않다고 여겨져 왔다. 이러한 한계를 해결하고자 카바졸 기반의 정공전달물질과 포스핀 옥사이드 기반의 전자전달 물질을 사용해 높은 발광 에너지를 갖는 엑시플렉스 시스템을 개발하였으며 이를 적용한 소자를 제작하였다. 소자는 높은 EQE 와 우수한 색 좌표를 나타내었으며 엑시플렉스 호스트가 청색에 적용될 수 있다는 것을 증명하였다.

3 장에서는 열 활성 지연 형광 특성을 보이는 발광체의 특성을 분석하였다. 열 활성 지연 형광 물질은 전자 주게 및 받게가

서로 연결되어 있으며 둘 간의 전자 교환으로 발광이 발생한다. 일반적으로 넓은 반치폭으로 인해 청색 발광이 쉽지 않을 것으로 여겨졌으나 청색 발광에 적합한 에너지 레벨을 가지며 단단한 구조를 갖는 전자 주게와 받게를 이용해 높은 발광 에너지와 좁은 반치폭을 갖는 청색 형광 발광체들을 개발하였다. DFT 계산을 이용해 분자의 특성을 예측하고 실험을 통해 특성이 잘 예측되었음을 확인하였다. 긴 분자구조로 80% 이상의 높은 수평 배향 쌍극자 배향 비율을 나타내었으며 발광체들을 이용해 소자를 제작한 결과 28.2% EQE, CIE 색좌표 (0.142, 0.090)을 보이는 소자를 구현할 수 있었다.

제 4 장에서는 삼중항–삼중항 소멸 (이하 TTA) 과정을 통해 삼중항 수확을 하는 소자의 특성을 분석하였다. TTA 물질의 높은 안정성으로 인해 아직까지 상용화된 디스플레이의 청색 소자에는 TTA 물질이 사용되고 있다. 그러나 TTA 를 이용한 소자의 경우 기존 형광에 비해 발광에 참여하는 여기자 비율이 증가하긴 하지만 앞서 2, 3 장에서 다루었던 100% 여기자 활용이 가능한 인광 및 TADF 에 비해 30% 수준의 낮은 발광 여기자 비율을 보인다. 4 장에서는 TTA 과정의 메커니즘 분석을 통해 TTA 효율의 한계를 분석하고자 하였으며 분석을 바탕으로 TTA 효율을 높일 수 있는 소자 구조를 제안하였다.

주요어: 진청색 유기발광다이오드, 인광, 형광, 열활성형광, 삼중항–삼중항 소멸, 지연 형광

학번: 2014 - 22529

CURRICULUM VITAE

Hyoungcheol Lim

Department of Materials Science & Engineering

Seoul National University, Seoul, 08826, Korea

+82-2-875-2412 (Office)

E-mail: leemhc0126@snu.ac.kr

Education

2014.09 ~ **Ph.D.** in Materials Science & Engineering

Supervisor: Professor Jang-Joo Kim

Seoul National University, Seoul, Korea

2007.03 ~ 2014.02 **B.S.** in Materials Science & Engineering

Seoul National University, Seoul, Korea

Research Interests

Exciplex host, Organic light emitting diodes, Phosphorescent OLEDs, Fluorescent OLEDs, TADF OLEDs, Triplet-triplet annihilation, deep-blue OLEDs

Professional Skills

- Design and fabrication of organic electroluminescent (EL) devices: Thermal deposition, Spin coating

- Electrochemical analysis of organic semiconduct materials: Cyclic voltammetry
- Optoelectronic analysis on organic semiconduct materials: UV-vis-NIR absorption spectroscopy, PL efficiency, Emitting dipole orientation, Time-resolved photoluminescence (PL) emission, Excitation source operation (Nd:Yag laser, N_2 laser, He:Cd laser), Detector operation (photomultiplier tube, spectrometer, streak camera, iCCD)
- EL characteristics analysis: Current density-voltage-luminescence (*J-V-L*) measurements, Electrically pumped transient PL, Transient EL, Emission pattern, Function generator, Delay generator, Oscilloscope
- The structural characterization of organic semiconductors: α-STEP
- Density functional theory (DFT) calculations

Scholarship and Fellowship

- Brain Korea 21 Scholarship (2014.09 ~)

List of Publications

1. **Hyoungcheol Lim**, Hyun Shin, Kwon-Hyeon Kim, Seung-Jun Yoo, Jin-Suk Huh, and Jang-Joo Kim*, "An Exciplex Host for Deep-Blue Phosphorescent Organic Light-Emitting Diodes" *ACS Appl. Mater. Interfaces,* **2017**, 9 (43), 37883–87.

2. **Hyoungcheol Lim**, Hyung Jin Cheon, Gyeong Seok Lee, Mikyung Kim, Yun-Hi Kim, and Jang-Joo Kim*, "Enhanced Triplet–Triplet Annihilation of Blue Fluorescent Organic Light-Emitting Diodes by Generating Excitons in Trapped Charge-Free Regions", *ACS Appl. Mater. Interfaces,* **2019**, 11 (51), 48121–48127.

3. Kyung-Hoon Han, Kwan Kim, Yoonjay Han, Yang-Doo Kim, **Hyoungcheol Lim**, Daihong Huh, Hyun Shin, Heon Lee, and Jang-Joo Kim*, "Highly Efficient Tandem White OLED Using a Hollow Structure", *Adv. Mater. Interfaces*, **2020**, 7 (9), 1901509.

4. **Hyoungcheol Lim**, Hyung Jin Cheon, Seung-Je Woo, Soon-Ki Kwon, Yun-Hi Kim, and Jang-Joo Kim*, "Highly efficient deep blue OLEDs using TADF emitter with narrow emission spectrum and high horizontal emitting dipole orientation ratio", **2020***, Submitted to Adv. Mater.*

List of Presentations

International Conference

1. **Hyoungcheol Lim**, Hyun Shin, Kwon-Hyeon Kim, Seung-Jun Yoo, Jin-Suk Huh, Jang-Joo Kim, "Deep-blue phosphorescent organic light-emitting diodes based on high triplet energy exciplex host", 2nd International TADF Workshop, July 19-21 (July 19), 2017, Japan (Poster)
2. **Hyoungcheol Lim**, Hyun Shin, Kwon-Hyeon Kim, Seung-Jun Yoo, Jin-Suk Huh, Jang-Joo Kim, "Deep Blue Emitting Exciplex Forming System and Its Application to Phosphorescent Organic Light-Emitting Diodes", The 9th Asian Conference on Organic Electronics (A-COE 2017), October 25-27 (October 26), 2017, Korea (Poster)
3. **Hyoungcheol Lim**, Hyun Shin, Kwon-Hyeon Kim, Seung-Jun Yoo, Jin-Suk Huh, and Jang-Joo Kim, "Blue phOLED with improved Operational Lifetime Using High Triplet Level Exciplex Forming Host", The 18th International Meeting on Information of Display(iMiD 2018), August 28-31 (August 30), 2018, Korea (Poster)
4. **Hyoungcheol Lim**, Hyun Shin, Kwon-Hyeon Kim, Seung-Jun Yoo, Jin-Suk Huh, and Jang-Joo Kim, "Blue PhOLED with Extended Operational Lifetime Using Deep Blue Emitting Exciplex System as a Host", The 12th International Conference on Electroluminescence and Optoelectronic Devices(ICEL 2018), October 14-17 (October 16), 2018, Korea (Poster)

5. Chang-Ki Moon, **Hyoungcheol Lim**, and Jang-Joo Kim, "Formation and Binding Energy of Charge-Transfer Excitons in Organic Donor-Acceptor Mixtures", The 11th Asian Conference on Electronics (A-COE), November 6-9 (November 8), 2019, Taiwan (Poster)
6. **Hyoungcheol Lim**, Hyung Jin Cheon, Gyeong Seok Lee, Mikyung Kim, Yun-Hi Kim, and Jang-Joo Kim, "Enhanced Triplet-Triplet Annihilation of Blue Fluorescent Organic Light Emitting Diode by Generationg Excitons in Trapped Charge Free Region",The 11th Asian Conference on Electronics (A-COE), November 6-9 (November 8), 2019, Taiwan (Poster)

Domestic Conference

1. **임형철**, 김장주, 신현, 김권현, 유승준, 허진석, "An exciplex host consisted of high triplet level materials for deep-blue phosphorescent organic light-emitting diodes", 2017 한국고분자학회 추계학술대회, October 11-13 (October 13), 2017, Korea (Poster)